Doctoral Thesis

Development of a Near-Field Scanning Microwave Microscopy for Semiconductors Characterization

Author:
Bendehiba Abadlia Bagdad

Supervisor:
Dr. Francisco Gámiz Pérez

A thesis submitted in fulfillment of the requirements
to obtain the **Degree of Doctor of Philosophy** as part of the
Programa de Doctorado en Física y Ciencias del Espacio
in the

Nanoelectronics Research Group
Departamento de Electrónica y Tecnología de los Computadores

Granada, June 27, 2019

Editor: Universidad de Granada. Tesis Doctorales
Autor: Abadlia Bagdad Bendehiba
ISBN: 978-84-1306-271-6
URI: http://hdl.handle.net/10481/56504

El doctorando/ *The doctoral candidate* **Bendehiba Abadlia Bagdad** y el director de la tesis/ *and the thesis supervisor* **Francisco Jesús Gámiz Pérez** garantizan, al firmar esta tesis doctoral, que el trabajo, titulado ***Development of a Near-Field Scanning Microwave Microscopy for Semiconductors Characterization***, ha sido realizado por el doctorando bajo la tutela del director de la tesis, y hasta donde nuestro conocimiento alcanza, en la realización del trabajo, se han respetado los derechos de otros autores a ser citados, cuando se han utilizado sus resultados o publicaciones.

Guarantee by signing this thesis: that the work entitled ***Development of a Near-Field Scanning Microwave Microscopy for Semiconductors Characterization*** , has been performed under the full guidance of the Ph.D Supervisor and, as far as our knowledge reaches, during the work, it has been respected the right of others authors to be cited, when their publications or their results have been used.

Granada, June 27, 2019

Director de la Tesis	Doctorando
Thesis supervisor	*Doctoral Candidate*
F.J. Gámiz Pérez	Bendehiba Abadlia Bagdad

I would like to dedicate this Doctoral Thesis to my beloved parents, Mohamed and Yamina Bounoua, to my brother Charef, my sisters : Nadia, Zineb, Djamila, Houaria, Mansouria, Naima, Fatiha and to my lovely nephews (Adem , Ayoub, Abdelilah), and also to my grandmother Setti Bounoua , my aunts (Kheira ABADLIA BAGDAD and Zohra) , and to all the ABADLIA BAGDAD family who are the most important people in my life.

To all the people I had the chance to meet in Granada and supported me during my whole stay, at the Islamic center in Granada with whom I spent unforgettable moments: Souhail, Meknassi, Anas Otman, Mohamed daoudi, Brahim, Mohamed benlemou, Mahi Imen, Dr. Said chham, Dr. Abdelhakim, Houada Zentar, Dr. Soumicha Mahdjour, Dr. Mohamed Grandi, Dr. Chadia Elfatini , Dorsaf cheikh, and José Antonio (my roommate).

To all my friends I studied with in Algeria and to whom I know from the university : Dr. Azzouzi Soufiane, Nekkaa Abdellah, Amel Benhalou, Bainine Abdelhamid, Dr. Batoul Benkadour, Dr. Amina Benallou, Mansour Benhoua, Mohamed Benatia, Hamou Mouradd, Nora, Moumia, Bouziane karim, Omar Idriss, Amine Benadidou, Nadia, Belguendouz Miloud, Abed Benkadour, Embarek Madjid, Mustapha Daho, Khetaf Habib, Seddik Mohamed, Torkiya, Chemseddine, Reda hadj ali, Belghachem Ali, Belayachi Feyçal, Mansour Attallah, Abdellah khelafi, and Amel rezali.

To all my Turkish teachers to whom I am really grateful : Özgue, Tuğba, Tuğçe, Gülşen, Dilek and all my friends I met and studied with in Turkey during the Academic year 2013/2014.

Finally, to all the amazing people and friends I had the chance to know this year, with whom I spent memorable moments : Rula, Duaa, Arkan, Majd, şubat, Hikma, youcef, Hiba, Bushra, Onur, Halis, Karim, Kalilou, Nassim, Reza, Souhail, Antonio, Sara, Olga, Dominika, Maribel, Parmis and others I may probably forget.

ABADLIA BAGDAD Bendehiba

Acknowledgments

In the name of ***God***, the Almighty, the most Beneficent and most Merciful. All praises are to Allah (the Supreme), the Creator and the Sustainer of the universe, on whom ultimately we depend for sustenance and guidance, for the strengths and His blessing to accomplish this project successfully.

First and foremost I offer my sincerest gratitude to the coordinator and all the responsibles of the programme ***Erasmus Mundus – Al Idrisi II***, for providing me the opportunity to be part of this exchange programme and for fully funding my scholarship for three beautiful years in "Physics and Space Science Programme" at the University of Granada - Spain.

My sincere appreciation goes to my supervisor, ***Pr.Francisco Gamiz*** to whom I am very grateful. Firstly, for accepting me to be part of his research group and gave me the opportunity to work on this doctoral thesis. Also for his coaching, availability, support and their valuable and wise advice throughout this project.

Besides my advisor, I would like to thank the members of jury, for their availability and the time spent for reading the manuscript and evaluating the work, and for serving as my committee members.

Similar, profound gratitude goes to ***Pr.Benachenhou Abdelhalim***, who has been a truly dedicated mentor. I am particularly indebted to him for his constant faith in the laboratory work, and for generously hosted me in "the Laboratory of Electromagnetism and Guided Optics" (LEGO). I could never forget the time I spend there and the great souvenirs.

I am also hugely appreciative to ***Pr.Juan Tejada***, especially for sharing his taxonomic expertise, and for being so dedicated to his role as my tutor, and also I want to thank ***Dr.Carlos Sampedro*** for his help during my experimental works.

Spercial thanks to ***Dr. Ahmadouche Ahmed***, and ***Dr. Abed Mansour***, from the University of Mostaganem – Abdelhamid Ibn Badis, Faculty of sciences and technology in Algeria, not only for their tremendous academic support, but also for giving me beneficial and wonderful advice. Without forgetting to thank the other teachers at the same University, the Faculty of sciences and technology ; Aibout abdellah, Oueld ali, Bense-

nane Bachir, Sabsadji Abdelrahmen, Mehidi Aicha, Neddar Houaria, Yaagoubi Benabdellah, Merah Mostefa, Farah Said, Bahous Hadj, Bechiri, Ouari Kheira, Beklaouz Hadj, Rebhi Mostapha, Ghomri Leila, Djelti Benbella, Benchellal Amel, Houcine Rachida, Hadri Baghdad , Benouddnine Hadjira, for the quality of education they offered to me, their support and encouragement during my stay abroad. I want also to thank all the staff in the department of Electrical engineering at the University of Mostaganem.

I thank my fellow ***labmates***, Dr. Celso, Dr. Cristina, José Maria, Alex, Manuelo, Dr. Carlos Navarro, Dr. Carlos Markez, and Santiago for the help, support they brought me back during this thesis and the great moments spent together. I can not forget the help of Dr. Pilar López, who has always supported me, from my first day in the laboratory until the end of my Ph.D. Really, I was very lucky to know someone like you in my life.

Special thanks go also to my best friends ever, kaddour benatia Mohamed and Dr. Azzouzi soufiane for their presence, support and for every single advice they provided me all along my stay abroad.

Very special thanks to my family. Words cannot express how grateful I am to my parents, Yamina and Mohamed for all the sacrifices they have made on my behalf, and also all my sisters and my younger brother.

Last but not least, I would like to thank the Algerian families I met in Granada, ***REHI family*** : Uncle Khaled, his wife Zakia and their daughters Bachira and Khadidja. Also ***NACER family*** , Nabahate, Feryal and her father who helped me a lot correcting the manuscript with the help of ***Dr. BELKHIR Yasmina***.

ABADLIA BAGDAD Bendehiba

"Knowledge comes from experience: Knowledge is not information, the only source of knowledge is experiment and experience. Knowledge is not just a collection of information that any of us can get without any effort, but the real knowledge is to work diligently to gain experience."

Albert Einstein

Abstract (Arabic version)

تعرف مؤخرا تقنيات الفحص بمجهر الميكروويف ذات المجال القريب تطوراً ملحوظاً ، و بشكل جيد لأنها أدوات متطورة ، مكرسة لتوصيف المواد. توفر هذه الطرق إمكانيات لتوصيف سطح المواد وتحت سطحها ، وتقدم قياسات بطريقة غير ملامسة ، والأهم من ذلك ، غير مدمرة لهاته المواد المراد توصيفها.

تتضمن تقنية ***NSMM*** على المرنان ذو تجويف محوري على ترددات الميكروويف المتصلة بمحلل شبكة المتجهات. يتم تغذية طرف حاد يمتد من الموصل الداخلي للتجويف بواسطة مصدر ميكروويف لتشكيل مسبار المجال القريب من أجل تحليل العينة قيد الاختبار. تبقى المسافة بين طرف المجس وسطح العينة أو الركيزة ثابتة بينما يتم فحص العينة بأكملها المراد تحليلها. يتم قياس وتسجيل التغييرات في وتيرة الرنين (f_r) في مرنان تجويف متحد المحور ومعامل الانعكاس (S_{11}) او النقل (S_{21}) على التوالي باستخدام نظام معلوماتي. هذه المعلمات تعتمد على الخصائص الكهرومغناطيسية المحلية للعينة. من خلال رسم هذه الكميات المقاسة فيما يتعلق بموضع طرف المجس ، يمكن الحصول على خريطة عازلة ، توفر معلومات حول خصائص العينة.

في هاته الدراسة ، قمنا بتحسين تطوير تقنية ***NSMM*** محلية الصنع للاستفادة الكاملة من إمكاناتها. تم إجراء العديد من اختبارات المحاكاة لمرنان التجويف المحوري والتفاعل بين العينة والطرف الابري من المرنان من أجل الحصول على قدرة استبانة مكانية عالية على مدى تردد واسع. تكون درجة الدقة المكانية أعلى عند استخدام رأس حاد للغاية ، يتم الحصول عليه عن طريق الحفر الكهروكيميائي لأسلاك التنغستن. وكان أفضل رأس ابري حاد متحصل عليه ذو قطر حوالي 1 ميكرمتر.

وبالتالي ، فإننا نبيّن أن استغلال تقنيات الفحص المجهري ذات المجال القريب يجب أن يسمح لنا بتوصيف بعض عينات أشباه الموصلات على الترددات العالية التي تتراوح من 1 جيجاهرتز إلى 20 جيجا هرتز. في النهج الثاني ، تمكنا من الجمع بنجاح مجهر القوة الذرية مشتراة من شركة تجارية مع تقنية ***NSMM*** المطورة في مخبرنا. هدفنا الرئيسي هو المقارنة بين النتائج التي تم الحصول عليها من كلا التقنيتين. على وجه الخصوص ، تم اقتراح بعض تطبيقات ***NSMM*** ، مثل اقتراح أتمتة منصتها باستخدام نظام محكمات وضع نانومترية بدقة عالية.

توضح النتائج التي تم الحصول عليها في هذا العمل أن التقنيات المقترحة ملائمة من حيث حساسية القياسات ومدى تردد التشغيل وفقًا لأحدث التقنيات. بالإضافة إلى ذلك ، أصبحت هذه التقنيات أداة مهمة لقياس خصائص المواد ، وخاصة أشباه الموصلات ، في مجال الميكرو و النانو الالكترونيات.

Abstract (English version)

Near-field Scanning Microwave Microscopy (NSMM) techniques experimented a remarkable development as they are cutting-edge tools, devoted to the characterization of materials. These methods provide possibilities to characterize the surface and sub-surface of materials, offering measurements in a non-contact, non-invasive and, the most important, non-destructive way.

The NSMM technique comprises a coaxial microwave resonant cavity connected to a vector network analyzer (VNA). A sharp tip extending from the inner conductor of the coaxial cavity resonator is fed by a microwave source to form a near field probe in order to analyze the sample to be tested. The distance between the probe tip and the surface or substrate of the sample is kept constant while the entire sample to be analyzed is "scanned". Changes in the resonance frequency of the coaxial cavity resonator f_r and reflection, or transmission coefficients S_{11}, S_{21} respectively are measured and recorded using a computing system. These parameters are dependent on the local electromagnetic properties of the sample. By plotting these measured quantities with respect to the probe tip position, a dielectric map can be obtained, providing information about the properties of the sample.

In this study, we implemented a set-up of a home-made NSMM in order to take full advantage of its potential. Several simulation tests of the coaxial cavity resonator and the tip-sample interaction were done, in order to achieve a high spatial resolution of the properties at a wide range of frequencies. The spatial resolution is higher when a very sharp tip is employed, obtained by electrochemical etching of a tungsten wire with diameters below $1 micron$.

Thus, we show that the exploitation of the developed home-made near-field microscope should allow us to characterize some semiconductor samples at high-frequency range from $1GHz$ up to $20GHz$. In a second approach, we were able to combine successfully a commercial Atomic Force Microscopy with NSMM technique. A comparison between the results obtained by both techniques was our major objective. In particular, some applications of NSMM were suggested, such as the automatization of NSMM platform using the nanopositioner system with high precision.

The results obtained in this work show that the proposed techniques are convenient in terms of the sensitivity of the measurements and the range of operating frequency according to the state of the art. In addition, these techniques become an important metrology tool for the characterization of materials, especially semiconductors, in the field of micro-nano electronics.

Abstract (Spanish version)

Las técnicas de microscopía de barrido de microondas de campo cercano (Near-field Scanning Microwave Microscopy, NSMM) suponen un desarrollo muy notable en el campo de la Nanotecnología, ya que son herramientas evolucionadas, dedicadas a la caracterización de materiales. Estos métodos ofrecen la posibilidad de caracterizar la superficie y la subsuperficie de los materiales a escala nanométrica, utilizando mediciones en los modos sin contacto, no invasivas y las más importantes no destructivas.

La técnica NSMM comprende una cavidad coaxial resonante de microondas conectada a un analizador vectorial de red. Una punta afilada que se extiende desde el conductor interno de la cavidad es alimentada por una fuente de microondas formando así una sonda de campo cercano para analizar la muestra situada bajo la misma. Mientras la distancia entre la punta y la superficie de la muestra o el sustrato se mantiene constante, la muestra entera a analizar "es barrida" por la punta y los cambios en la frecuencia de resonancia de la cavidad coaxial f_r y el coeficiente de reflexión, o de transmisión (S_{11}, S_{21} respectivamente), se miden y registran usando un sistema informático. Por lo tanto, estos parámetros dependen localmente de la composición y de las propiedades electromagnéticas en la muestra. Al representar estas cantidades medidas con respecto a la posición de la punta, se puede obtener un mapa de las propiedades electromagnéticas (composición, constante dieléctrica, etc.) de la muestra analizada.

En este estudio, se ha implementado físicamente un sistema de microscopía de microondas de campo cercano, y se ha utilizado para estudiar diferentes muestras semiconductoras. Se realizaron varias pruebas de simulación del resonador de cavidad coaxial y la interacción entre la punta y la muestra, con el fin de fijar las condiciones geométricas y de diseño del sistema que permitiesen lograr una resolución espacial muy alta en un amplio rango de frecuencias. Esta resolución espacial es muy elevada si se utiliza una punta muy afilada. En nuestro caso se utilizó un ataque electroquímico de un hilo de tungsteno para obtener puntas con diámetros inferiores a $1micra$.

De esta forma, hemos demostrado que la técnica de microscopía de microondas de campo cercano implementada en nuestro laboratorio nos permite caracterizar muestras semiconductoras en el rango de frecuencias de $1GHz$ hasta $20GHz$. En una imple-

mentación diferente de la técnica NSMM hemos usado un microscopio de fuerza atómica (AFM) comercial al que se le ha adaptado un microstrip y una analizador vectorial de redes para obtener imágenes NSMM de diferentes muestras semiconductoras. Una comparación entre los resultados obtenidos por ambas técnicas fue nuestro principal objetivo. En particular, se sugirieron algunas aplicaciones de NSMM, como la automatización de la plataforma NSMM que utiliza el sistema de nanoposición con alta precisión.

Los resultados obtenidos en este trabajo muestran que las técnicas propuestas son convenientes en términos de rango de operación de frecuencia y sensibilidad de las mediciones según el estado de la técnica. Además, estas técnicas se convirtieron en una importante herramienta de metrología para la caracterización nanométrica de materiales, especialmente semiconductores, en el campo de la micro-nanoelectrónica.

Abstract (French version)

Les techniques de microscopie microonde en champ proche connaissent un développement très remarquable, car ceux sont des outils évolués, dédiés à la caractérisation des matériaux.

Ces méthodes offrent la possibilité de caractériser la surface et la sous-surface des matériaux, en utilisant des mesures effectuées en modes non destructif sans contact et non invasif. La technique NSMM comprend une cavité coaxiale résonante sur les fréquences microonde connectées à un analyseur de réseau vectoriel.

Une sonde pointue qui s'étend du conducteur intérieur de la cavité est alimentée par une énergie micro-ondes afin de former une sonde à champ proche pour analyser l'échantillons mis sous test. Lorsque la distance entre l'extrémité de la sonde et la surface ou le substrat de l'échantillon reste constante, alors que tout l'échantillon à analyser est "scannée", les modifications de la fréquence de résonance du résonateur à cavité coaxiale F_r et le coefficients de réflexion ou de transmission (S_{11} ou S_{21}) sont mesurés et enregistrés à l'aide d'un système informatique. Ces paramètres dépendent de la constante diélectrique et des propriétés des semi-conducteurs de l'échantillon. En traçant ces quantités mesurées par rapport à la position de la sonde, une carte diélectrique du substrat et les propriétés du semi-conducteur peuvent ainsi être obtenues.

Dans cette étude, nous avons amélioré la mise au point d'une technique NSMM de fabrication artisanale afin de tirer pleinement parti de son potentiel. Plusieurs tests de simulation du résonateur à cavité coaxiale et de l'interaction entre l'échantillon et la sonde ont été effectués afin d'obtenir une puissance de résolution spatiale élevée sur une large plage de fréquences. Cette résolution spatiale est plus élevée lorsqu'on obtient une sonde très pointue à son extrémité en utilisant la gravure électrochimique d'un fil de tungstène. Dans notre cas, la gravure électrochimique du tungstène a été utilisée pour obtenir des sondes d'un diamètre inférieur à $1\mu m$.

Ainsi, nous montrons que l'exploitation des techniques de microscopie à champ proche développées au sein de notre laboaratoire devraient nous permettre de caractériser certains échantillons de semi-conducteurs à haute fréquence allant de $1GHz$ à $20GHz$. Nous avons pu combiner avec succès une microscopie à force atomique commerciale avec la technique NSMM. Notre objectif principal était de comparer les résultats obtenus

par les deux techniques utilisées dans notre étude. Certaines applications de NSMM ont notamment été suggérées, telles que son automatisation à l'aide d'un système de nanopositionneur à haute précision.

Les résultats obtenus dans ce travail montrent que les techniques proposées sont pratiques en termes de la plage de fréquence de fonctionnement et de sensibilité des mesures selon l'état de l'art de la technique. En outre, ces techniques sont devenues un outil de métrologie trés important impliqué dans la caractérisation des matériaux, en particulier des semi-conducteurs, dans le domaine de la micro-nanoélectronique.

List of Abbreviations and Symbols

Abbreviations

AFM	Atomic Force Microscopy
ADS	Advanced Design System
CC	Circulating current
CST	Computer Science Technology
DC	Direct current
DTS	Distance between probe Tip-Sample
EM	Electromagnetic field
Epoxy-FR4	Substrate material type
SNOM	Scanning Near Field Optical Microscopy
FEM	Finite Element Method
FDTD	Finite Difference Time Domain
FET	Field-Effect Transistor
GPIB	General Purpose Interface Bus
HF	High Frequency
HFSS	High Frequency Structural Simulator
MoM	Method of Moments
MRI	Magnetic Resonance Imaging
MWS	Microwave Studio Software
MMIC	Monolithic Microwave Integrated Circuits
MLN-C	Microstrip Line made of Copper
MLN-G	Microstrip Line made of Gold
NSMM	Near-field Scanning Microwave Microscopy

PNA-X	4-Port Network Analyzer
POT	Potentiometer
PCB	Printed Circuit Board
PET	Polyethylene Terephthalate
RF	Radio Frequency
SQUID	Scanning Superconducting Quantum Interference Device
STM	Scanning Tunneling Microscopy
TE	Transverse Electric Wave mode
TM	Transverse Magnetic Wave mode
TEM	Transverse Electric and Magnetic mode
VNA	Vector Network Analyzer

Symbols

B	Electromagnetic flux
$C_{coupling}$	Coupling capacitor
C_R	Effective capacitance
D	Electric flux
d	Distance
E	Electric field
$E(Q)$	Azimuthal component of electric field
f_0	Resonance frequency
f_r	Resonance frequency of working
f_0	Resonance frequency at first mode
f_r	Resonance frequency
Go	Graphene oxide
H	Electromagnetic field
$La - Ca - MnO$	Polycrystalline
L_R	Effective inductance
$NaOH$	Sodium hydroxide
P	RF energy lost per cycle
RGO	Reduced graphene oxide
SiO_2	Dioxide of silicon
S_{11}	Reflection coefficient
S_{21}	Transmission coefficient
Q	Quality factor
$TEnmp$	Propagation mode in waveguides
$tan\delta$	Loss tangent
U	RF energy stored in the cavity
V	Volume
Z	Calibration impedance
Z_L	Load impedance

Q_C	Quality factor of conduction
σ	Conductivity of metal used
Q_D	Quality factor of dielectric
ε_{re}	Effective relative dielectric
Q_{ext}	External quality factor
λ_0	Free space wavelength
Q_L	loaded quality factor
ϵ	Permittivity of Medium
ϵ_0	Permittivity of Vacuum
μ	Permeability of Medium
μ_0	Permeability of Vacuum
λ_g	Micro strip line wavelength
Q_R	Quality factor of radiation
ϵ_r	Relative permittivity
μ_r	Relative permeability
Δf	Shift in resonance frequency
Δf_0	Shift in frequency
Q_0	Unloaded quality factor
ν	Wave propagation velocity in free space
ω	wave pulsation

Contents

List of Figures

Chapter 1

Scanning microwave microscopy generalities

1.1 Introduction

Since the beginning of semiconductor device manufacturing such as bipolar transistor in 1947, Microelectronics has not left off to grow significantly. Today, dominated by Silicon, Microelectronics is experiencing ever more demanding requirements on the performance of components, particularly in the field of digital applications. In addition, with silicon technologies, the growth of semiconductors makes the possibility to develop new components and devices, for example in analog electronics, optoelectronic, power electronics, and telecommunications.

To realize even smaller components and devices with high efficiency, Research has enabled the emergence of tools to characterize them at micro and nanoscale range. Semiconductor characterization field is always an important issue. Traditional measurement methods for semiconductors characterization require pre-measurement sample preparation that may affect the properties of the material [1]. So to study these semiconductor components, material characterization techniques based on microscopy have been developed [2].

Over the past four decades, the field of microscopy has been changing by the new microscopic methods. The new techniques "see" the morphology of the surface of all types of materials samples with a spatial resolution which depends on the wavelength used [3], [4], [5], [6].

Various research centres around the World have focused their efforts on the creation of these new microscopes, that make possible to examine and understand the distinctive

characteristics of components [3]- [7]. These new instruments use evanescent microwave fields and are capable of analyzing with high spatial resolution different types of materials such as superconductors, conductors, dielectrics, insulators, semiconductors, and organic samples [5]- [8]. In addition, these techniques characterize not only the morphology of the surface but also the electrical, magnetic and physical properties of the surface of the sample, but also beneath the surface [3]- [5].

Unlike traditional optical microscopy, the scanning microwave technique performs sweeps of the sample surface in touch, or separated by a few microns up to nanometers from the sample surface. So, it gives rise to a non-invasive and non-destructive technique. Measurements can be presented in a wide range of temperatures, in the air or in the vacuum, or in samples that are fixed or in motion or altered by the presence of electric or magnetic fields or under the excitement of intense light beams. An example of such technique can be a laser for the study of the change of the concentration of carriers in a semiconductor [6], [7], [9].

Today, microscopes have advanced considerably employing wavelengths in different bands, but also employing probing particles technique instead of photons. These include notably microscopes in which they use electrons, such as the scanning tunnelling microscope (STM) [10], the transmission electron microscope (TEM) and the scanning electron microscope (SEM). These tools have become widely used and necessary for Materials Science, Physics, Chemistry, and Biology.

In addition, the forces between the particles have been used in the field of the Atomic Force Microscope (AFM): this technique has become a popular system of measurement in the fields listed previously. The microscopes mentioned above have reached an extremely high spatial resolution, some of them can resolve atoms individually. Microscopes that use photons will always motivate the scientists to reveal the interaction behavior of a material to electromagnetic waves at certain frequencies. In the past, microscopes using electromagnetic waves inherently implied the processes of wave propagation for imaging objects. The diffraction phenomena were, therefore, a major obstacle that limit the spatial resolution of microscopes, which researchers strived to overcome, through the use of the near field, then this limitation has been overcome later [11].

1.2 Work objectives

The objectives of this thesis are given as follows;

- **Development of Near-Field Scanning Microwave Microscopy technique (NSMM)**

  The first part of this research focuses on the design of an NSMM home-made technique. We start with an introductory chapter that provides a brief discussion of the

techniques used for material characterization. The goal of the study is to develop a NSMM technique that can pair with tools that we use in the laboratory. In order to have this system feasible, several simulation tests were conducted. The time needed for conducting these simulations was long as the technology that allows us to realize this design was limited. Three were the main challenging tasks to accomplish: the design of coaxial cavities, the microstrip line resonators, and the probe tips. Three different approaches have been implemented in the NSMM platform in order to achieve a good functioning system and a high spatial resolution regarding material characterization domain [12].

- **Design an integrated NSMM-Atomic Force Microscopy (AFM) platform system** The second part of the research focuses on the integration of the two techniques (NSMM and AFM). The integrated system design aims at tightly combining an NSMM technique with a commercial AFM, in which different microstrip line resonators were designed to ensure the proper functioning of the system. A quarter and a half wavelength microstrip line resonators have been designed and fabricated. In this part, our goal is to be able to image conductor materials like copper, a dielectric substrate (epoxy), SiO_2, graphene oxide (GO) and reduced graphene oxide (rGO). These materials were tested in order to study their characteristics by using this technique.

1.3 Methodology

The first section of the present work was focused on the design of the main part of a NSMM system, i.e. the coaxial resonators. These resonators operate in the near-field region. We have used a full-wave 3D Electromagnetic solver (High frequency structural simulator HFSS) to simulate the entire structure of the designed resonators. Furthermore, whenever an optimization of the coaxial cavity and the feeds, is required, many of such simulations are needed to be handled. Once the coaxial resonator was designed, and the whole NSMM system simulated, the next step was the fabrication of the resonators and the tungsten tip. The resonant cavity was then fully characterized in different conditions and in a very wide frequency range using a Vectorial Network Analyzer. Several tungsten tips were then fabricated using an electrochemical procedure. All the system was finally implemented using micropositioning stages to accommodate the sample under study.

Section II of the work deals mostly with scenarios of NSMM-AFM combination techniques, which typically require a good matching of NSMM with AFM technique. It is well known that the integration between two different techniques is not a simple task regarding their principles of functioning. For this reason, we used a 3D full-wave simulator (HFSS) and (Advanced Design Simulator (ADS)) to characterize the device that

establishes the integration between NSMM and AFM technique which is a micro strip line resonator.

1.4 Thesis outline

This study is organized into six main chapters where several aspects of the research were addressed: the design, the simulation and the experimental validation of the proposed NSMM platform concepts.

Part I

- **Chapter 01** presents an introduction to the study. First of all, it demonstrates the motivation why the technique of characterization by near field scanning microwave microscopy has been chosen at a special frequency range. Discussing later general characterization tools, in which are included four methods which explain the functioning of the characterization at wide frequency range.
- **Chapter 02** presents a brief introduction and concepts of the resonant cavities theory closely related to near-field scanning techniques and to the workings of the NSMM configuration used in the experiments. The goal of this chapter is to describe the main part of NSMM which is the resonator.
- **Chapter 03** focuses on the design and characterization of microwave coaxial cavity resonators used in the experiments. This chapter provides some useful design guidelines of the coaxial resonators used in the system. Several simulations including the interaction between the resonator and the sample under test were carried out.
- **Chapter 04** provides an alternative setup with respect to the concept of NSMM presented in previous chapters. The main goal of this chapter is to link these quantities such as the transmission or the reflection coefficient, the resonance frequency, and the quality factor to the electrical properties of the samples under test, and how these quantities can be measured. Details about the coupling between the probe tip of the coaxial cavity resonators are also included in this chapter.

Part II is devoted to the integration of the NSMM technique with a commercial AFM .

- **Chapter 05** focuses on the setting of integration techniques. It provides a brief description of the SNMM-AFM platform and investigates the combination methods and samples used in it.
- **Chapter 06** it summarizes final remarks on the results obtained in the thesis and future work planned.

1.5 Fundamentals

This section illustrates the concepts that are closely related to the application of scanning near-field microwave microscopy and to state Maxwell's equations in media

1.5.1 Maxwell's equations in matter

The relations and variations of the electric and magnetic fields, currents, and loads associated with electromagnetic waves in any kind of medium are governed by physicals laws. In a homogeneous medium, without charge, dispersive and isotropic, for a given frequency, Maxwell's equations system are described as follows [13];

$$\begin{aligned} \overrightarrow{\nabla}.\overrightarrow{E} &= 0 \\ \overrightarrow{\nabla}.\overrightarrow{H} &= 0 \\ \overrightarrow{\nabla} \wedge \overrightarrow{E} &= -\frac{\partial}{\partial t}\overrightarrow{B} \\ \overrightarrow{\nabla} \wedge \overrightarrow{H} &= \frac{\partial}{\partial t}\overrightarrow{D} \end{aligned} \tag{1.1}$$

For an isotropic, and linear medium, the density of the electric flux (D) and the intensity of the electric field (E) are described by the following relationship [24];

$$D = \epsilon.E = \epsilon_0.\epsilon_r.E \tag{1.2}$$

and even for the density of magnetic flux (B) and the magnetic intensity (H) are also described by this relationship;

$$B = \mu.H = \mu_0.\mu_r.H \tag{1.3}$$

Where, these parameters are defined as follows; ϵ is the permittivity of a given material,ϵ_0 represents the permittivity of free space and ϵ_r describes the relative permittivity normalized to the permittivity of vacuum for a given material of ϵ. μ is the permeability of a given material. Whereas μ_0 free space permeability, and μ_r describes the impact of the magnetic dipole moments of atoms inside the medium [13].

1.1.2 Wave propagation equation

The wave propagation equation in a homogeneous medium is obtained by combining Maxwell's equations :

$$\begin{aligned} &\nabla^2 \cdot \overrightarrow{E} + K^2 \cdot \overrightarrow{E} = 0 \\ &\nabla^2 \cdot \overrightarrow{H} + K^2 \cdot \overrightarrow{H} = 0 \\ &K^2 = \omega^2 \cdot \varepsilon \cdot \mu \end{aligned} \tag{1.4}$$

Where ; K=$\omega\nu$ =$2\pi/\lambda$, with ν represents the wave propagation velocity in free space and ω its pulsation, λ =ν/f, represents the wavelength ,f represents the wave frequency. The obtained equations are called three dimensional Helmholtz Equations [13].

1.1.3 Diffraction-limited system

The resolution of an optical imaging system such a microscope, telescope, or camera can be limited by factors such as imperfections in the lenses or misalignment. However, there is a principal limit to the resolution of any optical system, due to the physics of diffraction. An optical system with resolution performance at the instrument's theoretical limit is said to be diffraction-limited.

The observation of sub-wavelength structures with microscopes is difficult because of the **Abbe diffraction limit**. Ernst Abbe found in 1873 that light with wavelength λ, traveling in a medium with refractive index η and converging to a spot with half-angle θ will have a minimum resolvable distance of;

$$d = \frac{\lambda}{2(\eta \sin\theta)} \tag{1.5}$$

The portion of the denominator (1.5) ($\eta \sin\theta$) is called the numerical aperture (NA) and can reach about 1.4–1.6 in modern optics, hence the Abbe limit is around $d = \lambda/3$. This means that if a microwave of frequency $2.5GHz$ is employed in a microwave microscopy, a resolution of only 4cm will be achieved, too large to study material features at high resolution. However, this difraction limit only holds in the far-field region, and as demonstrated by Synge ([14]) in 1928, near field microscopy is capable of overcoming the Abbe diffraction limit.

1.1.4 Properties of materials

Different types of materials have diverse electrical and magnetic properties. Especially some of them are insulators, and some are conductors [15]. The electrical properties of the materials are what determine the behavior of a certain sample when the electric current passes through it.

The electromagnetic properties of matter can be represented by constitutive parameters: the permittivity ϵ and the permeability μ. Maxwell equations allow taking into account the electrical conductivity of the medium through an expression of the permittivity [16]. The permittivity and permeability must be represented by complex values;

$$\epsilon = \epsilon' - i\epsilon'' \ , \mu = \mu' - i\mu'' \tag{1.6}$$

Taking into consideration the dissipative effects (losses) inherent in any matter, the electromagnetic response of heterogeneous environments can be represented by an average of permittivity and permeability provided that the size of the heterogeneities of the matter remains low compared to the wavelength. Finally, about media with anisotropic electromagnetic properties, the permittivity, or permeability can be represented by tensors quantities [15], [17].

1.1.5 Wave-matter interaction

At the high-frequency range, the electromagnetic fields interaction phenomenon with materials became a wide use in the industry especially in the practical implementation and medical sciences with no exception [6]. Instruments that are invented for a particular purpose or probes are derived from these systems, in which the interaction between the electromagnetic field and material is produced by them. Various devices such as the microwave oven, medical therapeutic tools, industrial applications of rf/microwave plasma and other sensors are classified in the category of applicators and probes. It is well known that all matter is comprised of atoms. But subatomically, matter is made up of mostly empty space. For example, consider the hydrogen atom with its one proton, one neutron, and one electron. The diameter of a single proton has been measured to be about 10^{-15}meters. The diameter of a single hydrogen atom has been determined to be 10^{-10} meters, therefore the ratio of the size of a hydrogen atom to the size of the proton is $100,000 : 1$. For example, if the nucleus of the atom could be enlarged to the size of a tennis ball (about 7 cm), its electron would be approximately 7 kilometers away. Therefore, when electromagnetic waves pass through a material, they are primarily moving through free space, but may have a chance encounter with the nucleus or an electron of an atom. Because the encounters of photons with atom particles are by chance, a given photon has a finite probability of passing completely through the medium it is traversing. The probability that a photon will pass completely through a medium depends on numerous factors including the photon's energy and the medium's composition and thickness. The more densely packed a medium's atoms, the more likely the photon will encounter an atomic particle. In other words, the more subatomic particles in a material (higher Z number), the greater the likelihood that interactions will occur Similarly, the

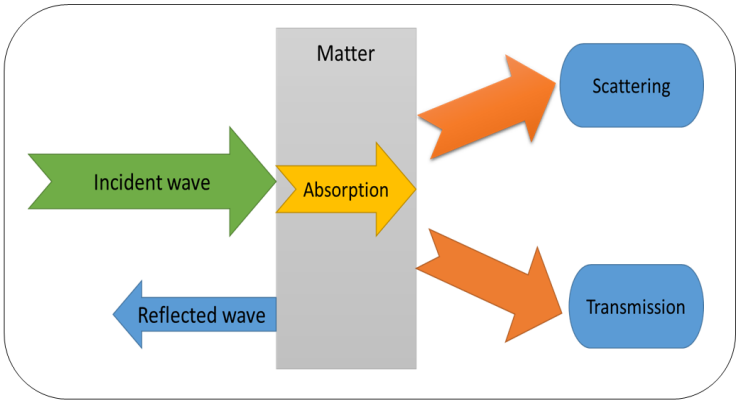

Figure 1.1: Summarizes the different interactions between waves and matter.

more material a photon must cross through, the more likely the chance of an encounter. When a photon does encounter an atomic particle, it transfers energy to the particle. The energy may be reemitted back the way it came (reflected), scattered in a different direction or transmitted forward into the material. Let us first consider the interaction of visible light. Reflection and transmission of light waves occur because the light waves transfer energy to the electrons of the material and cause them to vibrate. If the material is transparent, then the vibrations of the electrons are passed on to neighboring atoms through the bulk of the material and reemitted on the opposite side of the object. If the material is opaque, then the vibrations of the electrons are not passed from atom to atom through the bulk of the material, but rather the electrons vibrate for short periods of time and then reemit the energy as a reflected light wave. The light may be reemitted from the surface of the material at a different wavelength, thus changing its color [18].

1.6 Microwave techniques for materials characterization

1.6.1 Generalities

The characterization of materials requires the use of a characterization method and a model allowing the extraction of conductivity, permittivity and permeability parameters. There are several measurement methods that differ according to a set of parameters. The

frequency of determination is one of these parameters but the level of the dielectric and magnetic losses of the sample, the size of the available sample, the solid, liquid or gaseous state of the sample, the destructive or non-destructive nature of the method should also be considered. All these parameters are factors to determine the suitable technique. For each method, there are different models more or less complex to represent the measuring device and the sample tested [19].

Microwaves characterization of materials consists of measuring the variations of the electromagnetic waves reflected by or transmitted through, the object under test. These microwave signals depend on the level of incident power on the object, the dielectric constant, the permeability, conductivity of the material, and the measurement frequency.

We can quote measurements that can be described as destructive. This involves printing metal tracks on the unknown substrate and measuring the coefficient of reflection or transmission of the waves. The electrical parameters (permittivity, permeability, conductivity, etc.) are then deduced from these measurements. The non-destructive characterization methods, do not affect the material to be characterized. The range of millimetric frequencies and microwaves, although not rigorously defined, is usually between a few megahertz (MHz) and a few hundred gigahertz (GHz). The corresponding wavelengths are between $100cm$ and $1mm$. The frequency of use is usually chosen to optimize the interaction of electromagnetic energy with the nature of the material, its geometry, and its physical properties [18].

1.6.2 Potentialities of microwave techniques in the field of material characterization

In the field of the characterization of the materials, this section introduces briefly the microwave techniques used in non- destructive methods. This section will deal with the capability of these techniques. One of the major cases of microwave non destructive control has been studied in a patent in 1948, which describes a technique to assess the level of moisture in a dielectric material [20]. This work was an important application of non-destructive microwave control, till nowadays, because of the wide variation in the dielectric constant caused by the presence of water molecules in the matter [21]. The application of microwave in the non-destructive control field then developed slowly, but a number of publications began to appear in the 1960s, from which the title combined the words “microwaves” and “non-destructive testing” [22], [23].

1.7 Far-field material characterization techniques

This section presents various techniques used in materials characterization at high frequency with a wide range, especially in the region of far-field radiation.

1.7.1 Technique of free space

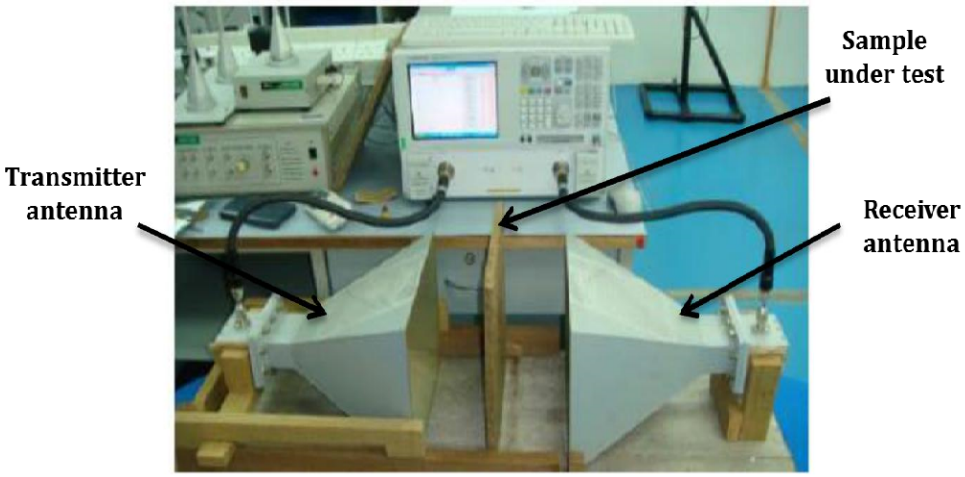

Figure 1.2: Bistatic measurement principle [25,29].

The typical free space technique consists of two antennas operating at a certain frequency range as shown in Figure 1.2. To make this technique in a normal operating mode, a flat sample is placed in parallel between these antennas which are well adjusted. For example, when there is a signal transmitting , the other works as a receiver. This channel between the transmitter and receiver antennas can record incident wave that pass through the sample. This distortion of the signal arises as attenuation of the signal and a shift in phase. They are easily measurable and the dielectric properties of the sample undergoing the test can be extracted.

Techniques of free space are contactless and non-destructive measurement methods to be used at a wide range, in particular, they would be more appropriate to characterize materials at a high-temperature level, and homogeneous and non-homogeneous dielectrics [24].Furthermore, to avoid the phenomena of diffraction by the edges of the sample, this latter must be flat to obtain a good quality characterization. For a known frequency value, the dimension of antennas is well identified to that they impose the size of the sample that will be characterized [25].

The advantage of these systems that operate in the mode of transmission is linked to their simplicity. The reflection in an interface matter-environment produces the main source of error associated with it; otherwise, the major limitation of these techniques is the need to have large enough sample of matter to achieve sufficient sensitivity. The reflection coefficient of the sample under test can be measured in addition to the transmission coefficient that should be noted [18], [26], [27].

1.7.2 Split-cylinder resonator technique

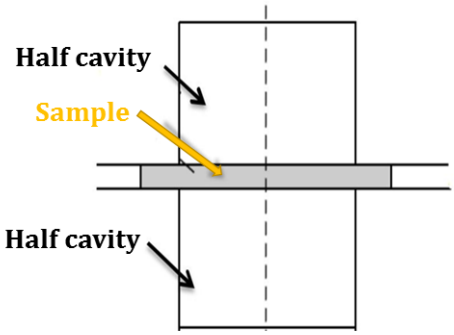

Figure 1.3: Split resonant cavity [29].

The split cylinder resonator method is originally proposed by Kent [28]. It is often used to determine the low losses of dielectric materials [29], [30]. Figure 1.3 shows the setup on this technique, which is based simply on an empty cylindrical cavity, separated into two sections of cylindrical waveguide short-circuited. The split cylinder resonator must be constructed to allow an adjustable, a variable gap between the two cavity sections for an introduction of the sample which must cover all section of the cavity.

In the split-cylinder resonator operation mode, in order to excite and detect its desired fundamental TE_{011} resonant mode, a coupling loop is introduced in the cavity wall through a small hole, in each of the two cavity regions, and from measurements of the resonant frequency and quality factor, the permittivity and loss tangent of the sample can be determined. The plane of the coupling loop should be parallel to the plane of the sample, in order to allow maximum interaction with the vertical component of the magnetic field. Each of the coupling loops is connected to a coaxial transmission line that is connected to the input port of a vector network analyzer. To minimize the effect of coupling losses, the distance to which the loops extend radially into each of the cavity sections must also be adjustable. In addition to the fundamental TE_{011} mode, higher

modes can be used to extend the measurement frequency. The main advantage of the split-cylinder technique is that the sample needs only to be planar form and extends sufficiently far beyond the diameter of the two cylindrical waveguide sections. Other models are not necessary, which makes it an attractive method for accurate and non-destructive measurements of low-loss substrates. [29], [31], [32], [33].

1.7.3 Methods based on reflection and radar

The main operating mode of the radar shown in Figure 1.4 is based on the signal transmission and signal reflection in a body. This feature is produced when the signals are emitted by the source and reflected later. So, the reflected signal provides a description of the body that runs through this signal. Inspiring this main function to be applied in the mode of material characterization, this technique of reflection consists of the source of the wave at a special frequency range, and also coaxial probe open-ended that will manage this operation.

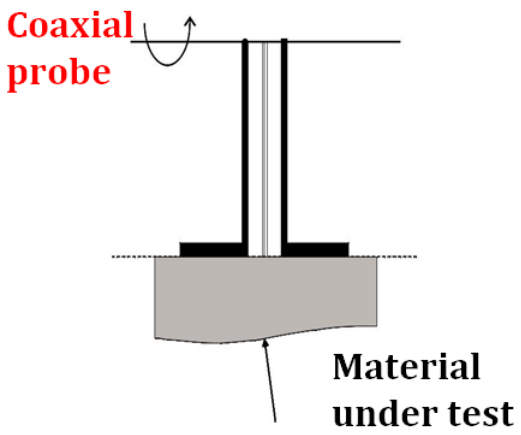

Figure 1.4: Reflection method by using a coaxial probe [18,29].

The measurement procedure consists of diving the coaxial probe in a liquid sample, or by placing the probe in contact with a solid sample as the sample must be flat in one of its faces. The properties of the materials are determined by measuring the phase, and the reflection coefficient module using the coaxial probe with materials under test in contact mode.

1.8 Near-field microwave microscopy NFMM

The first NFM (near field microscope) was proposed by E. Synge [34], and the first NFMM (near-field microwave microscope) was demonstrated by Soohoo in 1962 [35]. $\lambda/60$ of spatial resolution have been exhibited after being demonstrated by Ash and Nicolas using near-field microwave microscope, where λ represents the free space wavelength. For all the mentioned techniques of scanning microscopes, the use of wavelength above the microwave and below optical regimes has been important. NFMM is still the oldest technique, yet an active tool for the characterization of localized matter at high frequency. This technique implies a set of tools to characterize and to analyze materials.

Since the first use of NFMM, several applications were developed using this technique and among them we can cite :Non-destructive evaluation, passive and active circuits imaging, quality control, study of surfaces, as well as the qualitative and the quantitative characterization of dielectric materials including typically ferroelectric polarization [29], [36], sheet resistance [37], dielectric constant as well [38], [39], magnetic permeability [40], and the conductivity of material as well [12]. In addition, through these quantities, it can be possible to know the temperature as a function of frequency.

1.9 Scanning microscope techniques with nanometer resolution (STM, AFM, SOMM, NSMM)

Several techniques were developed many years ago to be useful tools for materials's characterization. They will be cited as follows:

1.9.1 Scanning tunneling microscopy STM

This technique (STM) was invented in 1981 by Heinrich Rohrer, Gerd Binnig, Christoph Gerber and Eddie Weibull at the IBM Research Laboratory in Rüschlikon (1981), near Zürich [10], [41], [42]. The STM and the "atomic landscapes" that they produced will become emblematic of what will be called nano sciences and nano technologies

The instrumental concept of STM makes possible to probe the closest electronic field which is constituted by a tunnel effect on the surface of a conductive material. Scanning Tunneling Microscope (STM) is used to observe the atomic structure of a surface in direct space. Its principal operating mode is focused on the measurement of the electron current I_t which passes through tunneling from one electrode (tip) to another (which is the sample) or vice versa, through a potential barrier formed by a vacuum or a fluid. When, the tip is moving over the sample with the smallest distance that separates the tip from the sample, the current will be measured with the function of the position of

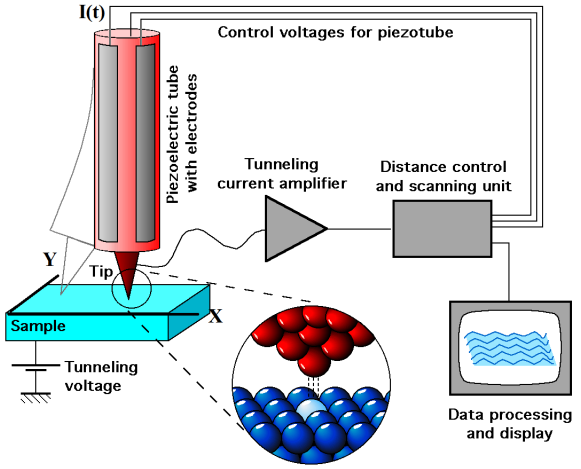

Figure 1.5: Schematic of Scanning Tunneling Microscopy (STM) [44].

the tip as shown in Figure 1.5. The distance between the tip and the sample changes as a function of the surface roughness. Furthermore, the current exponentially depends on the tip-sample distance. The local variation of the electron density in the (X, Y) plane, make a variation in the current I_t. This operation allows to obtain a scanned image by plotting the following function of the current I_t=f(X, Y). STM has become a fundamental tool in surface physics, enabling the study of nano object growth at the atomic scale, dynamics phenomena on the surface(diffusion, alloys, etc.), and the observation of the substrate-adsorbate interaction [10], [41], [42], [43]. To have a mapping of the surface, the tip which acts as an electrode probe is brought close to the surface by piezoelectric tubes. The tunnel current is the consequence of the junction polarization as it is shown in Figure 1.5. So, this approach is performed at a non-zero bias voltage to be able to measure the tunnel current once both electrodes are closer [10], [42], [44]. During the scan over the sample, the tip is moving over the surface by raising the tunnel current value, and this is repeated point by point. An amplification and processing unit controls the (x,y,z) piezoelectric movement, hence, to maintain the current constant. The surface image is produced, line by line, and by using a software, this latter can be shown on screen.

The scanning tunneling microscopy can be used to study friction and surface roughness of materials, and analyze the defects and reaction of the surface of materials such as catalysts in which the catalysis is the back- bone of synthetic chemistry. The main advantage of the scanning tunneling microscopy technique, that it allows to study at low temperature the precision of electronic properties of observed objects. In addition, it

permits to study the thermal reduced noise. The high stability obtained of STM makes it possible to observe extremely current depending on the polarization bias voltage [44].

1.9.2 Atomic force microscopy AFM

The Atomic Force Microscopy is a near-field microscope technique that was developed by Binnig, Quate et Gerber [42] in 1986. This technique enables us to have an atomic resolution of different types of surfaces. In general, an atomic force microscopy system is composed of ;

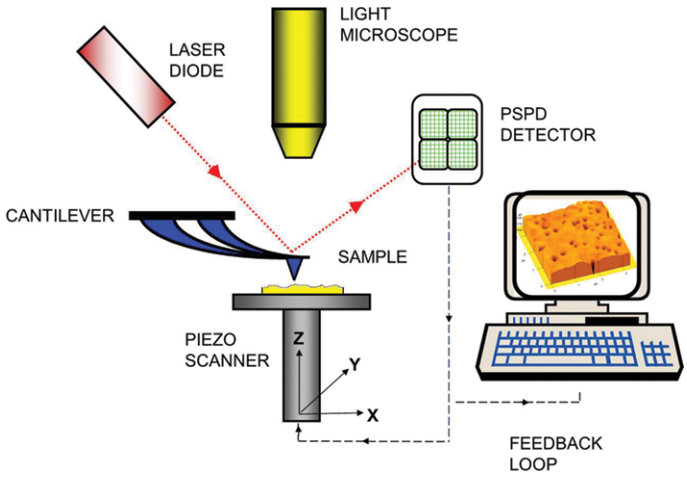

Figure 1.6: Schematic of Atomic Force Microscopy (AFM)[44].

- The sample holder(support): it is generally made of mica with a plane surface which helps to obtain a good analysis. The chosen material of sample holder(mica) allows fixing the sample very well, especially liquid samples. In fact, it helps also to avoid that some part of the sample under test to be carried by the probe during the measurement.

- Cantilever: it is made of Silicon in general, it moves over the sample under test during the measurement. It is very flexible and can be easily damaged, and this depends on the forces with low intensity that can be applied to it by the sample that is known as (Electrostatic or Van der Waals interactions).

- Laser: Laser radiation is sent at the end of the cantilever and it is reflected toward a photo diode to detect the variation of cantilever flexion.

- The probe tip: it is the main part of the atomic force microscope, it is also fabricated from Silicon and is connected to the cantilever. The size of the tip changes according to the samples to be analyzed: it can be rounded or pyramidal in shape.
- Motion system: This system offers the displacement of the sample holder in x,y directions to probe the surface of the sample under test. It is connected with a photo diode, therefore it can control the height z of the sample to keep a constant force between the sample under test, and the probe tip. The surface of the sample analyzed is represented in three dimensions after the displacement has been saved and transmitted to a computer system to process them and do the analysis of the sample.

Figure 1.6 illustrates how an AFM works. The cantilever tip receives a light beam on its back face; then this beam is recovered by a 4 dial detector. The deflection of the cantilever is induced by the forces that are produced by the interaction of the cantilever ended with a sharp tip, and the surface under test. This, deflection is being measured once the variation of the light beam position is carried on the 4 dial detector [45].

According to the interaction between the surface and the cantilever tip, there are several forces that are implied. The dependence of this interaction as a function of the distance between the surface and the tip, allows distinguishing three essential operation modes of the AFM. The first one is known as the contact mode in which the interaction is strongly repulsive, whereas the second mode is produced without contact (Non-contact), hence the interaction is totally weak attractive, and then the third which is more complex, it is an intermittent contact or (tapping mode). The last mode is between the contact and non-contact mode.

1.9.2.1 Contact Mode AFM

In this case, there is a repulsion of electron of the tip and the sample. The tip is kept at a constant distance from the sample, so that variations of the z position of the tip represent variations of the surface height [46]. In the context of general contact mode that is shown in Figure 1.7-A, the cantilever that carries the tip sensor supports on the sample [47].

1.9.2.2 Tapping Mode AFM

As it is illustrated in Figure 1.7-B, the cantilever is oscillating at a given frequency (in the range of kHz) combined with a fixed amplitude. The sample will exert an attractive force of (Van der Waals type- [46], [47]) with a short range on the cantilever and the tip. So, the amplitude is going to vary according to the displacement of the sample height in z direction.

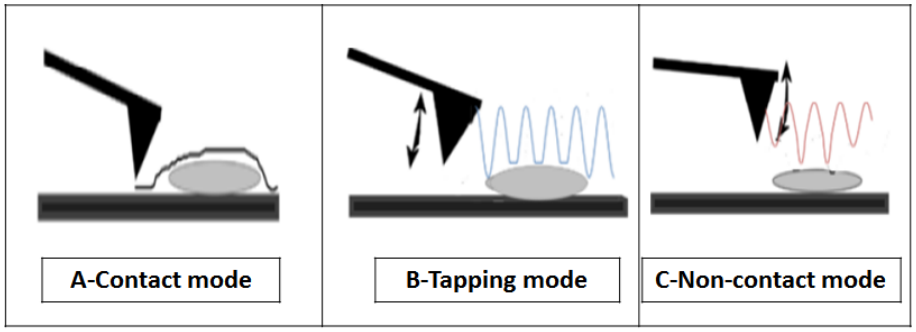

Figure 1.7: Different modes of the Atomic Force Microscopy (AFM)[46].

1.9.2.3 Non-contact Mode AFM

In Figure 1.7-C, we can see that this mode is similar to the contact mode, but, the distance between the sample and the tip is kept fixed at very small value (nm scale). At this point, the attractive forces induced by the sample on the cantilever and the tip also used [46], [47].

1.9.2.4 AFM applications

The application field of the atomic force microscope keeps expanding. With its nanometric resolution, its main use concerns those applications that are situated between the STM (using its atomic resolution), and the optical microscope (using its micrometric resolution).

This technique has become an important useful analysis tool in comparison with the electron microscope. In the fields of matter physics and biology, for example. One of the advantages of AFM is that it is able to study insulating samples. Among the advantages of an AFM are: its nano- metric resolution, and its ability to analyze different materials (conductors, semiconductors, Insulating, biological,etc) [48].

1.9.3 Near-field scanning optical microscopy NSOM

In the characterization of matter, to exceed the ultimate resolution of systems set by Rayleigh criteria, it is important to work with the closest field to the matter that is going to be characterized. The first principle of optical microscope was exposed by E.Synge in 1928 [34]. He proposed his idea by using an aperture smaller in dimensions than the wavelength of light λ, made in a metallic screen, in order to illuminate a sample locally [49]. E. Synge assured that it would be possible to observe some size around 50nm, that is much less than the resolution of the microscope. This assertion

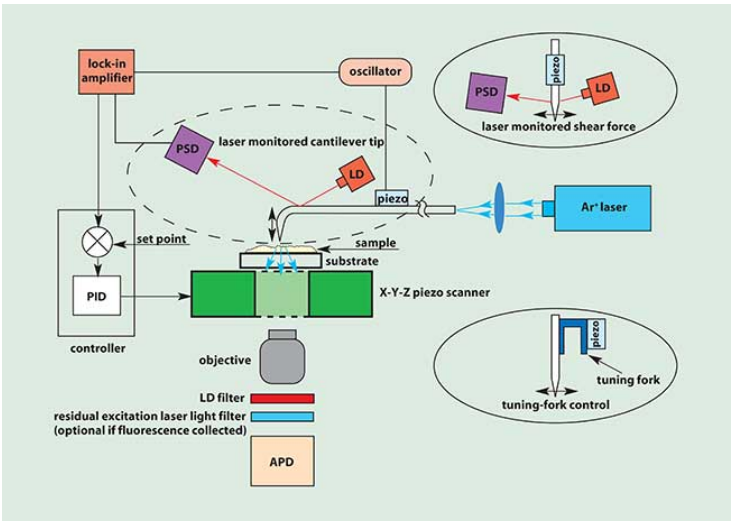

Figure 1.8: The SNOM system [51].

had been demonstrated experimentally in 1972 by E. Ash and G. Nicholls [34], [50]. They obtained images with $\lambda/60$ of resolution by using centimetric waves, whereas the criteria of Rayleigh gives a limitation of order $\lambda/2$ of resolution.

Near-field optical microscope can be presented in two principal groups of experimental configurations, as shown in Figure 1.8. Thus, if the probe is used as optical field detector then it works on collection mode otherwise, the mode called illumination mode. This operation is produced when the probe is used as a source of evanescent waves [51].

1.9.4 Near-field scanning microwave microscopy NSMM

Many research groups have been trying to develop the near-field microwave microscopy using different designs. A micro strip resonator ended by an open electric dipole and closed magnetic dipole. This design called an evanescent wave microscope was demonstrated by Tabib. Azar et al. in 1993 [52].

The first evanescent microscope based on a coaxial cavity resonator probe was published by Wei et al. in 1996 [53]. In addition, this technique was successfully implemented in the context of evanescent microwave microscopy studies using a transmission line. It was used by Vlahacos et al. [54] and Keilmann et al. [55].

A developed NSMM using a lumped-constant resonator probe is composed of an outer ring in conduction format that is integrated with a commercial microwave oscillator module using also a thin conducting needle. In the matter characterization domain, such characterization of the bulk, thin film structures, are employed to analyze quantitatively

their dielectric constant. This operation focuses on the measurement of gap-length that depends on resonance frequency shift [56]. On top of that, the coaxial resonant near-field microwave microscope was analyzed by a theoretical model, the set-up of quantitative adjustment of tip-sample distance applying a scanning evanescent microwave microscope over conductive samples; was developed using an analytical expression of the tip-sample capacitance as a function of tip-sample distance. At the same time, a non-contact mode imaging of topography and surface resistance of sample having a high spatial resolution range was demonstrated [57], [58], [59].

The main constraint of a near-field scanning microwave microscopy was the tip-sample distance control. To overcome this obstacle, a lot of techniques offering the control of the distance between the tip and the sample under test were developed by researchers [60]. An incorporating of a scanning tunnelling microscope feedback to an NSMM probe has been set up by Imtiaz et al. [61], in order to image capacitance and loss properties of La-Ca-MnO thin film, and some kind of doped silicon sample. This is the result of an association with STM topographic image to prove the shift in resonance frequency, and the difference of the quality factor between the doped and undoped region. Other approach to control the distance between the tip and the sample was proposed by Kim et al. by using a tunning shear force quad glued to the tip [61]. A high spatial resolution around $50nm$ reached by using NSMM provided by a coaxial resonator was applied to have a topographic imaging on metallic surfaces [62].

1.9.4.1 Different techniques of NSMM

The majority of scanning near-field microwave microscopy contain an antenna, whose edge is much smaller than the wavelength of propagation. This probe that is placed close to a sample under test, is connected to a microwave detection system. When the probe is over the sample under test with a respective distance of separation between the probe and sample h, at this stage, an electromagnetic response of the detection system can be collected. Additionally, this distance of separation h is less important than the size of the probe and especially its aperture in order to keep a measurable signal. Figure 1.9 illustrates some of the techniques used in microwave microscopy [63].

Generally, there are two different modes of the near-field scanning microwave microscopy, resonant mode as it is illustrated in Figure 1.9-a-c, and the non-resonant mode as shown in Figure 1.9-b-d-e. Figure 1.9-a represents a resonant cavity that is connected to a sample using an evanescent mode by a small hole existing in the cavity wall (aperture). The evanescent wave(signal) is applied locally to the sample, then the perturbation of the cavity that is affected by the presence of the sample under test is going to be measured by the changes in resonance frequency and the quality factor of the cavity. The size of the cavity aperture and the distance that separates the sample

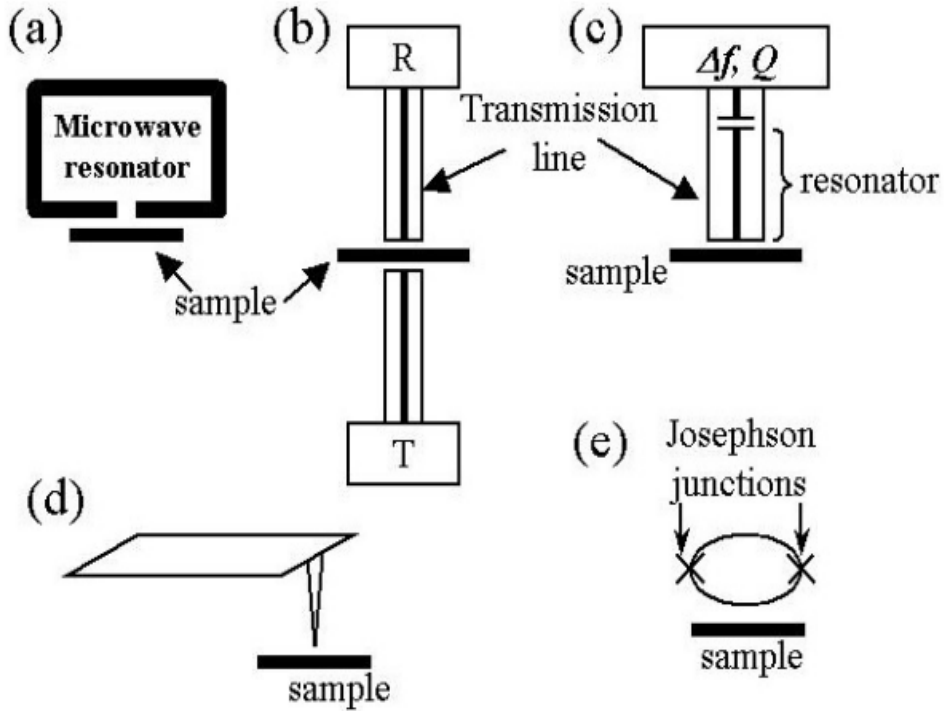

Figure 1.9: Different near-field microscopy techniques; a) shows a microwave resonator that contains a small hole in one of its wall. The shift in resonance frequency Δf and the quality factor Q are evaluated. b) shows the reflection and the transmission method. c) shows the scanned transmission line resonator technique where Δf and Q are evaluated. d) shows the cantilever tip method where quantities like force are evaluated. e) shows the scanning superconducting quantum interference device method [63].

of the cavity are factors used to determine the spatial resolution of this technique. As shown in Figure 1.9-c, it is noticeable that the same principle was used previously. It consists of a section of a coaxial transmission line or a resonator decoupled with the rest of microcircuit by a capacitor. Samples are placed closer to the end of the probe to ensure a good interaction with the resonator.

There are also techniques shown in Figure 1.9-b-d, that do not employ a resonator. These techniques based on sending a microwave signal to the sample. Then, those signals can be measured after they get reflected or transmitted through the sample. Figure 1.9-d represents the possibility of obtaining a very high spatial resolution by very sharp probe tip. This characteristic simplifies the control of the probe tip and the sample under test [18].

Figure 1.9-e shows another different method of microwave microscopy which is based on the scanning superconducting quantum interference device (SQUID). This technique implies to generate a circulating current (CC). This happens when a (DC) bias is placed across the loop, these currents have a frequency that will be directly proportional to the applied bias voltage. A magnetic field is generated by these currents that touch the sample. A response current will be generated by the sample itself which changes the inductance of (SQUID) loop. By measuring the feedback signal of the magnetic field to maintain the (SQUID) in a state that has a constant flux we are allowed to obtain a map of the electromagnetic response of the sample. This technique is used at a wide range frequency up to $100GHz$ that makes it advantageous in comparison to other techniques [63].

1.9.4.2 The basic component of NSMM

In general, a typical NSMM as shown in Figure 1.10 contains the following main components [64];

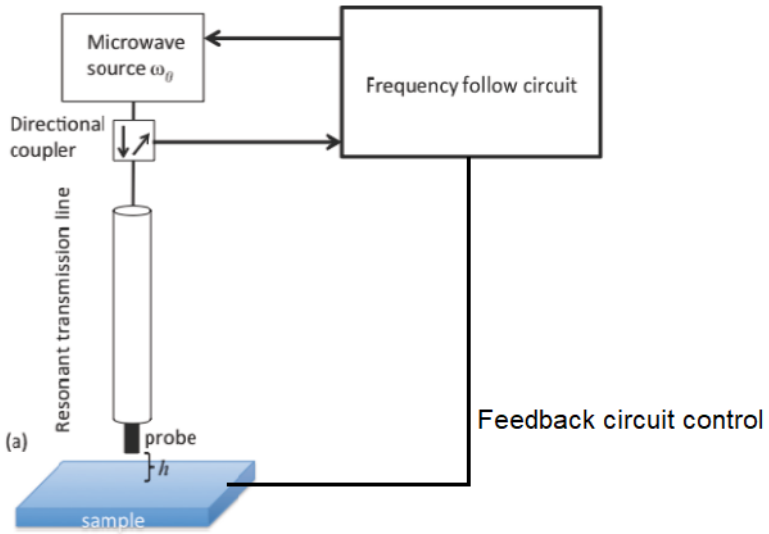

Figure 1.10: The basic component of a NSMM. a) Typical schema of the microwave microscopy introduced by Steinhauer et al. b) Different probing techniques [64].

- A microwave generator: the microwave source is represented by a vector network analyzer that is used frequently as a detector as well as a microwave source.

- Resonator:

  In NSMM concept, several types of resonators were proposed by different research groups. For example (Micro strip Resonator, a quarter and half wavelength coaxial resonators). In the schematic of NSMM in Figure 1.10, a transmission line is represented by a coaxial resonator is used. In the absence of the sample, the resonator is a half wavelength resonator because it is open-ended. On the other hand, a contact with a metallic sample turns the boundary condition into a short circuit and giving rise to a quarter wavelength resonator. For both cases, the shift of resonance frequency obtained, is very sensitive to the probe tip-sample separation distance, and the electrical properties of the sample (Conductivity, dielectric constant, permeability..).

- Feedback circuit:

  The main objective of using a feedback circuit is to keep the microwave source locked to the resonance frequency of the transmission line. The resonance frequency due to the sample is proportional to the feedback output voltage. When the open-ended coaxial probe is scanned over the sample, a computer system is recording information about the shift in frequency of resonance and the quality factor.

1.9.4.3 Properties of NSMM

- **Near-field** : The graph shown in Figure 1.11 illustrates that there are four zones

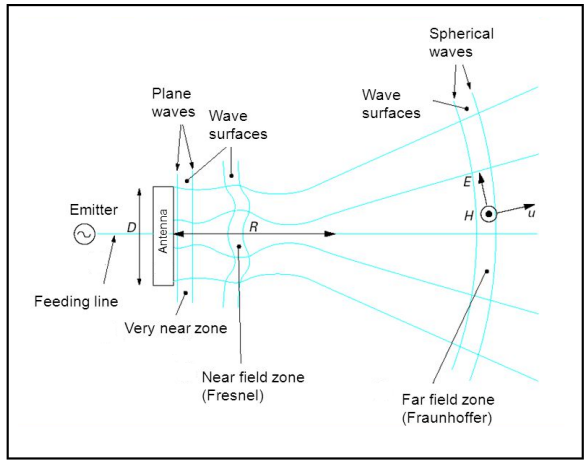

Figure 1.11: Different radiation zones around a transmitter antenna.

of radiation around a transmitter antenna, from the far field zone till the very near

field zone. The near field region is located near the antenna. This region is divided into two parts; the reactive and the radiative regions of the near field. The far-field region is the region that is located after the near radiative of the near field. In this region , the electric and magnetic fields are dominated by radiating fields. Fields E and H are orthogonal to each other and to the direction of propagation [18].

- **Evanescent wave definition** :

  An evanescent wave is a wave in which the intensity decreases exponentially with the distance from the source. In the reactive field zone (very near-field) the waves are evanescent and the phenomena of propagation are negligible. Evanescent waves appear possible solutions as Maxwell's equations. They are part of a general type of near-field solutions, however many of them are used in near-field microscopes.

- **Spatial resolution** : The size of the smallest object that can be observed on a sample defines the meaning of imaging resolution.

  Additionally, it has been clearly demonstrated that to have a high spatial resolution of the smallest object for an NSMM probe depends at first on the sharpness of the probe, the size of its end, and the separation distance between the probe and sample. Also to get this high imaging resolution, the end of the tip must be as small as possible and kept close to the surface of the sample.

  The quantitative resolution can be defined as the size of such a zone or volume in which the probe response is insensitive to the matter properties, this resolution depends on essentially the geometry of the probe [18], [63].

NSMM exploits the microwave signal that is generated by the vector network analyzer to feed the transmission line which ends with a sharp tip. It is important to employ a resonant frequency when the tip of the probe is away from the sample, which means the resonator resonates in the air. But, when it begins to approach the sample with a well-known distance of separation, then the resonance frequency shifts. This change of resonance frequency is explored in order to extract the properties of the sample under test. The main advantages of near-field scanning microscopy are the higher spatial resolution that it offers and sensitivity to the electromagnetic properties of the scanned materials. The limits of this resolution are no longer fixed by the wavelength of the microwave signals, but mainly by the geometry of the probe tip of the microscope. More details concerning NSMM are given in the next chapter.

1.10 Conclusion

In this chapter, a review of the history of NSMM, the main components of NSMM, its operation mode, and different techniques based on near- field microscopy are presented. NSMM is a powerful technique that can be used to study a different kind of materials such as smooth bulk materials, lossy liquids, and thin films with sub-wavelength resolution. A comparison between several microwave probe designs show the advantages and limitations of each design with regard of the spatial resolution of the technique, materials that can be studied and vacuum requirements as well. In the next chapters, two different coaxial cavity resonators designs that use a microwave probe will be presented and used for the measurement of electromagnetic properties of materials and structures such as $Sio2$, graphene oxide (GO), and reduced graphene oxide (rGO). Finally, some possible advantages of NSMM technique are highlighted, in terms of use and design.

Chapter 2

Resonant cavity based on near-field scanning microwave microscopy

2.1 Introduction

An electromagnetic resonant cavity is an empty volume or filled with a dielectric, whose walls are electric (metallic cavities) or magnetic cavity type (dielectric resonators). The cavity is completely surrounded by the conductive walls, in which the electromagnetic fields can have a special configuration for certain frequencies. Fields are established in the form of a quasi-stationary wave regime and allow the cavity to store electromagnetic energy for very long periods; the cavity is called "resonant". It is possible to use this stored energy to be transfered to a particle crossing the cavity; the particle is thus accelerated and its energy increases [17].

The resonant cavity operates at microwave frequencies ; the front face to the sample has a tiny hole smaller than the wavelength of used signal. If the sample is placed very close to the hole, the area on the sample with a surface equal to the diameter of the hole will then disturb the resonance of the cavity, producing a change in both resonance frequency and quality factor of the cavity. If, for example, the hole is smaller in the order of μm and the sample causes a small disturbance to the cavity, this response could be used to examine some property related to the analyzed sample [65].

The variation of a complex pulse of resonance resulting from a small modification of the cavity is determined by the method of perturbation, according to the same principle as for the waveguides. It is used in particular to assess the effect of losses in the walls,

and the introduction of samples of materials or even a modification of the form [66] as shown in Figure 2.1.

2.2 Perturbation theory

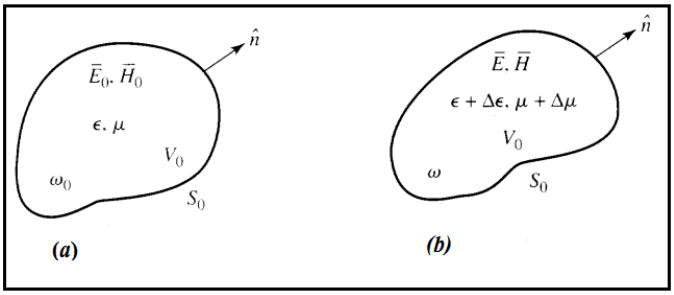

Figure 2.1: A resonant cavity perturbed by a change in the permeability or the permittivity of the material in the cavity. a) Cavity in normal situation. b) Perturbed cavity.

In general, when a small change is made in the form of a resonant cavity by the introduction of small pieces of material, the properties of the cavity are modified. The change of fields and the resonance frequencies are then produced. The shift in frequency Δf represents the frequency of the measured disturbed mode f_1 difference, and the frequency measured in the air f_r. This shift in frequency depends on the electromagnetic field disturbed at the position of the disruptive element [17], [67].

In NSMM applications, the interaction between the tip and the sample under characterization will produce a shift in resonance frequency and quality factor. In the case when the sample is a dielectric material and homogeneous with low loss of permittivity $\varepsilon = \varepsilon^{'} \cdot (1 - j\tan(\delta))$, so the theory of perturbation is given by [68]:

$$\frac{\Delta f}{f} \cong -(\varepsilon^{'} - 1)\frac{\varepsilon_0}{4w}\int_{Vs} E_1 E_2 dV \tag{2.1}$$

$$\Delta(\frac{1}{Q}) = -\tan(\delta)\frac{2\varepsilon^{'}}{\varepsilon - 1}\frac{\Delta f}{f} \tag{2.2}$$

In the equation (2.1), E_1, and E_2 represent the electric fields calculated in the case of the sample being considered with substrate permittivity ε. On the other hand, where the air $\varepsilon = 1$. w represents the total energy stored inside the resonator. The volume of the substrate is represented by Vs [68].

2.3 Propagation modes of resonant cavities

Electromagnetic waves in a wave guide do not have the properties of a progressive plane wave, in which the wave is propagating in a vacuum. For example, the electric and the magnetic fields are not always perpendicular to the direction of propagation. The purpose of this section is to define different modes in a wave guide. The *TE (Transverse Electric Wave mode)* and *TM (Transverse Magnetic Wave mode)* in a wave guide are electromagnetic waves in which the electric field or the magnetic field, respectively, are normal to the direction of propagation Oz defined by the wave guide axis. Thus, the modes of resonators constitute a real case that depends on the technique where the cavity is excited and the application from which it is used. The cavity resonator has modes listed as TE_{mnl}, TM_{mnl}. The index values correspond to periodicity (corresponds to the number of sine or cosine waves) in three directions. The z direction is used as reference to define the transverse electric or magnetic fields, Indices are allowed with the following values :

$$TE = \left\{ \begin{array}{l} m = 0, 1, 2, ... \\ n = 0, 1, 2, ... \\ l = 0, 1, 2, ... \end{array} \right\}, TM = \left\{ \begin{array}{l} m = 0, 1, 2, ... \\ n = 0, 1, 2, ... \\ l = 0, 1, 2, ... \end{array} \right\}$$

The **dominant mode** is the mode in which the resonance frequency is the lowest. The Transverse Electric and Magnetic ***TEM*** mode is characterized by both of electric and magnetic fields that are transverse at each point of the cavity to the direction of travel in three-dimensional space.

2.3.1 Cylindrical cavity resonator

In general, the cylindrical cavities based on a circular waveguide as illustrated in Figure 2.2 closed at both ends by metallic walls that are perpendicular to the longitudinal axis of guided wave. Its excitation (feeding) may be made by a magnetic antenna (loop) or an electric antenna type (monopole). When resonance conditions exist in the cavity and this latter is excited by an electromagnetic field, standing waves are produced and the energy is stored. Therefore, the study of the resonance conditions allows determining the eigenmodes and their relative frequencies in the cavity.

Insofar the actual cavity has losses (types of metal losses on the walls, dielectric losses, coupling losses, etc.), it will also be important to determine the over-voltage coefficients of the cavity.

A resonant cavity coupled by a single port operates in absorption or reflection, and in transmission when it is coupled by two ports. The resonant cavities are used as

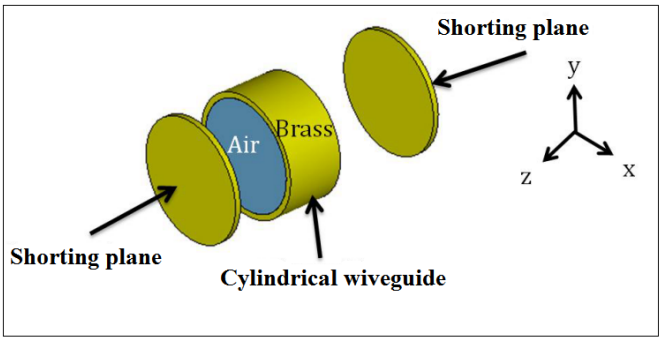

Figure 2.2: Cylindrical cavity structure.

resonant elements or as frequency meters in microwave devices, but can also be used for the characterization of materials: determination of the complex permittivity of a gas, and/or characterization of material properties with small dimensions. Furthermore, the cavities are also used in wide range domain such as fixing the resonant frequencies of tube oscillators (metal cavities for sources such as klystron) or solid state (dielectric resonators for field effect transistors) [17], [69].

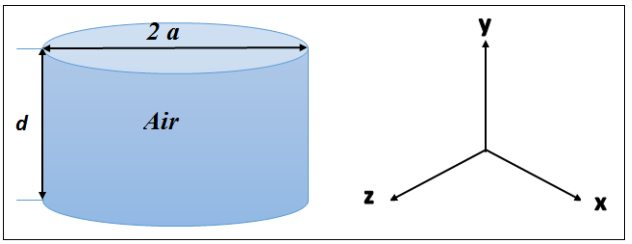

Figure 2.3: Air dimension inside the cavity.

As shown in Figure 2.3, the application of the boundary conditions at the cylindrical cavity walls permits to get:

$\overline{E}_t = 0, z{=}0, z{=}b.$

The resonant frequency for the TE_{mnl} mode is given by [17]:

$$f_{mnl} = \frac{c}{2 \cdot \pi \cdot \sqrt{\mu_r \cdot \varepsilon_r}} \sqrt{\left(\frac{p_{nm}}{a}\right)^2 + \left(\frac{l\pi}{d}\right)^2} \tag{2.3}$$

For the TM_{mnl} mode, the same equation 2.3 holds by simply replacing p by $p^{'}$.

Where; f_{mnl}, represents the operation frequency of the cylindrical cavity resonator.

c , is the speed of light in vacuum.
μ_r, is the permeability of the filled material inside the cylindrical cavity resonator.
ε_r, is the permittivity of the filled material inside the cylindrical cavity resonator.
P_{nm} denotes the $n-th$ zero of the $m-th$ Bessel function.
a, Cavity radius.
d, is the height of the cylindrical cavity resonator.
$l\pi$, Wave number of the resonant wave.

2.3.2 Rectangular cavity resonator

The rectangular resonant cavity consists of a rectangular waveguide section surrounded by conducting plates at its two ends, z=0 and z=b, refer to Figure 2.4-a

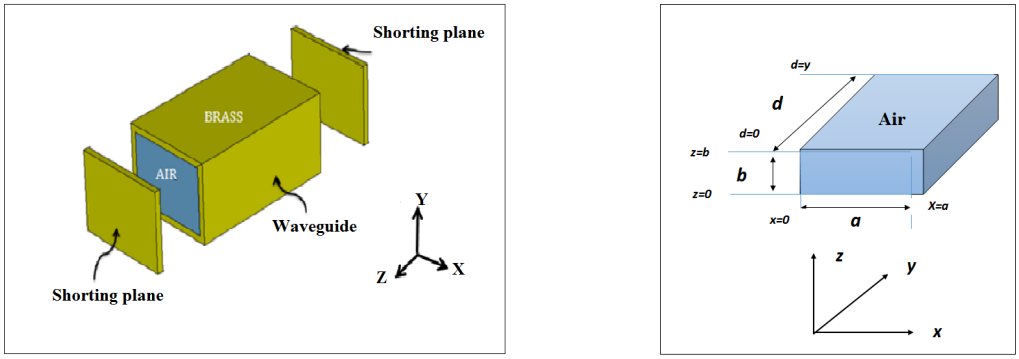

Figure 2.4: a) Rectangular cavity structure. b) Air dimension inside the cavity.

As we can see in Figure 2.4-b, the boundary conditions of a short circuit at the two ends, z=0 and z=b, will be satisfied once two opposite travelling waves along $+z$, $-z$ exist simultaneously and form a standing wave in the the z direction. Moreover, the rectangular cavity contains standing waves formed, in all of its three directions, by the internel field. The boundary conditions on the cavity walls hold at:x=0, y=0,y=d, z=0, z=b. These conditions are the same as those for a rectangular waveguide.

The resonant frequency of the TE_{mnl}, TM_{mnl} of the rectangular cavity resonator is then given by [70];

$$f_{mnl} = \frac{c}{2 \cdot \pi \cdot \sqrt{\mu_r \cdot \varepsilon_r}} \sqrt{\left(\frac{m\pi}{a}\right)^2 + \left(\frac{n\pi}{b}\right)^2 + \left(\frac{l\pi}{d}\right)^2} \tag{2.4}$$

2.3.3 Coaxial cavity resonator

A coaxial cavity designed with geometric parameters a, b, z, as shown in Figure 2.5 has an infinity of resonant frequencies, defined by implicit equations that result from the writing of the boundary conditions.

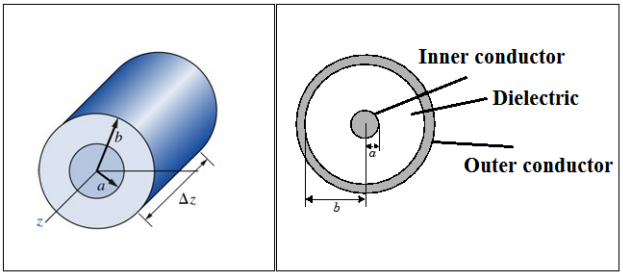

Figure 2.5: Coaxial transmission line structure.

Generally, the coaxial resonators are made from the coaxial transmission line. There are three different kinds of coaxial resonators.

2.3.3.1 Half wavelength resonator

Half wavelength resonator as shown in Figure 2.6 consists of a section of a coaxial transmission line with length $\boldsymbol{l}$ over its two ends.

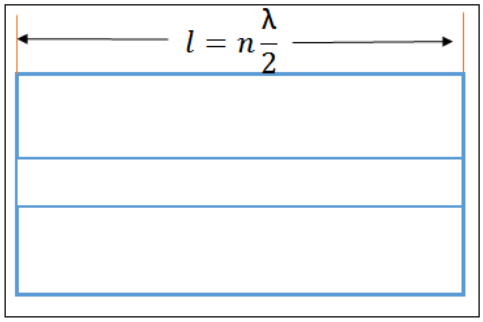

Figure 2.6: A half-wavelength coaxial resonator [71].

Usually, a coaxial resonator operates at ***TEM*** mode (transverse electromagnetic mode). It is recommended that the following conditions must be satisfied to avoid the resonance along the $\boldsymbol{z}$ direction [71].

$$\pi.(a+b) \leq \lambda_{min}, \tag{2.5}$$

where :

- ***a*** represents the radius of the inner conductor.
- ***b*** represents the radius of the outer conductor.
- λ_{min}, represents the shortest wavelength that corresponds to the highest working frequency.

The relationship that links the resonant wavelength λ_0 and the length of the resonator l is:

$$l = n \cdot \frac{\lambda_0}{2} \tag{2.6}$$

This equation (2.6) indicates that the length of the coaxial resonator is a multiple of the half wavelength, and through that it is called *half-wavelength coaxial resonator* [71].

2.3.3.2 Quarter wavelength resonator

The quarter wavelength resonator as illustrated in Figure 2.7-b is formed by one shorted end, and the other one is opened. A standing wave is produced from the open load that causes total reflection.

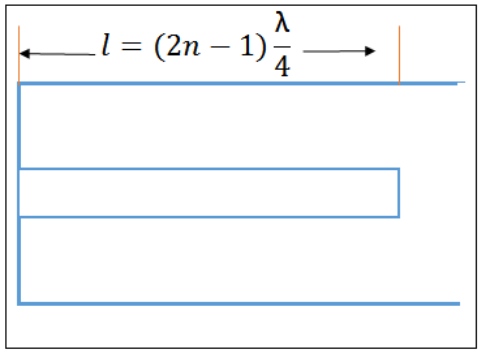

Figure 2.7: A quarter wavelength coaxial resonator [71].

The relationship between the resonator's length l and the resonant wavelength λ_0 is given by:

$$l = (2n-1) \cdot \frac{\lambda_0}{4}, n = (0, 1, 2, ..) \tag{2.7}$$

This equation indicates (2.7) that the length of the resonator is odd number times the quarter wavelength. The structure for a quarter wavelength resonator at its open end will have generally some radiation losses. In order to overcome this drawback, a segment of cutting-off TM_{01} circular wave guide is formed by the extension of the outer conductor.

2.3.3.3 Capacitor-loaded resonator

The Capacitor-loaded resonator, shown in Figure 2.8-c, consists of a coaxial transmission line section as the quarter wavelength resonator unless this latter is shorted at its two ends.

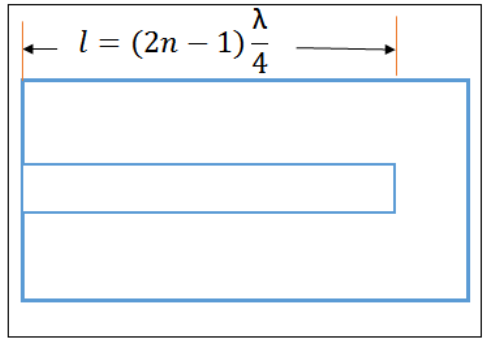

Figure 2.8: A capacitor-loaded resonator [71].

It has a small space between the inner conductor and short plate of one of its ends. This space can be modeled by a lumped capacitor.

2.3.4 Cavities coupling

Cavity resonators will be useful as circuit elements only if they can be coupled to other circuit elements. Energy has to be fed into the cavity and taken out from it to be useful as a filtering element. Excitation techniques used for launching waves into the waveguide can be used for coupling or exciting waves in a resonator as well as shown in Figures 2.9, 2.10, and 2.11 respectively. The common methods used for coupling are as follows:

2.3.4.1 Probe coupling mode

This technique is an alternative coupling loop that is particularly useful one wants to isolate the centre of the coaxial entry line of a cavity from the walls of the cavity to avoid low frequency . Since the probe for coupling is different from the loop, the probe does

not need mechanical support for the end of the central conductor. Besides, an insulating or lossy watertight can be put at the entrance of the cavity [70], [72].

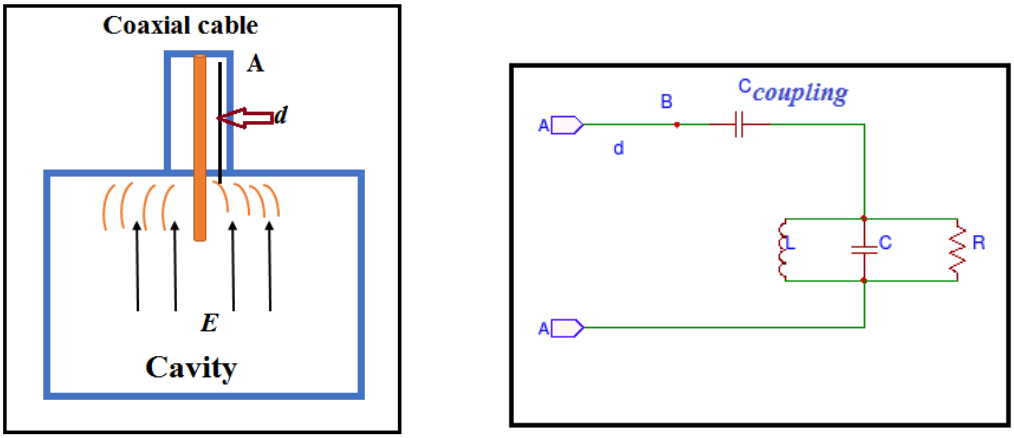

Figure 2.9: a) Waveguide and resonator fed by an electric probe. b) Equivalent circuit of coupling probe mode [73].

Such probes are generally an extension of the central conductor of the coaxial line. The equivalent circuit for a resonator with a coupling probe can be obtained by the same general method used for the coupling loops. A short circuit is placed in such a way as to have either a quarter-wave antenna or a half-wave antenna. It can be seen that in the case of a half-wave antenna (open circuit), the resonance frequency of the tip is lower than the natural frequency of the cavity. This derivative in frequency is clearly seen for the resonator of Figure 2.9-a because the tip consists of a capacitance at the end of the resonant line.

The open circuit probe can be considered to be equivalent to two capacitors connected in series. Thereby, the quarter-wave short-circuit resonance frequency is lower than the one of half-wave open circuit, and the equivalent circuit for the input impedance is presented in Figure 2.9-b. The coupling capacitor $\mathbf{C}_{coupling}$ is approximately the capacitor at a low frequency between the tip and the conductor of the resonator [73].

2.3.4.2 Coupling magnetic loop mode

The most useful method of coupling a coaxial line to a resonant cavity is, the use of a small loop formed at the end of the central conductor of the coaxial line and the wall of the cavity. As illustrated in Figure 2.10-a, the loop is connected by the magnetic flux of the considered natural mode.

By this flux linking, a voltage is generated in the loop by the oscillations of the cavity. A resonator is fed in its entry using a coupling loop. The equivalent circuit is shown in

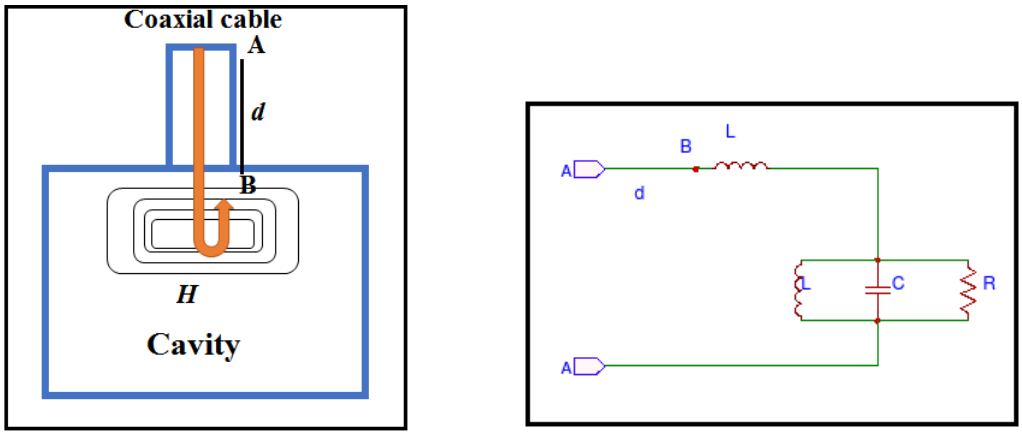

Figure 2.10: a) Waveguide and resonator fed by a magnetic loop. b) Equivalent circuit of a magnetic coupling loop mode [73].

Figure 2.10-b where ***d*** represents the arbitrary distance from a reference plane to the internal surface of the walls of the cavity. The format of the equivalent circuit depends on the relationship of an open circuit and a short circuit of the natural frequencies of the cavity, and also a combined coupling loop [73].

2.3.4.3 Aperture coupling mode

The holes are commonly used to connect a coaxial line, or a waveguide to a cavity, especially when an adjustable coupling is not required. The holes are physically simple, but the calculation of

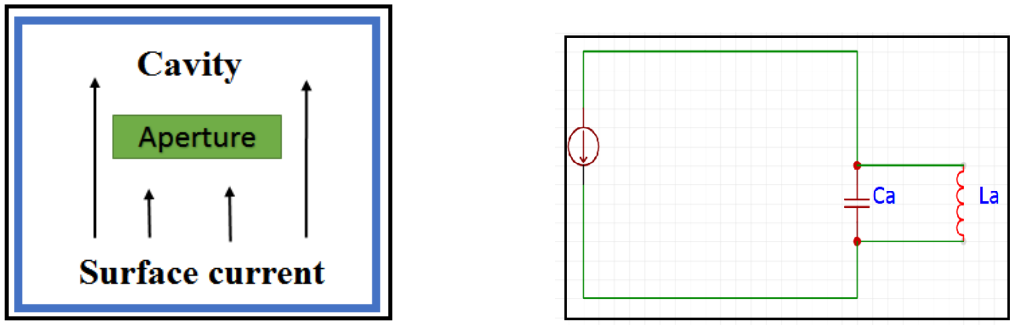

Figure 2.11: a) Waveguide and resonator fed by an aperture. b) Equivalent circuit of coupling using aperture [73].

their performance is often difficult. Coupling is produced by an aperture in the metal wall between the cavity and the wavesguide. Figure 2.11-a shows a structure of a cavity

assembly using the hole and the equivalent circuit of this aperture [73].

2.3.5 Quality factors of resonant cavities

For a given closed non-ideal (real) cavity of volume V in which fields oscillate in a given mode at the frequency f_0. RF losses will then be generated by the presence of these electromagnetic fields. These losses can be quantified by the "quality factor" of the cavity denoted by Q_0 and given by:

$$Q_0 = \omega \cdot \frac{\mathrm{U}}{\mathrm{P}} \tag{2.8}$$

Where : $\boldsymbol{U}$ represents the RF energy stored in the cavity, and $\boldsymbol{P}$ represents energy lost per cycle. These RF losses are generally composed of two types: the losses due to the dissipations in the dielectric medium composing the volume of the cavity, and the losses due to Joule effects on the metal walls of the cavity [68].

When the cavity is coupled with a waveguide, the quality factor can be expressed as follow ;

- The quality factor of the resonator corresponds to the unloaded quality factor , $\mathbf{Q}_0$.
- This quality factor corresponds the energy coupled out of the cavity. The losses of this energy are produced when the cavity is fed by a wire element. So, this energy can be taken out from the wire element and this feature is called external quality factor $\mathbf{Q}_{ext}$.
- The total losses can be defined as a loaded quality factor of these quantities as follow;

$$\frac{1}{Q_L} = \frac{1}{Q_0} + \frac{1}{Q_{ext}} \tag{2.9}$$

- The ratio $S = \frac{Q_0}{Q_{ext}}$ of the losses in the external circuit to the losses in the cavity depends on the coupling to the waveguide so that:
- $if S < 1$, the cavity is under coupling .
- $if S > 1$, the cavity is coupled.
- $if S = 1$, the cavity is in critical coupling.

In a cavity resonator, several types of losses often occur according to its geometry and construction. For example, a dielectric resonator will have a loss in dielectric due to its loss tangent. Furthermore, in the case of the open-ended cavity resonator, its losses will

be produced from the radiation leakage of its open ends. The walls of the cavity will induce losses such as finite conductivity as they represent the conductive components of the resonator. All these quantities increase the unloaded quality factor and they can be presented and gathered as follow [68] :

$$\frac{1}{Q_L} = \frac{1}{Q_R} + \frac{1}{Q_C} + \frac{1}{Q_D}, \tag{2.10}$$

Where :

- $\mathbf{Q}_R$ represents the quality factor of radiation.
- $\mathbf{Q}_D$ represents the quality factor of dielectric.
- $\mathbf{Q}_C$ represents the quality factor of conduction.

2.3.6 Conclusion

In this section, we gave a description of resonant cavities including the propagation modes that are used. We presented different kinds of cavity resonators, their operating principle and coupling modes properties that depend on the intended application. An estimation of the stored energy and losses of the cavity resonators during its operation has been modeled by a quality factor. This latter is defined as the ratio of the energy stored in the cavity divided by the energy lost per cycle.

2.4 Microwave simulation

Microwave simulation of components and 3D structures require powerful tools. The main objective of the electromagnetic simulation is to find an approximate solution to Maxwell's equations that satisfies a given boundary conditions and set of a initial conditions. To solve Maxwell's equations numerically, several methods have been developed, namely:

- Method of Moments (MoM)
- Finite Element Method (FEM)
- Finite Difference Time Domain (FDTD).

For each method, a specific convenient tool was designed. In this section, the best known electromagnetic simulation softwares that can be used in near field microscopy. These softwares are generally based on finite elements analysis like the famous HFSS software package. HFSS and CST are $3DEM$ simulators based upon different computational

techniques. HFSS is based on Finite Element Method (FEM) which is more accurate for designing microwaves devices such antennas while CST is based upon Finite Integration in Technique (FIT) and is also popular among microwave devices designers due to ease in simulations. However, results of both simulators are not the same because of the different computational techniques involved. HFSS results are close to experimental results with more insight into the structure available.

ADS is used for circuit co-simulations where active components are also involved. It can be used for planar antennas as well and is based upon MoM (Method of Moment). HFSS can offer a reliable mesh adaptation algorithm, and several simulation coverage criteria are sufficient to obtain reliable data in one simulation. CST also includes several coverage criteria but its suitable simulation mesh adaptation procedure for multi-channel MRI (Magnetic Resonance Imaging) coil is based on increasing the *Lines per wavelength* and *Lower mesh limits* settings. This refinement over the entire volume of the model is a less robust approach, compared with the refinement of HFSS mesh, which is performed mainly in volumes containing the maximum field values [74].

2.4.1 CST simulator

The Computer Science Technology (CST) as illustrated in Figure 2.12 Microwave Studio (MWS) software is an electromagnetic simulation software for passive structures in 3-Dimensions. The MWS simulations are based on the finite integration technique FIT-Finite, in order to determine solutions to electromagnetic problems by Maxwell equations in integral form. Regarding to the technical form, this method digitalizes over a discretization space as for FDTD (Finite Difference Time Domain). The MWS software

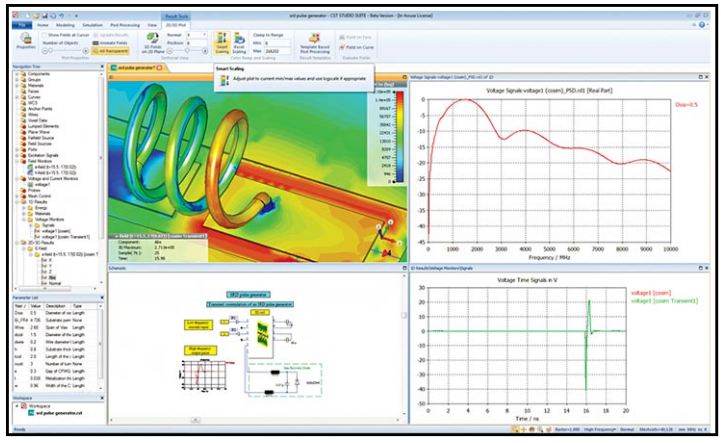

Figure 2.12: CST graphic interface.

meshes the structure using parallelepiped voluminous elements which allow a direct description in 3-D of all the components of the described systems. It is possible to describe the microwave devices to be controlled as they are made in practice by a stack of layers of materials with their own characteristics; permittivity and tangent losses in the case of a semiconductor and electrical conductivity in the case of a metal with losses. Like all 3D simulators that exist today, the advantage of this tool is its ability to process all sorts of homogeneous and non-homogeneous structures, regardless the desired technology. However, the implementation of the software is very cumbersome for planar circuits which are simple circuits. The software requires significant computer resources and in addition, calculations require the resolution of large matrix systems [75].

2.4.2 HFSS simulator

HFSS (High Frequency Structure Simulator) is an electromagnetic simulator for 3D models as it is presented in Figure 2.13. It integrates simulations, visualizations and an easy-to-use automated interface in order to solve quickly and efficiently 3D electromagnetic problems. Its calculation code is based on the finite element method. This software can be used to calculate many quantities such as S parameters, resonance frequencies and fields. It is a tool for calculating the electromagnetic behavior of a structure and possesses post-processing tools for more detailed analysis.

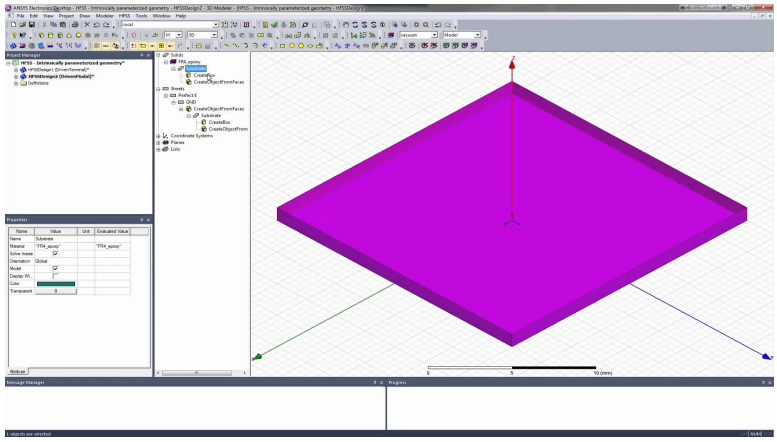

Figure 2.13: HFSS graphic interface.

It allows the calculation of:

- Basic quantities: near field, far field.
- Characteristic impedances of ports and their propagation constants.

- Normalized S parameters relative to a specific port impedance.

In order to generate a solution for the electromagnetic field, HFSS uses the FEM. In general, this method divides the problem-solving space, according to computational capacity and accuracy, into several thousand smaller regions and, represents the field in each sub-region (element) with a local function. The geometry of the model, studied under HFSS, is automatically divided into a large number of tetrahedra. The value of a field vector ($E, or H$) at a point inside a tetrahedron is calculated by polynomial interpolation of the field values in the vertices of this latter. Thus, by representing field values in this way, HFSS transforms Maxwell equations in matrix equations solved by numerical classic methods.

This is produced by dividing the structure into several small regions. HFSS calculates the fields separately in each element by setting convergence criteria. The smaller the elements are, the more precise the solution is, yet the computation time is longer. This tool is suitable for inhomogeneous and discontinuous structures. One of the main advantages of this software is also its adaptive mesh, that is ideal for analyzing resonant structures and low bandwidths [75].

2.4.3 ADS simulator

Advanced Design System (ADS), developed by AgilentEEsof EDA, is a software for the design and modelling of electronic systems working in the microwaves and radio frequency ranges as shown in Figure 2.14. The targeted applications are very large including, among others, the field of mobile telephony, pagers, wireless networks, radar and satellite communications systems.

With its easy-to-use powerful interface, the software offers design and simulation possibilities for the radiofrequency and microwave domains, and is divided into Analog RF Designer and Digital Signal Processing Designer modules that can interact with each other:

- Design of monolithic microwave integrated circuits (MMIC) or hybrids (with Surface Mounted Components).
- Design of new architectures for future wireless telecommunications standards.

ADS pioneers are the most innovative and performing technologies in commerce, such as X-parameters and EM 3D simulators. It is used by leading companies in wireless communication and networks and aerospace and defense industries.

There have been significant advances in the recent development of modeling tools for the design of the microwave components, especially with electromagnetic simulations

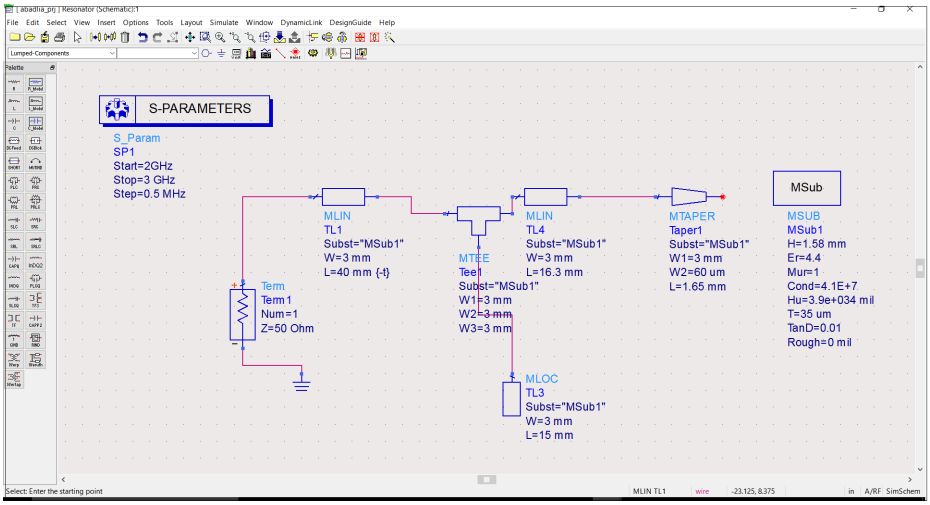

Figure 2.14: ADS graphic interface-Micro strip resonator simulation.

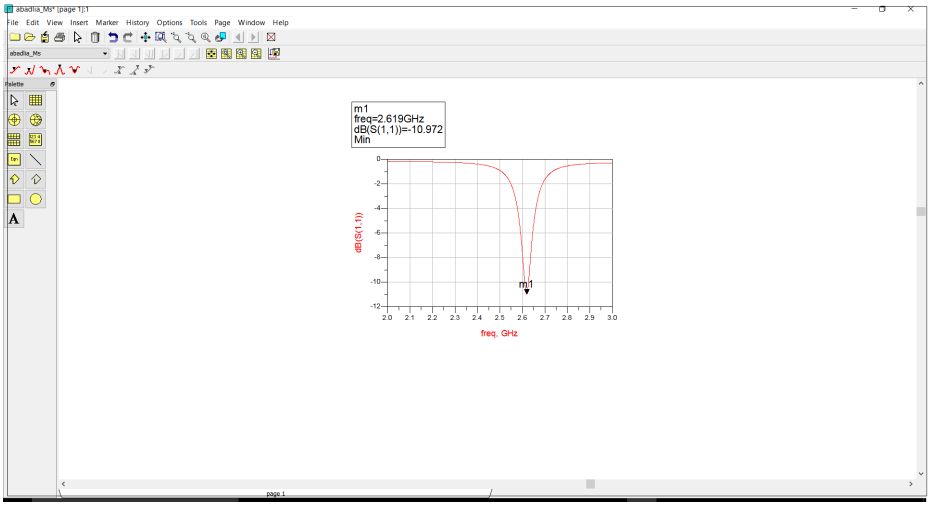

Figure 2.15: ADS result interface .

(EM) components. Today's software tools use models developed to provide a representation of the microwave including mounting devices or chip surface or whatever the shape of the component in the simulation. Depending on the type of the modelled component, linear and non-linear simulators are normally required. Furthermore, time-domain and EM simulators may also be required.

2.5 Conclusion

In this chapter, the theory of resonant cavity and the simulation tools are presented. The first section was dedicated to the introduction of the environment of the resonant cavity, with different function modes and also various kinds of resonators. In addition to theoretical concepts, we have introduced ADS, HFSS, and CST softwares for the design and simulation of different types of resonators. In our study, the ADS and the HFSS were the main tools used to model, design and simulate the investigated resonators with different structures namely coaxial resonators. Note that micro strip resonators could also be designed and simulated. The related study will be described in details in the next chapter.

Chapter 3

Design of coaxial cavity resonators

3.1 Introduction

This chapter is devoted to the design the main parts of an NSMM platform. The NSMM consists of a near-field probe and a microwave measurement system as it has been previously mentioned. According to the measurement configuration, this system has to allow the determination of the variations of the coefficient of reflection and/or transmission, of the shift of the resonant frequency and/or the variation of the quality factor when a sample is present to near the probe. Besides, when the system determines these parameters without the presence of the sample, it is said that the measurements are done in air [68].

Several academic and industrial research laboratories are more and more interested in the development of near field scanning microwave and they also take into account the range of possible applications of this technique (characterization of materials, imaging, biomedical applications, chemical analysis, etc ...).

In this section, different platforms of near field microscopes will be presented. The platform developed by Wang et al [18] at MITEC group of L'IEMN, the Agilent Technologies platform developed by Karbassi et al [13] and the microscope developed by Wei et al in Xiang's research group from Lawrence Berkeley national lab [13].

Figure 3.1 represents the NSMM configuration platform developed by Wang et al [18] at the group of L'IEMN. This system consists of a probe that is designed using a

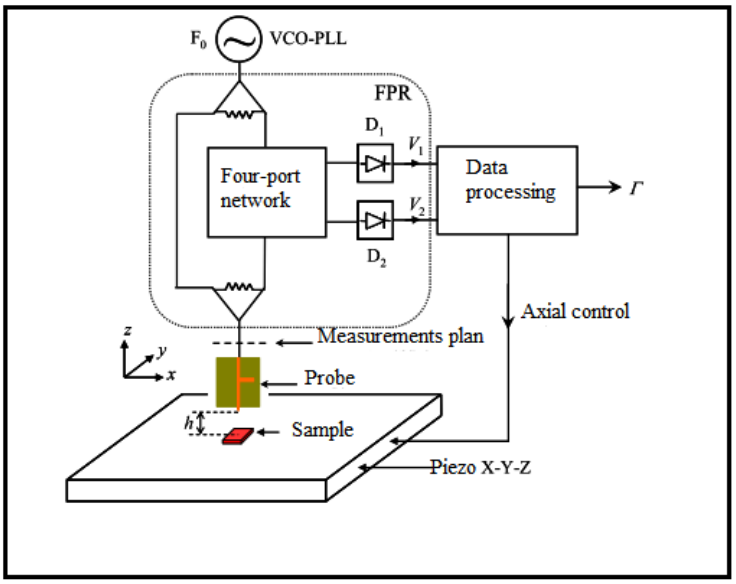

Figure 3.1: Near field microwave microscope developed by Wang et al [18].

micro strip line of 50Ω. This micro strip line has been tapered at its end to a width of approximately $60\mu m$, and was associated with a simple stub in order to realize the adaptation of the network. Taking into account the high impedance of the near-field probe, an adaptation at 50Ω has to be set to improve the measurements sensitivity.

To measure the reflection coefficient, a four-port reflectometer (FPR) has been used in this platform [68]. This reflectometer consists of six Wilkinson dividers, a 90° phase shifter and two detectors D_1 and D_2. The voltages V_1 and V_2 that were measured by the detectors are used for the calculation of the reflection coefficient at the level of the access plane of the measurement port of the sample under test. The measurement unit contains a controlled source (Voltage Control Oscillator-Phase Locked Loop VCO-PLL), this latter allows generating the microwave signal at the resonance frequency of the microstrip line resonator. Additionally, the control of the position of the sample has been developed using a data processing unit, to save the output voltages of the detectors and to calculate the complex reflection coefficient S_{11}. This platform offers operation in real time and with high spatial resolution around $\lambda/2000$ [68], [18].

The combined NSMM-AFM head presented in Figure 3.2, is a system that has been designed and fabricated by Agilent Technologies. This system uses a conventional reflectometer (i.e. VNA coupler) to measure the impedance variations between the AFM

tip and the sample. The AFM tip has a high impedance, compared to 50Ω. Moreover, to improve the measurement sensitivity of the reflectometer, a half-wavelength resonant coaxial line, and a 50Ω shielded resistor are inserted between the measuring system and the probe. The main principle is related to the measurement of the impedance at the end of the AFM cantilever when it is in contact with the material under test. This impedance can be measured using a network analyzer at a frequency close to the resonance frequency of the resonator. The probe used is a commercial AFM probe, consisting of a tungsten

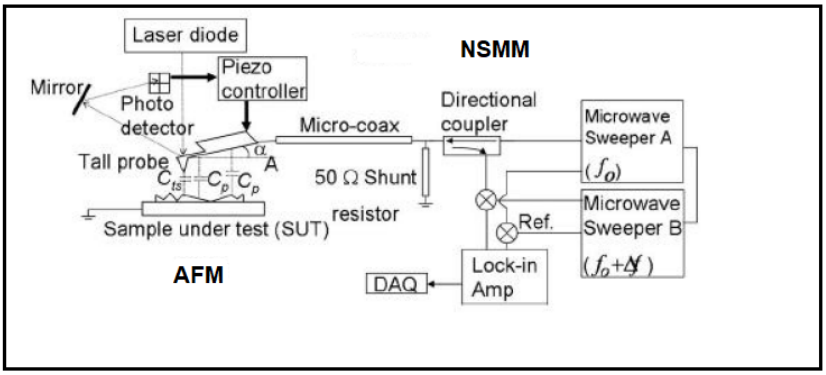

Figure 3.2: Near-field scanning microwave microscopy assisted system developed by Karbassi et al [67].

tip mounted on a stainless steel lever. According to the AFM operation principle, an optical detection method is used to track the topography of the sample under test. By adding a microwave signal to the probe tip, it is possible to have topographical imaging of the sample under test via microwave signal and AFM. The reflected signal delivered to the directional coupler is converted through a mixer and sent to the input of a lock-in amplifier referenced to the reference signal of a microwave scanner. The perturbation of the electric field at a near-field of the probe aperture is produced by the area of the sample under test which is scanned. This perturbation could be measured by controlling the reflected voltage wave. However, information about the sample under test such as resistivity, permittivity, or doping level in the case of semiconductors sample, can be carried on this reflected voltage wave. All these parameters are accessible to be figured out using AFM which makes it a specific technique [13], [68] .

The schematic platform illustrated in Figure 3.3, represents an experimental set-up of NSMM that was developed by Wei et al at Xiang's research group from National Labs in US [68]. They designed a $\frac{\lambda}{4}$ coaxial cavity resonator which is fed by an electromagnetic coupling loop. This coaxial resonator has an outer and inner conductor from copper. The

inner conductor is tapered at its end and ended by a sharpened tip usually made from tungsten. This tip is extended with $1mm$ to $2mm$ out of the cavity resonator through a hole that exists in the bottom of the end plate of the resonator, and this will be done without contacting the end plate because this feature can avoid the electrical contact. As it is mentioned before, the coaxial resonator is energetically coupled via two conducting loops formed from the inner conductors of coaxial cables to the ports 1 and 2 of vector network analyzer (VNA).

The monitoring of the changes in the resonance frequency and the quality factor in this

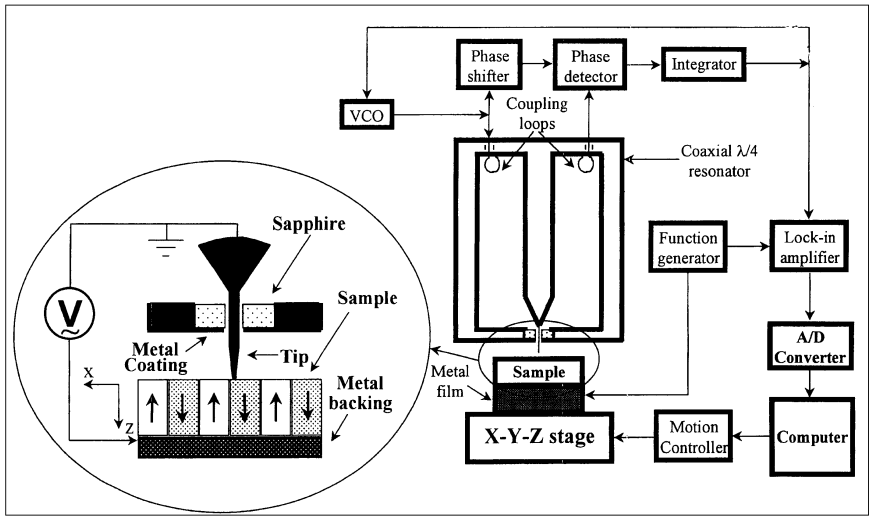

Figure 3.3: Near-field scanning microwave microscopy assisted system developed by Wei et al in Xiang's research group from Lawrence Berkeley national lab [13].

set-up is, therefore controlled by the vector network analyzer. This operation can be done when a sample under test is placed closer to the tip or with contact. This experimental set-up was admitted as a patent of Xiang et al [13].

3.2 Approaches to design different resonators

In this section, we will pay attention to those platforms presented previously. Our study focuses on making a contribution to developing an NSMM platform among these ones. We have designed a $\lambda/4$ microstrip line probe using HFSS and ADS software, and then we reinforced our platform where our contribution was designing different coaxial cavity resonators. The first coaxial cavity resonator was a cylindrical one and the second one was a conical one. In the following sections, each resonator will be presented with its

simulation using HFSS and ADS. During our study, several simulations have been done according to the design of these resonators and also their interaction with the material to be analyzed. Nevertheless, the interaction of the probe tip connected to the end of the resonator and the sample under test had been simulated just in the HFSS environment.

3.2.1 Design of the microstrip line resonator

The technique of printed circuits, originally developed in the field of Electronics, has spread in the field of microwaves since it allows the creation of transmission lines and micro-(isolators, phase shifters, circulators, etc.). The advantages of microstrip lines in comparison to coaxial lines or microwave guides are low cost, small footprint, and ease of manufacture. However, the microstrip lines carry low power and have greater losses due to the absence of shielding [17].
The microstrip line consists of a metal strip deposited on a dielectric plate which is completely metalized on the other side (ground plane) (Figure 3.4,).

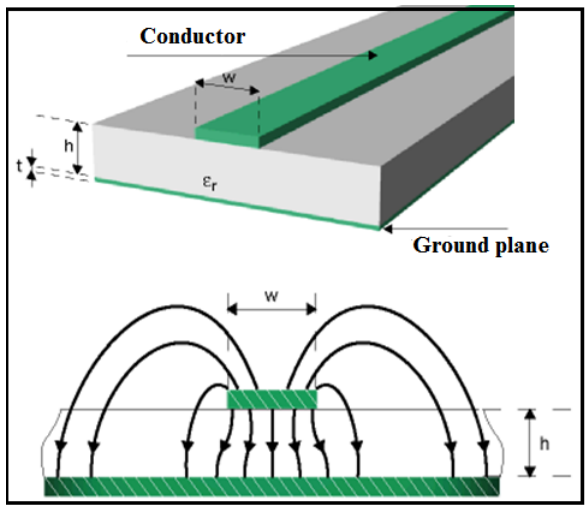

Figure 3.4: Geometry of a microstrip line with its configuration of electromagnetic field.

The line is characterized by the relative permittivity of its substrate ϵ_r, by the thickness h, by the width w of the ribbon which determines the characteristic impedance, and finally by thickness t of the ribbon. The propagation medium is therefore not homogeneous, part of the field lines is located in the substrate, the other part is in the air.
Strictly, the propagation cannot take place in the T.E.M. (Transverse Electro Magnetic). There are necessarily longitudinal components E_z and H_z of the fields. However, if they

are operated at a frequency that is not too high, these components are small compared to the transverse components and can be neglected. The micro-ribbon line is usually used in the quasi-T.E.M approximation [76].

The first microstrip line resonators ended by a probe tip were introduced by Tabib-Azar et al as shown in Figure 3.5, [52], [77]. These microstrip line resonators were used for materials characterization. The microstrip line resonators developed by Tabib-Azar et al are quarter-wavelength ($\lambda_g/4$) or half-wavelength ($\lambda_g/2$) lines terminated by a radiating element (tip).

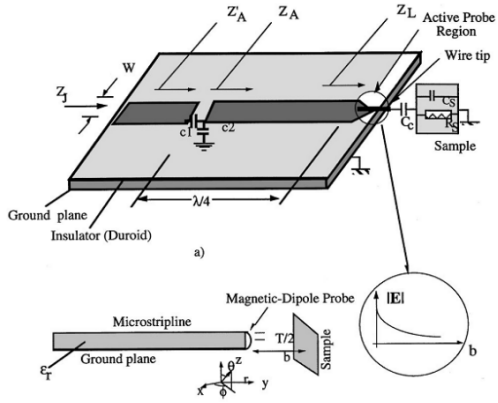

Figure 3.5: Microstrip line resonator and probe tip assembly [09].

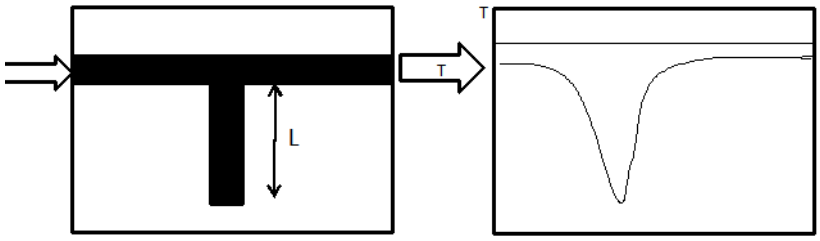

Figure 3.6: Simple stub mounted in parallel on a microstrip line.

The resonance frequency of the probe tip is fixed by the effective permittivity and the length l of the resonant line ($\lambda_g/4$, or $\lambda_g/2$) and its quality factor, therefore, depends on the length of the gap between the feed and the resonant line.
If a stub of length l in an open circuit is mounted in parallel on a microstrip line as shown in Figure 3.6, for certain frequencies such that $l = ((2K+1)\lambda_g)/4, , 3..)$, the impedance

returned in parallel on the line will be a short circuit. The structure then behaves like a band-cut filter and the transmission is attenuated significantly.

3.2.2 Simulation of the microstrip line resonator under ADS environment

Wang et al from the group of L'IEMN [18] used a 50Ω microstrip line tapered at its end coupled to a simple stub for matching the circuit with the network. Our idea was to integrate it into our platform, and also use it for combining a commercial atomic force microscopy with an NSMM, in which specific microstrip line resonators were designed to realize this coupling and will be detailed in the next chapter. The microstrip line works at a frequency of resonance around $f_r = 2.5GHz$, so to match connectors, the characteristic impedance is set to 50Ω. This microstrip line resonator was designed according to the following characteristics; a $FR4$ *Epoxy* substrate with ($\epsilon_r = 4.4$) that was conducted on it, the conductivity of the conductor in the line which is copper ($\sigma = 5.8 \times 10^7 Sm^{-1}$), and a metallization thickness of $35\mu m$.

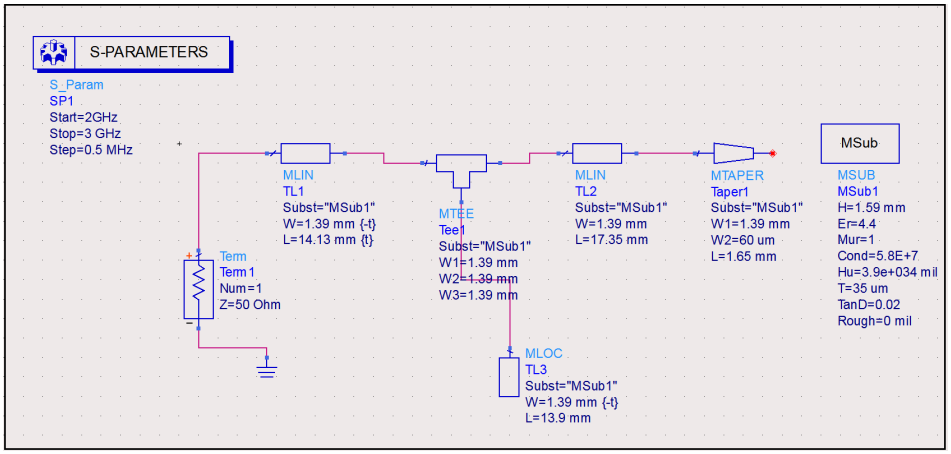

Figure 3.7: Microstrip line resonator designed in ADS.

Figure 3.7 illustrates the design of the microstrip line resonator under ADS environment, by using an open circuit, and a simple stub circuit matching, the resonator then is well matched with 50Ω impedance where it resonates at *fr=2.601 GHz.* The simulation of the design was performed under ADS simulator. Furthermore, the module of the reflection coefficient S_{11} is presented in Figure 3.8. The resonance frequency obtained in the simulation is close to the resonance frequency of the experimental measurement.

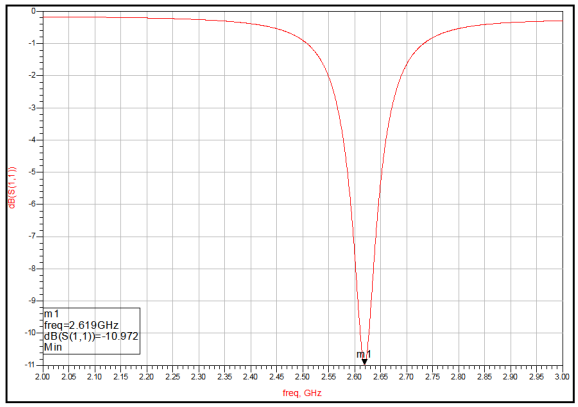

Figure 3.8: S_{11} module of the microstrip line resonator using ADS simulator.

3.2.3 Microstrip line resonator simulated under HFSS and fabricated on PCB

The design shown in Figure 3.9-a, represents the microstrip line resonator fabricated on an Epoxy substrate as it was mentioned previously. The fabricated microstrip line was also simulated using HFSS package as shown in Figure 3.9-b.

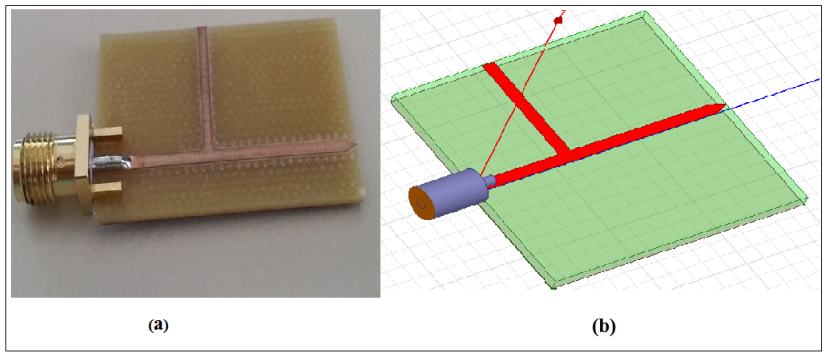

Figure 3.9: a) Microstrip line resonator fabricated. b) Microstrip line resonator designed in HFSS [18].

Figure 3.10 shows the module of the *S11* parameter of the microstrip line resonator using HFSS. Figure 3.11 shows a screen shot from the vector network analyzer (VNA). We see here the module of S_{11} parameter as a function of the frequency around the

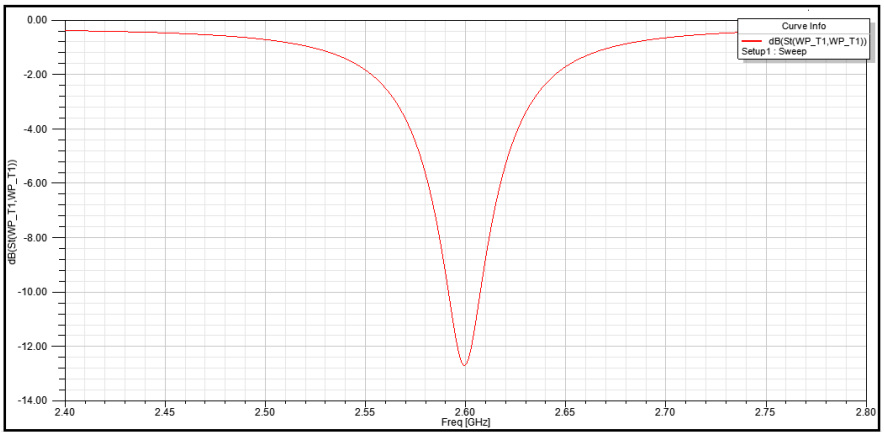

Figure 3.10: S_{11} module of the microstrip line resonator using HFSS simulator.

resonance frequency which experimentally results to be $fr = 2.615GHz$.

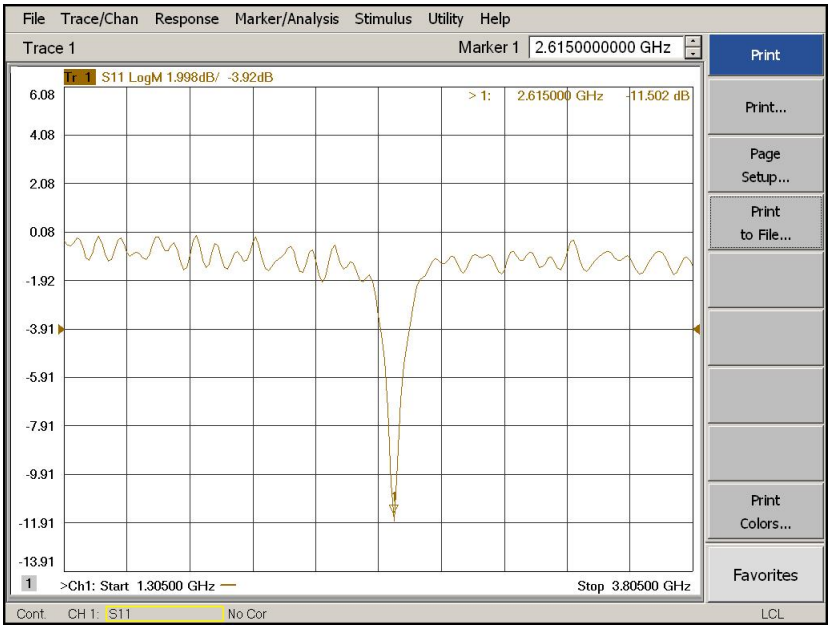

Figure 3.11: Screen shot from the VNA showing a frequency sweep of the microstrip line resonator.

Figure 3.12 the S_{11} module related to the microstrip line resonator measured experimentally and calculated with HFSS and ADS packages: the red curve represents the

measurement of the fabricated resonator measured using a *VNA* vector network analyzer, its resonance frequency is $fr = 2.615GHz$; the blue and brown curves represent the module S_{11} of the microstrip resonator $fr = 2.619GHz$, $fr = 2,6005GHz$ simulated in ADS and HFSS environment respectively.

Both simulation enviroments reproduce with high precision the experimental behavior

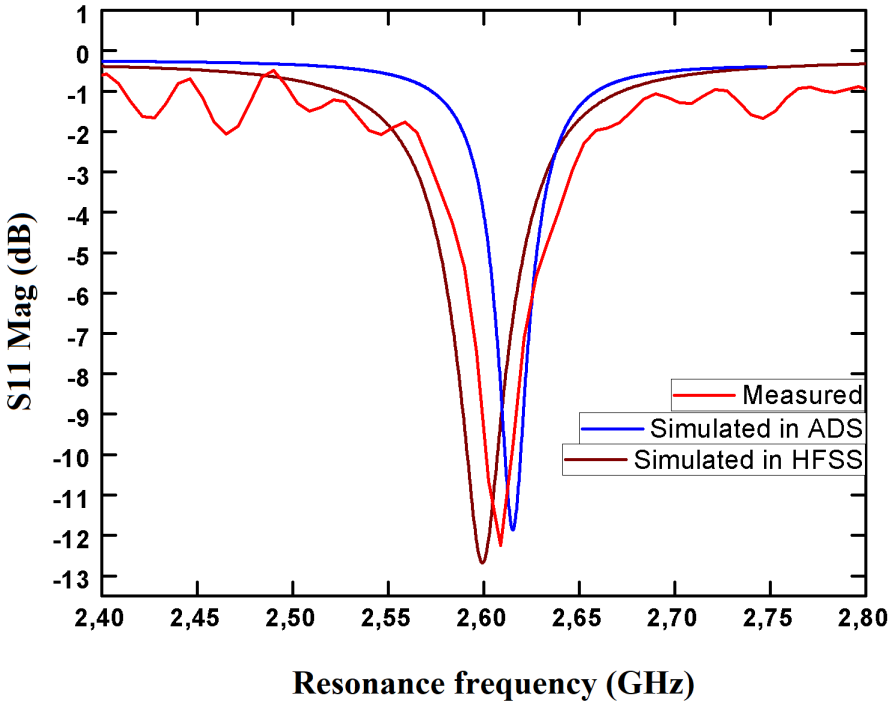

Figure 3.12: Comparison of simulated and measured reflection coefficients S_{11} of the microstrip line resonator.

of the microstrip.

Through the experimental measurements, and the simulations under ADS we can figure out that the resonator works at $fr = 2.615GHz$, with simple stub length $l_{stub} = 13.9mm$ that contributes to the circuit matching. The parameters of the microstrip line resonator will be determined as follow:

- Calculate the effective relative dielectric

$$l = \frac{\lambda}{4} = \frac{c}{4*f*\sqrt{\epsilon_e}}, l = 13.9mm, \Rightarrow \varepsilon_e = 4.25.$$

Where $l_{stub} = 13.9mm$ corresponds to the stub length and λ corresponds to the free space wavelength.
ε_{re} corresponds to the effective relative dielectric of the microstrip line $\varepsilon_e = 4.25$.

- The propagation constant of the micro strip line is given by;

  $\beta l = \frac{2\pi}{\lambda}\frac{\lambda}{4} \Rightarrow \beta = 112rad/m$

3.2.4 Simulation under HFSS the interaction between the resonator and the material under test

In Figure 3.13 we presented a sample of material to be tested under HFSS environment. This sample consists of transmission line, fabricated on a substrate of Epoxy including the same characteristic in which the microstrip line resonator is made of. It has a conductor line with $100\mu m$ width and $35\mu m$ of thick. In this example, the sample size was $6 \times 6mm$.

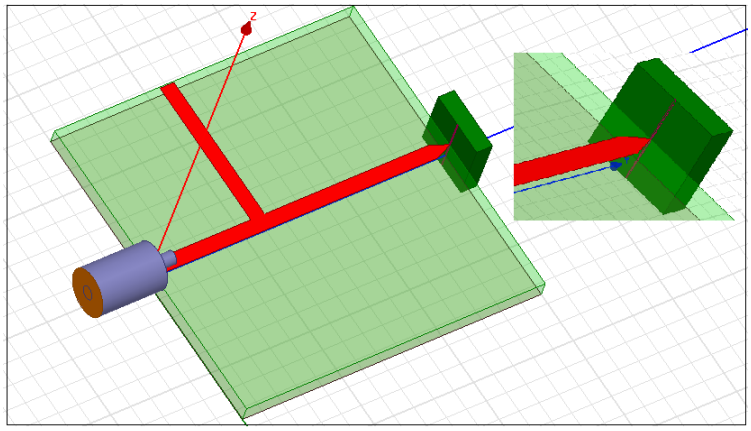

Figure 3.13: Micro strip line resonator over a sample under test.

To show the operation mode of the resonator ended with a tapered line forming a probe, the resonance frequency is determined by testing this resonator in the air at first. Different kind of samples in material and size have been used in the simulation to see the interaction between the tapered line of the resonator and the sample under test. The sample is placed at a fixed distance from the probe (distance tip-sample) and is kept constant during the scanning. In this simulation, the distance between the sample and

the tip was kept at $40nm$. The influence of the resonator when the tip is in the air or near the sample is different. These variations in resonance frequency are clearly shown in Figure 3.14.

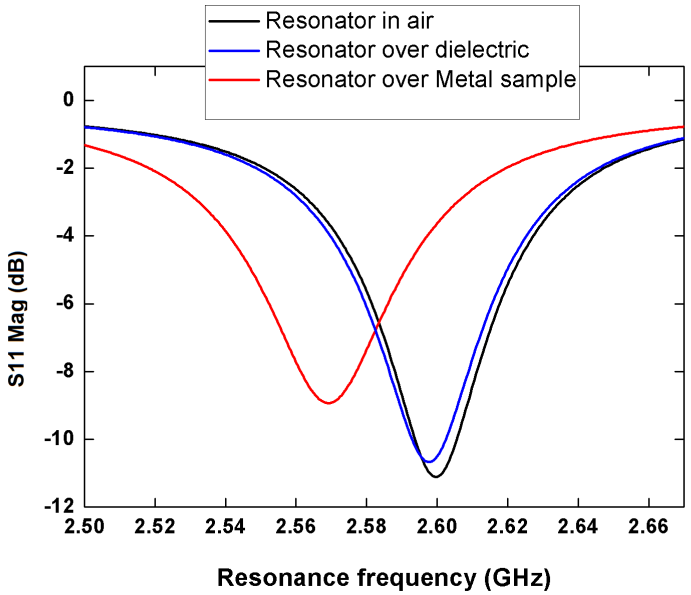

Figure 3.14: Microstrip line resonator simulation, in the air, over a metallic region of the sample under test, and over a dielectric substrate with a separation distance of $d = 0.4\mu m$.

The blue curve shows the magnitude of S_{11} parameter of the microstrip resonator when the probe is in the air (i.e. very far from the sample). In this case the resonance frequency is $fr_{air} = 2,60GHz$. When the tip is over a sample (on the metallized part, in red, or in the dielectric part, in green) the magnitude of the S_{11} parameter changes. In these cases, a variation of $100MHz$ of the resonance frequency from each one is produced. The resonance frequencies of the probe over the metal part and the dielectric part of the sample are respectively: $fr_{metal} = 2,58GHz$, $fr_{dielsub} = 2,57GHz$.

As it was previously mentioned, the resonator was matched using a 50Ω microstrip line, indeed, as the microstrip line has tapered at its end, a variation in resonance frequency was produced. The presented microstrip line resonator is ended by a tapered line, which has an aperture width of $60\mu m$ as shown in Figure 3.15.

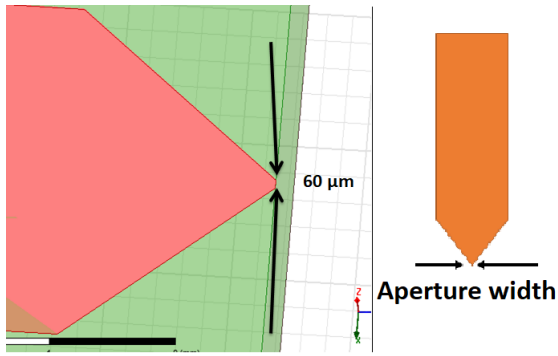

Figure 3.15: Microstrip line resonator ended by a tapered line.

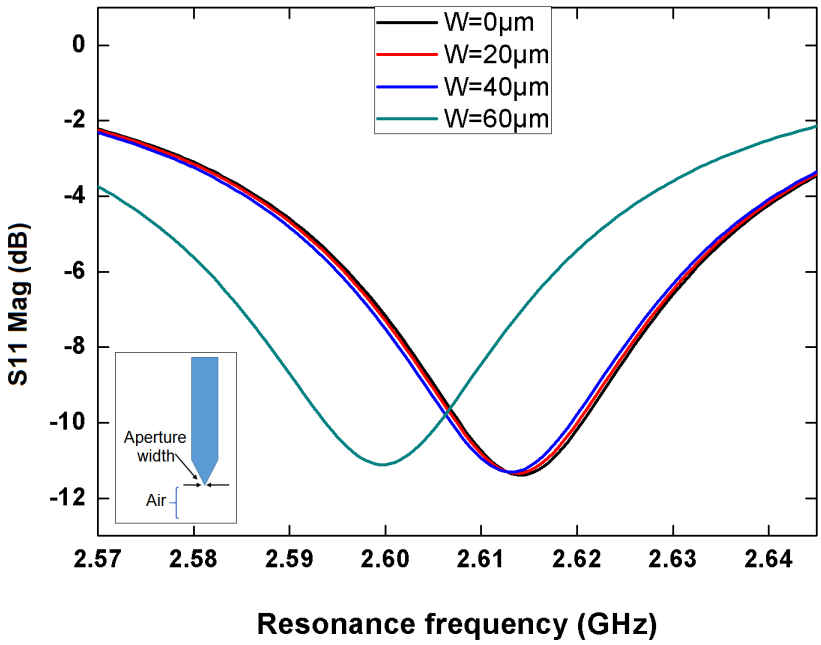

Figure 3.16: Variation of the resonance frequency according to the aperture width of the tapered line resonator in the air.

Figure 3.16 shows the variation in resonance frequency when the aperture width of the tapered line changes. According to the simulation, measurement tools that allow

us to reach this resolution, the best aperture width of the tapered line should be set at $d = 60\mu m$ to offer a good interpretation of the interaction between the tapered line of the resonator and the material under test.

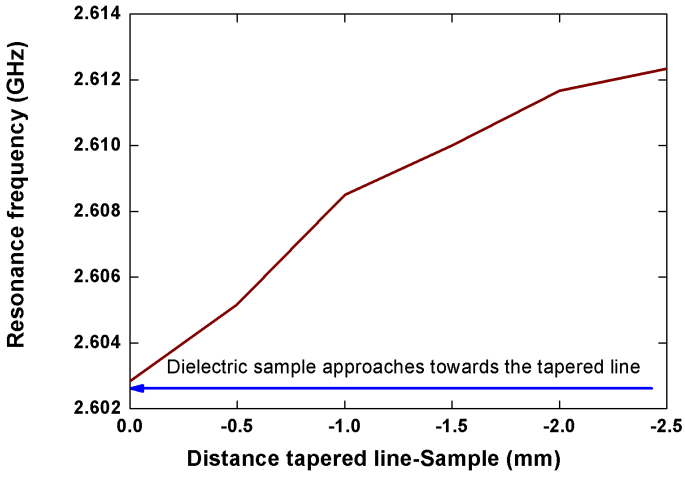

Figure 3.17: Approaching of the dielectric sample towards the tapered line resonator with a separation distance step of $d = 2.5mm$ with a step of $0.5mm$.

To demonstrate the interaction between the tapered line resonator and the material under test, a sample from copper was chosen to this operation. The sample was sized $3 \times 3mm$, and with a thickness of $1.59mm$.

The curve presented in Figure 3.17 shows how the resonance frequency decreases when the distance between the tapered line and the dielectric sample decreases also. The separation distance between them was set at $D = 2.5mm$, and the dielectric sample was approaching with $-0.5mm$ of a step towards the tapered line. The lowest resonance frequency, $f_r = 2.603GHz$, is obtained when the dielectric sample and the tapered line are in contact.

Figure 3.18 represents the evolution of the approaching mode of the metal sample towards the tapered line. The metal sample was sized $0.1 \times 6mm$ and with $35\mu m$ of thickness. The distance between the tapered line and the sample under test was set also at $d = 2.5mm$, and the approaching of the sample towards the tapered line have been done with a step of $-0.5mm$. The resonance frequency was decreasing slowly as the separation distance decreases until $d = 1mm$, a quick decreasing in resonance frequency have been recorded. The contact between the tapered line and the metal sample was produced at the resonance frequency value $f_r = 2.53GHz$.

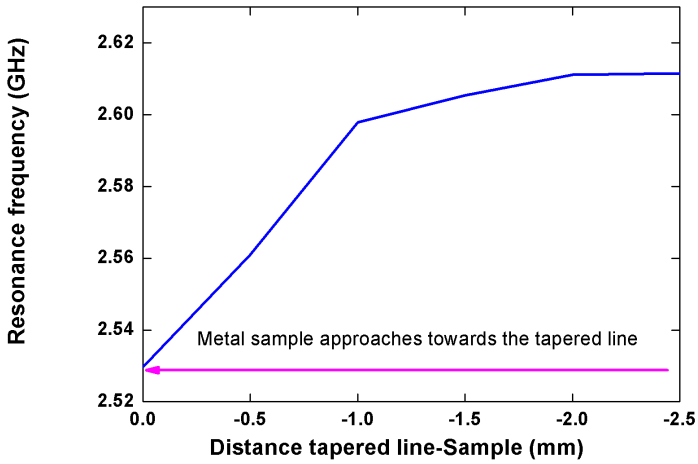

Figure 3.18: Approaching of the metal sample towards the tapered line resonator with a separation distance of $d = 2.5mm$ with a step of $0.5mm$.

The section above presented a brief explanation about the introduction of the microstrip line resonator, in our work, several simulations have been done using two simulators, ADS, and HFSS. The simulation results of the resonator obtained are close to the real operation mode of this resonator in comparison with the measurement realized using VNA.

In addition, a small sample consists of a section of transmission line was used to study the interaction between the probe resonator and the nature of the sample under test in order to calibrate our SNMM platform. The fabrication of the microstrip line resonator was restricted with the technology and the tools that our laboratory offers. The smaller width of the aperture probe resonator was $60\mu m$ which gave a good response.

3.3 Coaxial cylindrical cavity resonator ended with a sharp tip

It was noted previously that a coaxial cavity resonator consists of a $\frac{\lambda}{4}$ cavity resonator with a high-quality factor. It is associated with a metallic tip sharpened at its end in which it is mounted on the inner conductor of the cavity. However, the tip is extended outside the cavity some microns through a hole at the center of the endplate of the cavity. Two types of coaxial cavity resonators have been simulated and fabricated in

this thesis. In this chapter, we will discuss the concept of several types of the coaxial cavity, and their simulations using HFSS tools. Nevertheless, the fabricated cavities were designed in accordance with the technology of fabrication that the laboratory offers.

3.3.1 Design of coaxial cylindrical cavity resonator

In the literature, we can find different simulation models that describe the previous NSMM platform. In the following sections, a more detailed description of NSMM's main components will be simulated. The design of a cylindrical coaxial cavity requires the

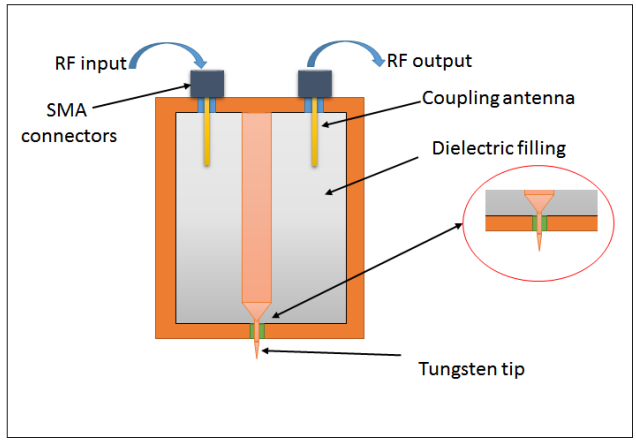

Figure 3.19: Geometry of coaxial cylindrical cavity resonator.

determination of radii and the length of the inner and outer conductors. The considered coaxial cavity resonator in this thesis according to the calculations, is open at one end and closed at the other one which means an open-ended coaxial resonator cavity ($\lambda_g/4$) of wavelength as shown in Figure(3.19. In order to get a high-quality factor and high spatial resolution, different sizes of the cylindrical cavities were designed and simulated, but the fabricated one has length $l = 38.6mm$, its radii of the outer and inner conductors are $a = 17mm$, $b = 2mm$ respectively.

The quasi ($\lambda/4$) Transverse Electro-Magnetic (TEM) mode is the fundamental mode in which the designed coaxial resonators are generally operating in it.
Before the fabrication of those coaxial cavities resonators, an optimization design has been done for each one using HFSS. The main goal of these simulations is to obtain a resonator adequate with the application of the NSMM platform. In addition, some examples of several simulations describing the interaction between the material to be

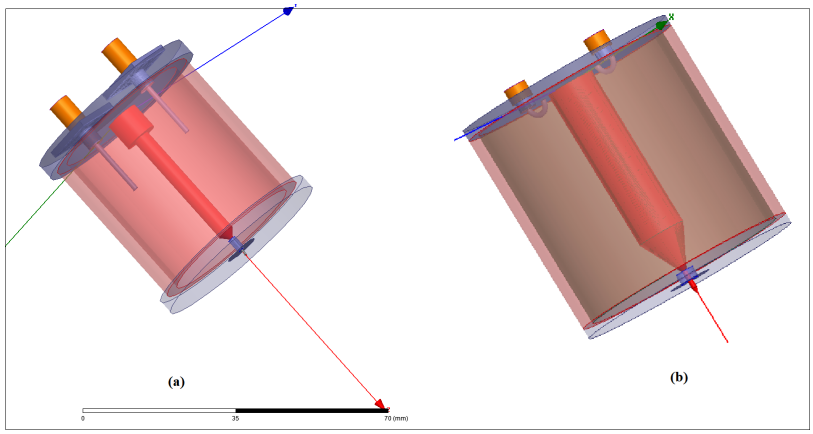

Figure 3.20: Design of the coaxial cylindrical cavity resonators under HFSS. a) The optimized cavity according to the fabricated one, fed with an electric coupling. b) The simulated cavity fed with a magnetic coupling.

analyzed and the metal tip connected to the end of the inner conductor of the coaxial cavities will be presented in the following sections.

3.3.2 Characteristics of coaxial cylindrical cavity resonator

The coaxial cylindrical cavity resonator is characterized by two important components:

3.3.2.1 Resonant structure

This structure consists of the designed shape with a tuned length and diameter of the inner conductor and the outer shield conductor. Those parameters are calculated in order to adjust the frequency of resonance in which the resonator operates in. The inner and outer conductors are made from aeronautical copper, the inside coaxial resonator is filled out with a specific dielectric or by the air. The resonance frequency of this coaxial cavity is around $f_0 = 1.1GHz$. The inner conductor is tapered at its end, forming a straight tapered. This shape allows a gradual transformation of impedance between the inner conductor and the probe tip that behaves as a radiating element. In fact, this mechanism was used to design a coaxial cone resonator for concentrating the energy toward the probe tip to have a better interaction between the tip and the material under test.

3.3.2.2 Metallic tip

The radiating element is a metallic tip usually fabricated from copper or tungsten. This element is located at the end of the tapered inner conductor as shown in Figure 3.20. It permits to channel the radiation coming from the resonator to the sample to be characterized and to collect information about the properties of the sample. Figure 3.21 presents an illustration of the effect of the probe tip to the resonance of the cavity.

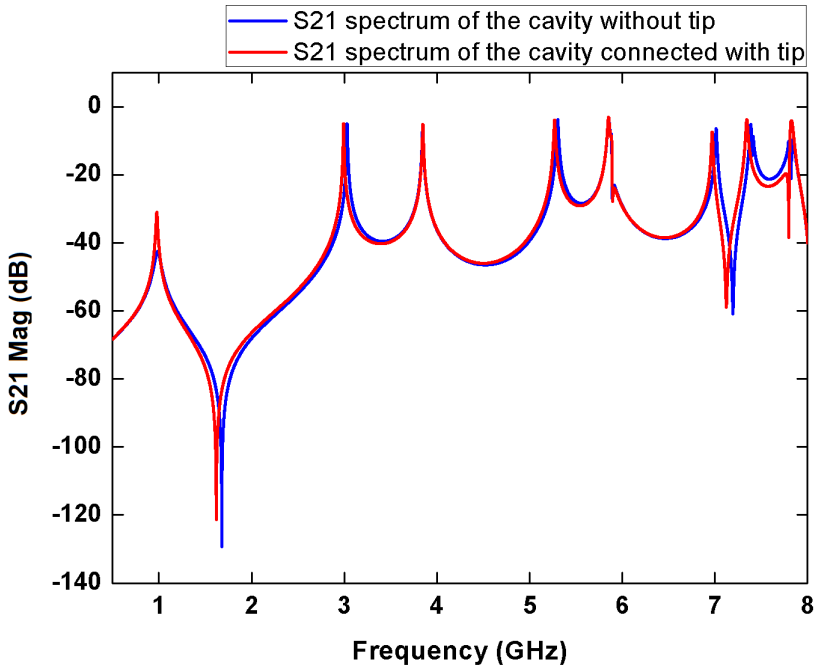

Figure 3.21: The broadband spectrum of the coaxial cylindrical cavity resonator under HFSS from $0.5 - 8GHz$ connected with the tip and without the tip.

When the connection between the probe tip and the inner conductor is produced, an increase in resonance frequency and in power transmission is obtained especially if it is well connected, which means that there is a good matching of the tip and the inner conductor. Several simulations using different shapes and material of probe tip connected the cavity were done. In addition, the steps of the probe tip fabrication will be detailed in Chapter 04.

During the simulations, the frequency band that was chosen to study some samples from different materials is shown in Figure 3.22. The selected frequency notch of the coaxial cavity shown in Figure (3.20-b) is $f_r = 2.9910GHz$. This frequency represents

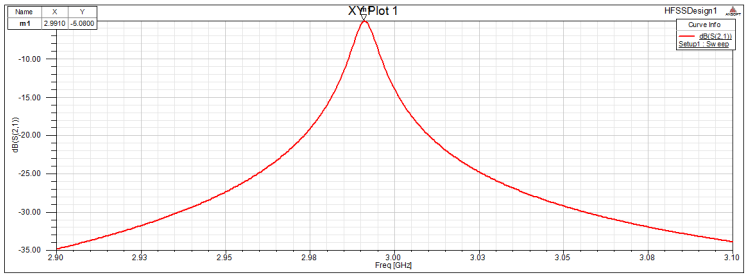

Figure 3.22: Selected of proper resonance notch. Response of the transmission coefficient (S_{21}).

($3\lambda/4$) resonance TEM mode and it provides a good interpretation of the probe tip-sample interaction.

3.3.3 Simulations of the coaxial cylindrical cavity resonator ended by different probe tips

In this simulation, two types of probe tips and the cavity fed with a magnetic coupled were used. The first part of the coaxial cavity simulations considers a probe tip made from tungsten and designed as the commercial one, with a length of $2mm$, $500\mu m$ of its sharpened area, its radius is $0.25mm$, and an aperture of $2\mu m$. The cavity was filled out with a dielectric from teflon with relative permittivity $\varepsilon_r = 2,1$. The second part of the coaxial cavity simulations used a probe tip made from copper having the same size as the tungsten tip unless its radius is double. For the cavity filling, a simulation with air-filled was done in order to figure out the changes obtained when the cavity is filled with different materials. The coaxial cavity of the cylindrical resonator is fed by magnetic and electrical coupling energy in the simulation.

3.3.3.1 Simulations of the coaxial cylindrical cavity resonator ended by a probe tip made of tungsten

In this section different simulations were done using coaxial cavity resonator connected with a sharpened tip made of tungsten. Also, the type of cavity used in this set-up is a cylindrical one filled with a Teflon dielectric and fed with a magnetic coupling (Figure 3.20-b). The sample used to study the interaction between the probe tip-sample is a transmission line with an Epoxy substrate of $1.58mm$ thickness and gold metallization $1\mu m$, where the width of the conductor line was set at $10\mu m$ and the length of both

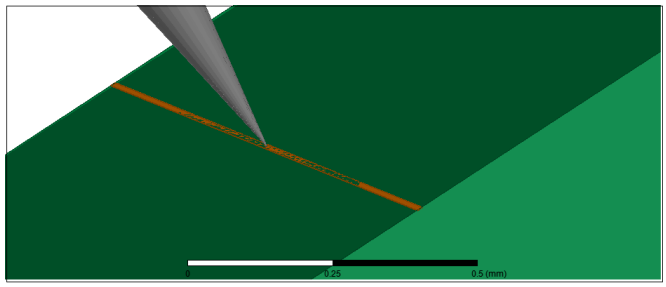

Figure 3.23: Sample under test.

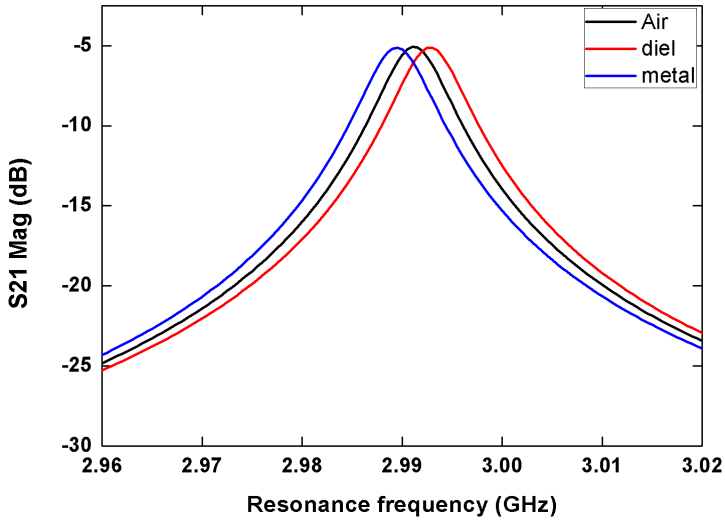

Figure 3.24: The change in resonance frequency due to the presence of sample under test.

substrate and conductor line is the same $10mm$, the mentioned sample is shown in Figure 3.23.

To verify the coaxial resonator operating mode, the sample was placed close to the tip with keeping a distance of $10nm$. This distance was kept both when the tip is over the metallization and the dielectric regions, then the resonator was tested in the air. This procedure enables us to determine the shift in frequency and the quality factor of the resonator when it is over different materials. The plotted curves in Figure 3.24 demonstrate how the probe tip interacts when it is closer to a material being tested, for that, different curves were obtained by the tip-sample interaction using different materials. The black

curve corresponds to the case when there is no sampled under the tip (tip in the air). The red and the blue curves describe clearly the interaction of the tip-sample over dielectric and metallization regions respectively. The shift in frequency was around $\Delta f_0 = 10MHz$.

3.3.3.2 Simulations of the coaxial cylindrical cavity resonator ended by a probe tip made of Copper

This part reveals another approach for connecting the coaxial cavity resonator with a tip made of Copper and with different dimensions.
The characteristic of this Copper probe tip used in this approach lies in its sharpened end diameter that is $D_{sharpened-tip} = 2\mu m$. This time we varied the DTS by approaching the tip to the sample until the contact is produced. The working frequency plotted in Figure 3.25, $f_r = 2.71GHz$, is smaller than the working frequency of the coaxial resonator connected to a tungsten tip.

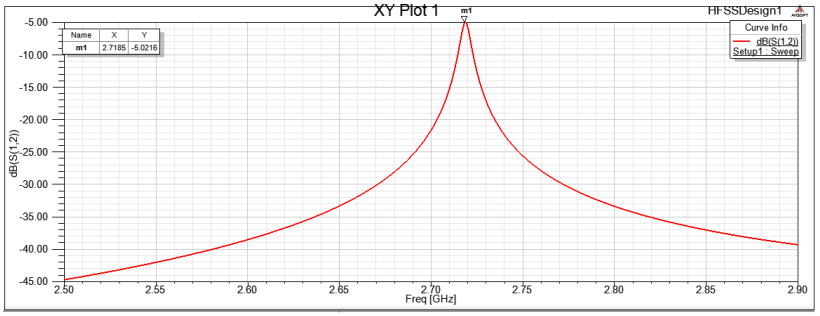

Figure 3.25: Resonance frequency of the coaxial resonator connected with a Copper tip.

By exploiting the chosen frequency, the tip was approaching the sample by a separation of $DTS = 45\mu m$ with a step of $DTS = 1\mu m$ until it reaches the $DTS = 0\mu m$ that means the tip is in contact with the sample under test. The approaching curve to the metallic region (Gold strip line) is illustrated in Figure 3.26, therefore, it is the same sample tested previously with the other probe tip.

While the Copper tip is approaching the metallic region of the sample which is represented by the red curve, the resonance frequency is almost constant until the distance between the tip and the sample registered at $DTS = 10\mu m$. So, from this separation point the resonance frequency decreased until the tip was in contact with metallic part of the sample. But, for the dielectric region of the sample, it is clearly shown with a blue

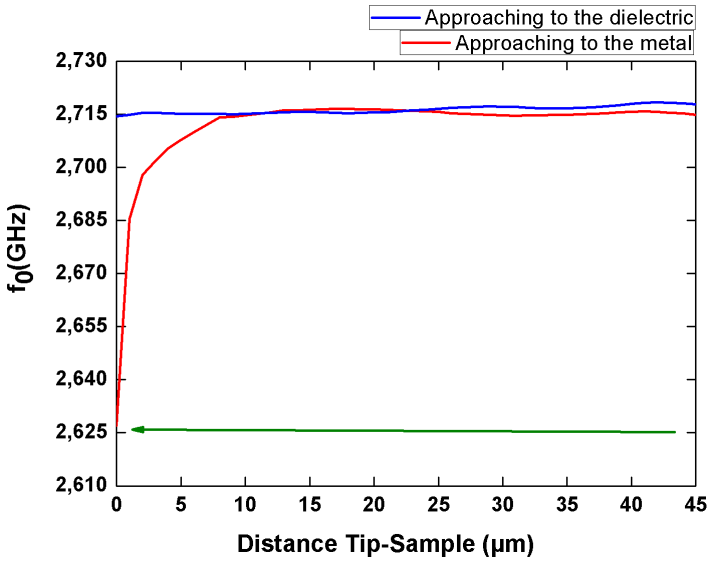

Figure 3.26: The changes of the resonator resonance frequency, when the metal and dielectric regions of the sample were approaching towards the probe tip.

curve, the approach of the Copper tip was practically constant. We conclude that there was a weak variation in resonance frequency completely different when the tip approaches the dielectric region.

The following study is devoted to the evaluation of the sensitivity of this technique to the variations of the patterns under test. Also, we address the effects of peaks (in simulations) on the resolution of the technique. This technique consists of a coaxial cavity cylindrical resonator ended by a sharpened tip put closer to a sample in order to study the interaction tip-sample.

To determine the sensitivity to geometric variations, we used the sharpened tip of $length = 500\mu m$ and $D_{tip} = 1\mu m$ of its sharpened diameter to scan lines of widths from $[-5.5, +5.5\mu m]$. To obtain a higher spatial resolution, the distance between the probe tip and the sample must be at least half the diameter of the sharpened tip $DTS = D_{tip}/2$ [78]. This line is considered etched at a depth $h = 10\mu m$ on an Epoxy substrate (thickness of the substrate is $T_{sub} = 1.58mm$). Then, these lines are metallized in gold. Note that the lengths of these lines are considered infinite.

In ths case, a constant $DTS = 50nm$ was considered. By doing a lateral scan above the sample along $[-x, 0, +x]$, the engraved metallic line is scanned with a step of $S_{step} = 5nm$. The variations of the module of the reflection coefficient S_{21} is shown

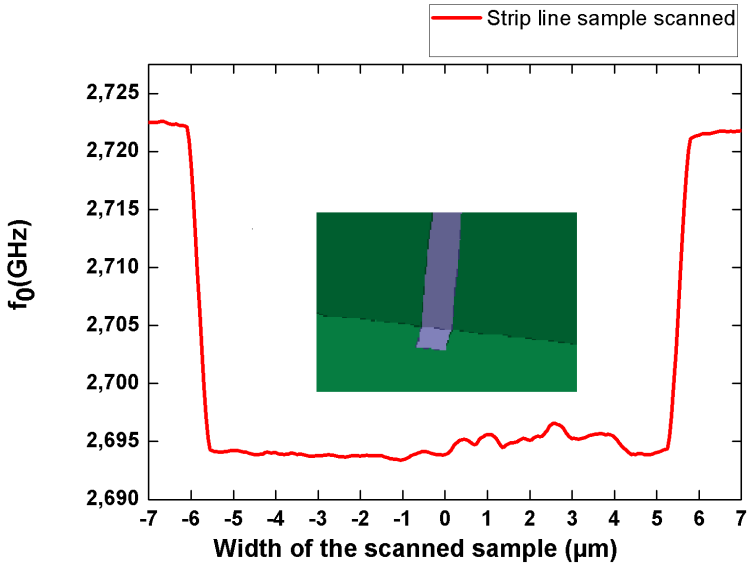

Figure 3.27: Profile of the probe tip scan over strip line sample using a Copper tip with a kept distance of $DTS = 50nm$.

in Figure 3.27. The profile of the scanned sample represented by the transmission coefficient module, demonstrates explicitly the change in resonance frequency when the tip is on the dielectric and on a conduction region. From this information, a characteristic of a sample that composed of different materials can be determined.

3.4 Coaxial conical cavity resonator

The designs presented in Figures 3.28, and 3.29 consider another approach to design coaxial resonators. This design consists of a coaxial cavity having a cone format. This kind of coaxial resonator which is similar to the cylindrical one, in the material of fabrication and in its dimension, is shorter than the cylindrical coaxial cavity.

This resonator is fed by an electrical energy of coupling, the idea to design such kind of resonator was to concentrate the energy carried by the inner conductor to the probe tip in order to have a good interaction between the sample and the probe tip. The details related to this resonator will be described in the next chapter in its fabrication part. This resonator is fed by an electrical energy of coupling, the idea to design such kind of resonator was to concentrate the energy carried by the inner conductor to the probe tip in order to have a good interaction between the sample and the probe tip. The

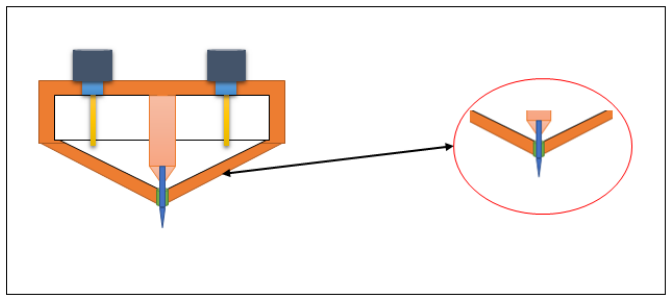

Figure 3.28: Geometry of coaxial cone cavity resonator.

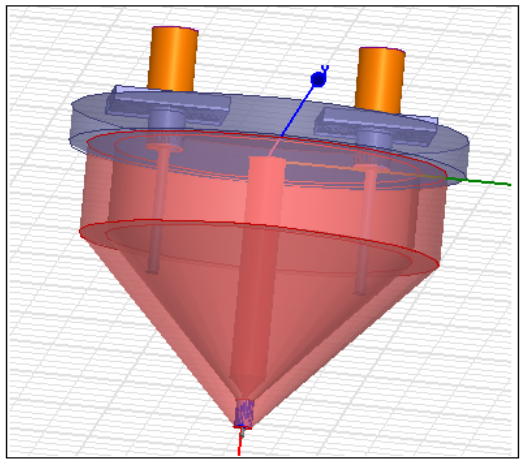

Figure 3.29: Design of the conical coaxial cavity resonator under HFSS.

details related to this resonator will be described in the next chapter in its fabrication part. The coaxial cone resonator was simulated in HFSS environment in order to figure out the desired working frequency in which was $f_0 = 2.6GHz$ mentioned in Figure 3.30 with an operating frequency range of [2.592 to $2.61GHz$].

As seen in the mentioned Figure 3.30, there is a match between the simulation and the measurements results. The slight differences obtained between these results can be caused by the attachment of SMA connector to the bottom of the both cavities and the probe tip connection. The graphs mentioned in Figure 3.30, present the magnitude of the transmission coefficient S_{21} of the conical coaxial cavity resonator when it is not connected to the probe tip.

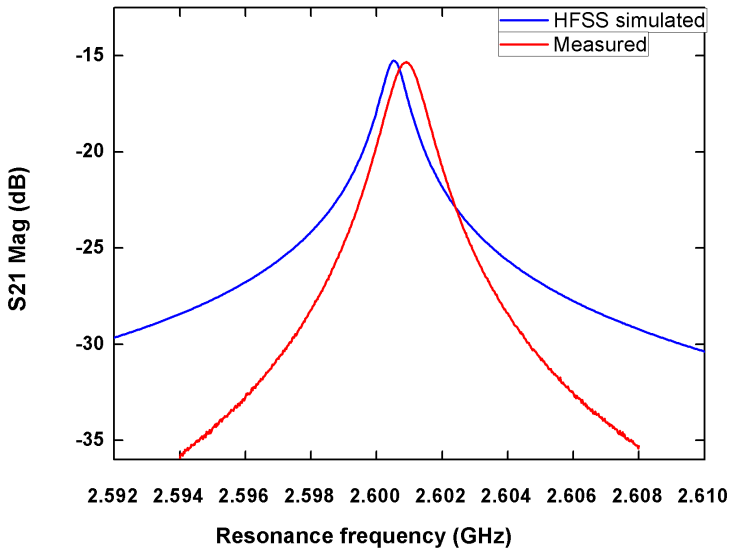

Figure 3.30: Tha magnitude of the transmission coefficient (S_{21}) measured and simulated.

3.5 Conclusion

This chapter is concentrated on the main tool design of such an NSMM platform. The most important and complicated part of this platform was the resonator. Following the improvement of the resonators' quality factor, it was deduced that:

- The simulations were useful to design a coaxial cavity resonator with good quality factor suitable for our platform on which we worked.
- Change in the diameter of the connected sharpened tip affect directly the resonator response and also improves the interaction tip-material under test.
- The resonator's dielectric filling could affect also the response of the resonator in term of frequency of resonance.
- To extract out the characteristics of such sample under test, the interaction between the tip-sample depends on the geometry of the sample and the size of the sharpened tip, and also the distance that separates them.
- In our case, we conclude that in order to obtain a good profile of material's characterization, the thickness of the sample used for any kind of material especially semiconductors structures, has to be bigger than the radius of the sharpened tip

$h_{sample} > r_{sharpened-tip}$ used to interact with the material under test, where **h** represents the thickness of the sample and **r** represents the radius of the sharpened tip.

Several simulations of both cavities were done, in order to optimize the final design that would be fabricated and used for our measurements. The design and fabrication of the coaxial cone cavity resonator were easier than the cylindrical one. The final optimized coaxial cavity resonator used in our work will be detailed in the following chapter.

Chapter 4

Experimental set-up of the NSMM platform

4.1 Introduction

In the fourth chapter, we will evaluate the potential of a near-field resonant technique based on coaxial cavity resonators to detect the thickness of a material stuck on a different material. The measurement steps will describe the characteristic of samples such as silicon dioxide, graphene, graphene oxide, and reduced graphene oxide, and a metallic track printed on a dielectric substrate.

In the previous chapters, we discussed the fundamentals of the NSMM. It is important to note that there are several measurable quantities in which NSMM is based on; the transmission coefficient, S_{21}, the reflection coefficient, S_{11}, the quality factor, Q and the resonance frequency f_r.

This chapter is devoted to describe the material and the fabrication methods of different parts of the NSMM platform. We pay particular attention to the coaxial resonators and the probe tip in order to carry out the feasibility of this study as it is shown in Figure 4.1 . This Figure represents the NSMM platform set-up. We thus highlight a number of constraints that need to be taken into account in order to define a near-field resonant technique compatible with the technical means of the laboratory. In sections 2 and 3, we justified, first of all, the choice of a coaxial cylindrical cavity resonator used to characterize the materials cited above, and by the following parts, we discuss the simulation and measurement results obtained. Finally, in the last section, we discuss the performance of the NSMM technique.

4.2 Components and functioning of the NSMM platform

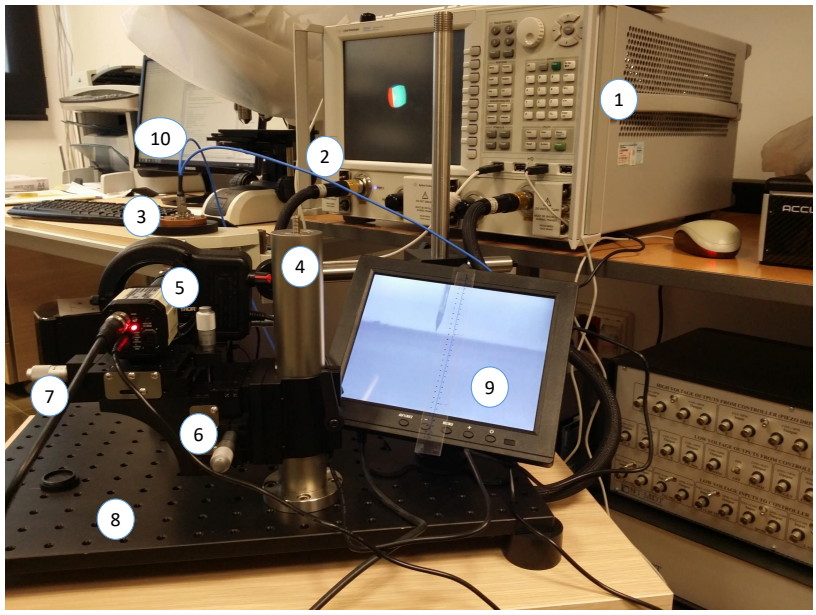

Figure 4.1: The setup of NSMM platform.

The term Components of an NSMM means the "hardware string" that includes the test model, the displacement table X, Y, Z, the measuring devices, and the technological techniques that provide the possibility to make the coaxial cavity resonators and the probe tips.

A general NSMM platform is presented as shown in Figure 4.1 with basic components, and each of them have been numerically labelled in the figure. An adjustable mechanism support (6) and (7) which is movable in x, y, and z directions using two placed manual linear translation steppers (RB13 Series 3-Axis Translation Stage, Thorlabs). The entire structure is mounted on an anti-vibration table (8) in order to avoid any kind of noise which may be caused by external vibrations.

Once of the coaxial resonators ended by a sharp probe tip (3), is connected to a

4-Port Network Analyzer (PNA-X) (1, Agilent Technologies N5242A) via coaxial RF cables. The microwaves source required to form the evanescent waves at probe tip's end is, therefore provided by this PNA-X. The resonance frequency, the reflection and transmission coefficients are measured depending on the given frequency range through the PNAX.

The metallic mounting bracket (4) has been used to hold the resonator, and this latter is supported by a mounting rod which is fixed to the anti-vibration table. In this system, the terminated coaxial resonator by a probe tip and the platform that holds the sample are fixed, and three-dimensional motion is provided by moving the sample with respect to the probe tip. To observe the position of the probe tip in respect with the sample being analyzed, a system of camera (5) mounted to the bracket is put close to the tip-sample interface. The camara used (5) is connected to an LCD screen (9) that provides a real-time image according to the tip-sample position.

4.2.1 Vector network analyzer (VNA)

The VNA used in our experimental work is a 4-Port Network Analyzer (PNA-X), is of (Agilent Technologies N5242A) type, and it offers a frequency range from $10MHz$ to $26.5GHz$ that covers the working frequency from $1GHz$ to $15GHz$ for both coaxial cavities. The PNA-X is the main device of NSMM platform, as it can be used as microwaves generator and detector at the same time of the transmitted and the reflected signals that would have been sent back during the tip-sample measurements. Before starting the experimental process, the PNA-X has been well calibrated on the frequency band using a 50Ω transmission line, and a calibration kit of impedances $Z = \infty$ (open), $Z = 0$ (Short).

4.2.2 Probe tips

After the optimization simulation of the cavities connected to different tips that will be used in our experiments, the tungsten tip has been chosen as the adequate tip that responds to the required issues. This choice furthermore, comes back to the rigid characteristic of the tungsten tip in comparison with other tips made from different materials. A technique for preparing probe tips of a few micrometers even nanometers of radius from a tungsten wire is investigated. The sharpened form has been obtained by electrochemical etching and the additional treatments are carried out in ultra-high vacuum.

The tungsten tip was prepared by doing an electrochemical etching process. A small length of the tungsten wire was cut and connected to the inner conductor of the cavity.

Another recipient made of epoxy was filled with a sodium hydroxide solution (4.1). A control circuit was used to manage the etching tip at the right time in order to avoid any damage. Once this circuit is put on, we placed the cavity on bracket support, and the tip was connected as an anode. In the other support we put the chemical product and at its edge surface, a ring made of platinum was placed and he acted as a cathode. The tip was slightly immersed in the (chemical product) with a deep of $2mm$, after some time, the tip began to be sharped at its end. Once the etching process is finished, the etched tip is cleaned by a distilled water.

4.2.2.1 Basic schemes of probe tip etching procedure

The general idea to design this circuit comes from the fact that while the electrochemical etching of the tip is in process, there is a relatively good connection through the solution between the electrodes. Once the tip etches through and drops off, the resistance between electrodes goes up. A number of earlier papers have suggested stopping the etching as soon as possible after the tip drops, or the continued etching will blunt the tip.

$$W + 2H_2O + 2NaOH \longrightarrow 3H_2 + Na_2WO_4 \tag{4.1}$$

According to this chemical reaction, different etching techniques were given by Melmed to create a sharp tip [79]. The Tungsten wire and stainless steel counter electrode (Platinum in our case), is dipped into a chemical liquid that contains $2-3M$ of **NaOH**. This reaction is formed by a simple etching procedure.
To realize the etching procedure, we need to apply it to the electrodes a DC voltage around $2.5 - 9V$. The platinum wire is placed as an electrode and on the other hand, the Tungsten wire acts as the anode. During the etching procedure, the current reaches a value of the order of mA that provided by the cited equation of reaction 4.1 [79].

4.2.2.2 Experimental set-up of the tip etching procedure

Figure 4.2 demonstrates the global procedure for etching the tungsten tip with the help of a DC circuit. To do so, this operation has been reinforced with a specifically designed mechanism to improve the etching.

The shown design in Figure 4.3 aims to connect the tungsten wire of $0.25mm$ in diameter into the cavity and leave an extension around $2.5mm$ out of the cavity. We used a special support to put the liquid of etching and to adjust the tungsten wire inside it. Once the connection between tungsten wire and cavity is well adjusted above the support, at this time, comes the role of the DC circuit that allows the control of the etching procedure . The operation of etching takes around 15 minutes of time as it was described in the previous parts, so that the tungsten wire will be etched and the probe

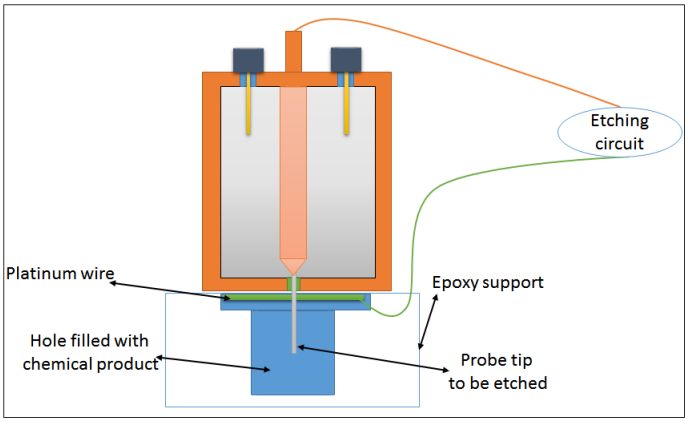

Figure 4.2: Synoptic scheme of the DC etching probe tip technique.

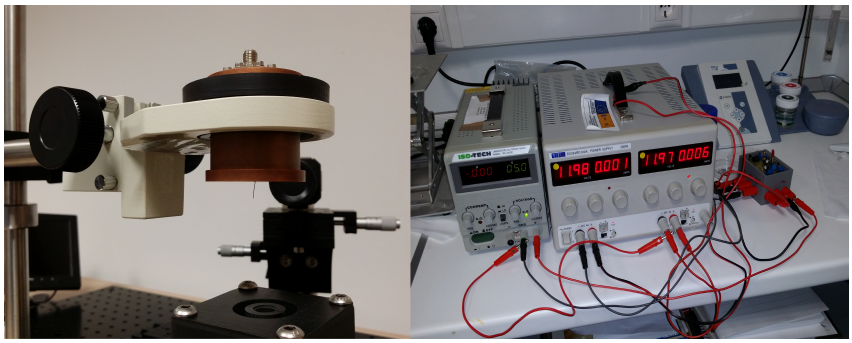

Figure 4.3: Experimental procedure using a DC circuit for probe tip etching.

tip will be formed [79], [80].

4.2.2.3 Description of the function of a DC circuit used in the tip etching procedure

The LM311 comparator watches effectively the resistance across the etching electrodes. Figure 4.4 right shows the resistance drawn between points A and B(-), it will be low during the etching, but jumps up when the tip drops. The 500Ω resistor (above A) and the variable resistor (potentiometer 1, below B) act as a voltage divider along with the cell itself. When the tip drops off and the cell resistance jumps up, point B is pulled closer to ground (as its resistance to the 12 V supply has increased). The idea is to have the set point for the comparator lower than the value of B during the etching, but higher than the value of B when it has stopped.

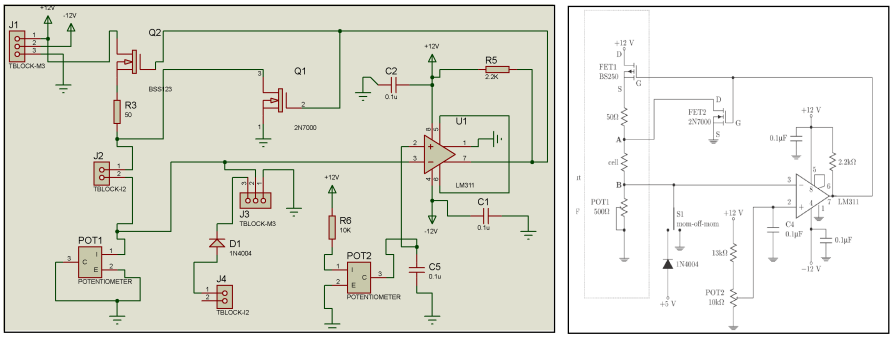

Figure 4.4: Schematic diagram of the DC etching control circuit. The right schematic is the general circuit. The left circuit designed under Proteus software (Labcenter Electronics).

Once B drops below the set point, the output of the comparator goes high. $FET1$ then breaks the connection between the voltage supply and A, and at the same time, $FET2$ connects A directly to the ground. (Note the $FETs$ are of opposite polarity [81].

4.2.2.4 Results of tip etching without the use of DC circuit

Following the experiments' steps, the results obtained as they are illustrated in Figure 4.5, show clearly the etching procedure of the tungsten wire manually, without using the DC circuit. This technique allows the control of the etching when the tungsten wire is put in the chemical solution by applying a direct bias of $12V$ to the electrodes. The tungsten wire acts as the anode and the platinum ring acts as a cathode. After a few seconds, around $12s$, the etching process is done.

As a result, this procedure cannot provide a good improvement to form the tip. It is

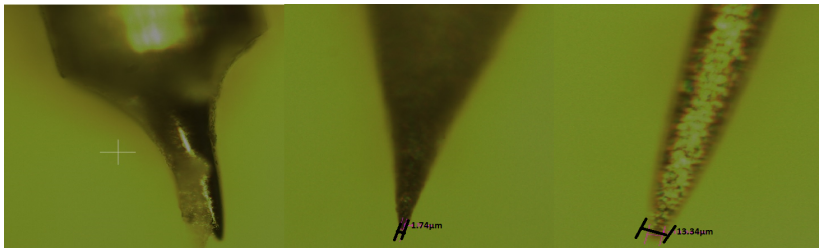

Figure 4.5: Different shapes of the tungsten wire during the etching manually (without using the DC circuit-Direct DC etching).

clearly shown in Figure 4.5, if the voltage did not cut off during the etching at a specific moment, the etching will go on and at the same time is maintained by a voltage which causes the damage of the tip. Due to this reason, the DC circuit controls accurately the etching of the tungsten wire [82].

4.2.2.5 Results of tip etching using DC circuit

It's clearly seen in Figure 4.6 that we could obtain very nice shaped tips around $200\mu m$ in length and $1.80\mu m$ in sharpened diameter during this process.

Figure 4.6: Different shapes of the tungsten wire during the etching automatically (Using a DC circuit and a tip mechanism holder).

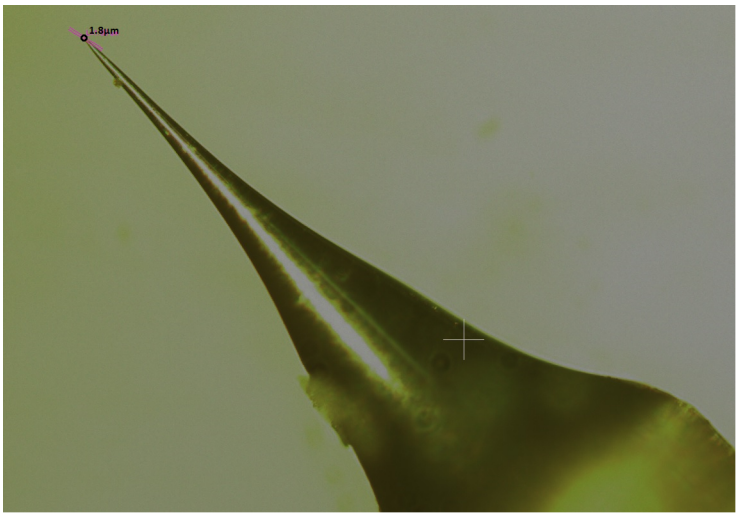

Figure 4.7: Tip after etching procedure.

As it was mentioned before, the DC circuit allows the control of the etching process in real time and helps the tip to be not damaged once the etching is done.

During the experimental tests, the tip that has been used is the one illustrated in Figure 4.7. This tip has the following characteristics; Diameter around $0.25mm$, sharpened part length $200\mu m$, and the sharpened head diameter was $1.8\mu m$. The obtained tip was extended out from the cavity $1.7mm$, and it was used in the cylindrical and the conical coaxial cavity resonators.

4.2.3 Coaxial cavity resonators

Figure 4.8 refers to the structure of the resonant coaxial cavity terminated by a sharpened probe tip [8], [53], [83]. This type of resonator makes it possible to obtain very high-quality factors and its potential to characterize metallic materials has been well demonstrated [8].

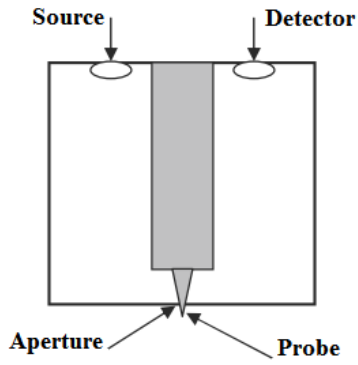

Figure 4.8: Structure of a resonant coaxial cavity ended by a sharp probe tip.

However, the realization of such kind of coaxial cavities is relatively complex. To achieve a very high spatial resolution and good quality factor, it is necessary to produce a very sharp tip with a small radius of curvature [69], [83]. On the other hand, an iris (aperture) in which, it does not exceed a few tens of microns in diameter at the end of the coaxial cavity has to be realized. This operation makes the probe tip passes through this opening avoiding twisting or breaking of the probe tip.

4.2.3.1 Realization of the structure

The fabricated cylindrical coaxial cavity resonator was designed to work at high frequency, and it has the following geometrical parameters [84] :

- *l= 38.6 mm* , represents the length of the cavity.

- a=17mm, and b=2mm are the radii of the outer and the center conductor respectively of the coaxial cavity.
- d=3mm, represents the thickness of the cylindrical walls.
- t=2mm, represents the radius of the cavity aperture.
- h=13.87mm, represnts the length of the coupling wires.

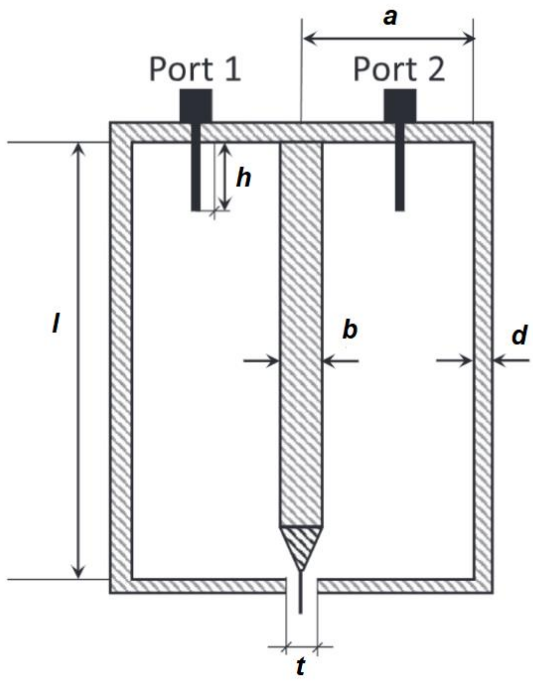

Figure 4.9: Scheme of the coaxial cavity resonator with the corresponding parameter definition.

4.2.4 Modelization of NSMM System with a Lumped Series Resonant Circuit

A resonator circuit is characterized by a resonance frequency f_0. This frequency determines the rate at which electric and magnetic energy are exchanged in the system. The important parameter of any resonator is its quality factor Q, that is a measure of the losses in the circuit. Minor losses implies a high Q. The easiest way to describe a

resonator is to modelize it in terms of the well-known circuit such as LRC. To make a connection of this system with the microwaves, the behavior of the circuit is modelized in the vicinity of the resonant frequency of the resonator. Consider the circuit in Figure 4.10 [85] ;

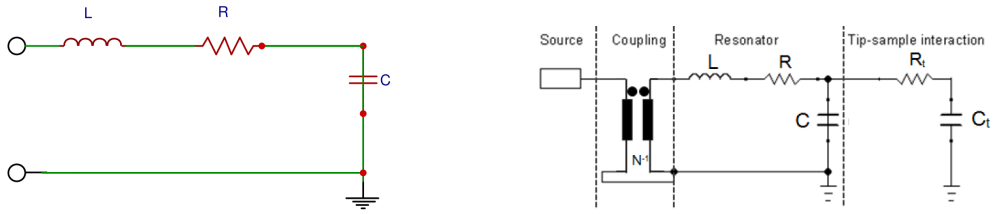

Figure 4.10: In the left side, Lumped circuit of the resonator. In the right side the lumped series resonant circuit of the NSMM set-up with the present of tip-sample interaction [14].

The interaction between the resonator and the sample under test was modelized by a lumped series elements circuit. This system consists of blocks of a transmission line containing the resonator , the probe tip, and also the section where the evanescent waves are produced by the interaction of tip-sample. This entire system can be represented by circuital components that would be able to have a load impedance Z_L [14], [86], [87].

The main reason to use this method is that it summarizes the treatment of each component that will have a certain resistance R, inductance L, of capacitance C as it is shown in Figure 4.10.

$$L_R = \frac{1}{2}\frac{\mu_0 \ln(\frac{b}{a})}{\pi} l \tag{4.2}$$

$$C_R = \frac{2\pi\epsilon_0}{\ln(\frac{b}{a})} l \tag{4.3}$$

$$R = \frac{\sqrt[2]{\frac{\omega\mu_0}{2\sigma}}}{\pi^3} l(\frac{1}{b} + \frac{1}{a}) \tag{4.4}$$

$$F_R = \frac{1}{2\pi\sqrt{L_R C_R}} \tag{4.5}$$

Where, L_R is the effective inductance and C_R is the effective capacitance of the R-L-C circuit. l represents the effective cavity length that is around $l \approx \lambda/4$, a and b are the radii of the outer and the center conductor of the coaxial cavity. ε_0 , μ_0 are the permittivity and permeability of vacuum respectively. σ corresponds to the conductivity of the metal used to fabricate the cavity [14], [86]. The presence of the sample under test closer to the tip, as it is summarized in RLC lumped circuit affects directly the resonant frequency f_r of the circuit, which then affects the value of the load impedance Z_L and

then the value transmission coefficient S_{21} of the system. Thus, the electromagnetic properties of the sample can be quantified by comparing the resonance frequency f_0 and the transmission coefficient amplitude S_{21} of the system with respect to the state of the system without the sample. In the next section, the relationship between shifts produced in the resonance frequency, Δf to the variation of the electromagnetic property of the sample (for example the permittivity of the material ε) will be determined.

Regarding the quantitative measurements of dielectrics, near-field microwave microscopy must be well calibrated. For calibration, frequency off- set and quality factor degradation due to the presence of the sample in contact with or near the tip must be related to the permittivity and loss tangent of a reference sample respectively. This can be done with standard analytical models and samples. Different analytical models have been proposed to describe the behavior of the NSMM system and especially the interaction between the tip and the sample to be analyzed.

In general, among them, the best-known model is the image loading model of C. Gao and X.D, Xiang [29], [79]. This model remains the most used analytical model because it does not only describe the response of thick samples, but also the response of thin films structures [58]. This model can provide a physical picture of the interaction behaviour between the probe tip and the sample under test.

The proposed model by C.Gao and X.D, Xiang [79], therefore, it describes the frequency shift and degradation of the quality factor of a coaxial $\lambda/4$ resonator when a dielectric sample is set closer to the tip. The model presents the tip as an infinitely charged sphere over a sample, and it is modelized as a sphere because the electric field on the surface of a charged object is proportional to its radius of curvature. As the end of the tip is sharpened and has much smaller radius of curvature than the rest of the tip. When it is closer to the sample to be analyzed, a neglectable coupling is supposed in the sample with respect to the end of the tip because of the electric field produced in the rest of the tip.

To obtain an effective interpretation about the interaction between the tip and the sample under test, the thickness of the sample is also assumed to be greater than the radius of the sharpened part of the probe tip [29].

The image loading model summarizes the shift in resonance frequency of the resonator, the quality factor degradation to the permittivity , and the loss tangent of the thick sample, this is when the tip is in contact with the sample, these parameters can be presented in the following relationships;

$$\frac{\Delta f_r}{f_r} = \frac{f_r - f_{r'}}{f_r} = A(\frac{ln(1-b)}{b} + 1); b = \frac{\varepsilon_r - 1}{\varepsilon_r + 1} \tag{4.6}$$

$$\Delta(\frac{1}{Q_0}) = \frac{1}{Q_0} - \frac{1}{Q_{0'}} = -(B + tan\delta)\frac{\Delta f_r}{fr} \tag{4.7}$$

By applying those relations, the permittivity of dielectric samples using these techniques of the cavity resonators can be determined .

4.3 Experimental results of the coaxial cavity resonator

After the electromagnetic study and the simulation test carried out under HFSS, the coaxial cavities and their supports were also manufactured in the Laboratory of Mechatronics of the University of Granada. For the excitation system, we used semi-rigid cables connected to connectors of the SMA type modified to obtain the best electrical coupling to the coaxial cavities (50Ω) [88].

Figure 4.11: Different fabricated coaxial cavity resonators.

4.3.1 Influence of the cavity dimension to the resonance frequency and the quality factor

The change in the cavity (cavity not connected to the probe tip) length affects primarily on the resonance frequecy and the quality factor as shown in Figure 4.12. The cavity length was optimized at $l = 38.6mm$, then a change was done by increasing the length by step of $1mm$ till $l = 44mm$. The step has been chosen in order to figure out clearly the change in resonance frequency.

Figure 4.13 shows clearly the change in quality factor, and also the resonance frequency when the diameter of the cavity changes. The optimized cavity radius was set at $a = 17mm$, then a decreasing of the diameter by a step of $-0.5mm$ was done till $a = 15mm$ in order to show these changes behaviour.

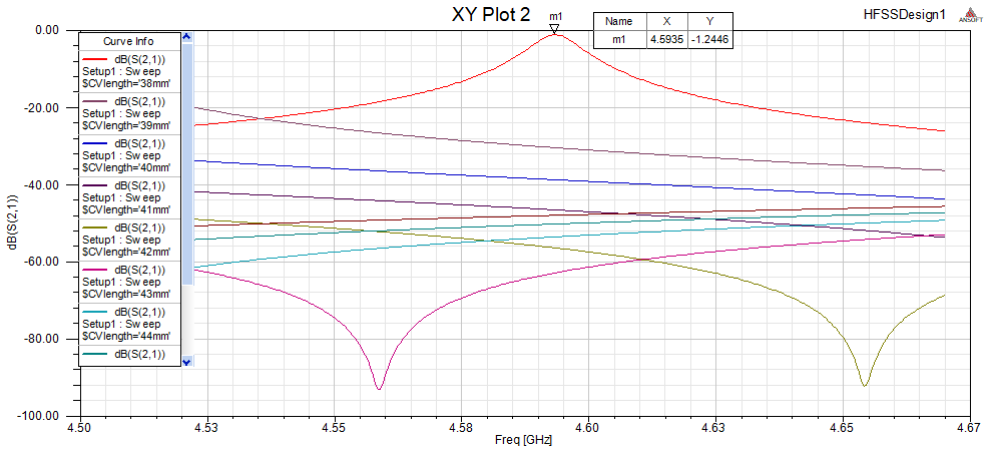

Figure 4.12: Change in resonance frequency as a function of the cavity length.

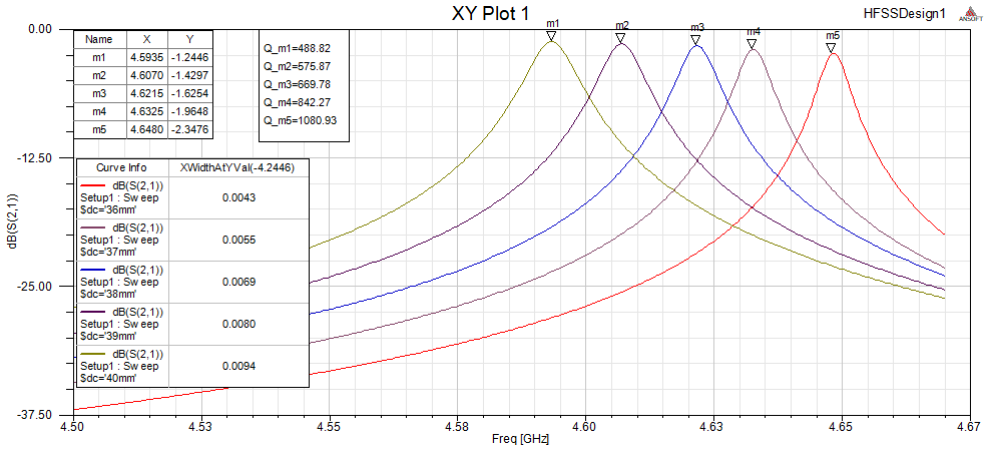

Figure 4.13: Change in resonance frequency and quality factor as a function of the cavity diameter.

The best quality factor was obtained when the cavity has the following radius $a = 15mm$, after the optimization, the cavity and the probe tip-sample interaction, the best diameter that gives precise measurements was set at $a = 17mm$.

4.3.2 Influence of the feeding connectors to the response of the cavity resonator

The coupling energy makes an influence on the response frequency of the resonator. The electromagnetic waves are driven to the cavity through coupling wires (SMA connectors) producing an electric field coupling. The coupling wires provide a smaller coupling and a higher quality factor and also offer more flexibility in modifying the coupling force. Figure 4.14 shows how the length of the connectors SMA extended inside the cavity can affect the coupling factor and therefore determine the quality factor of the coaxial cavity resonator. These connectors are placed on the top of the cavity, the depth to which they

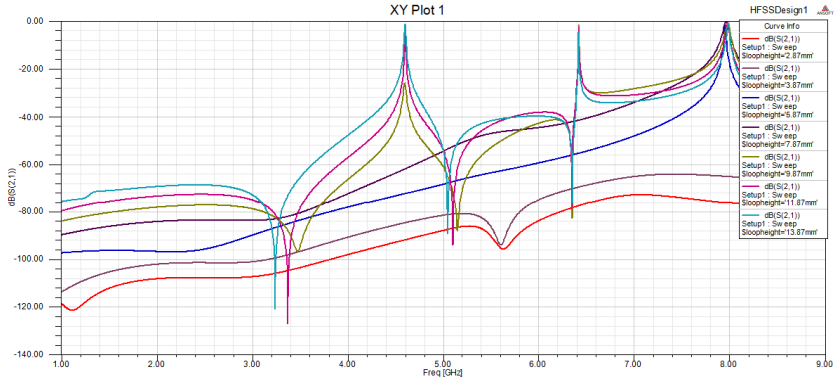

Figure 4.14: Diagram of the several simulations traces of $|S_{21}|$ from $1GHz$ to $9GHz$ for several different coupling wire lengths.

are inserted inside the cavity was varying from $2.87mm$ till $13.87mm$ for both connectors in this simulation. The length of the connectors inside the cavity was carefully adjusted at the value $13.87mm$ in order to optimize the coupling and the quality factor of the resonator.

The unloaded resonance frequency of this cavity was calculated using relations (4.2), (4.3), and (4.5) we have got ;

$$C_R = \frac{2\pi\epsilon_0}{\ln(\frac{b}{a})} l = 0.152pF,$$

$$L_R = \frac{1}{2}\frac{\mu_0 \ln(\frac{b}{a})}{\pi} l = 1.45nH,$$

$$F_0 = \frac{1}{2\pi\sqrt{L_R C_R}} = 1.19GHz.$$

where; $\epsilon_0 = 8,85 \cdot 10^{-12} F/m$, $\mu_0 = 4\pi \cdot 10^{-7} H/m$ represent the permittivity and permeability of the vacuum respectively.
A first measurement of the fabricated structure was carried out using a vector network analyzer PNA-X 5242-A . Figure(4.15) shows the measured transmission coefficient S_{21} in dB. The resonance frequency of the $3\lambda/4TEM$ mode is $4.56GHz$, the level of S_{21} is $-9dB$ and the vacuum quality factor Q_0 is of the order of $Q = 500$ [88].

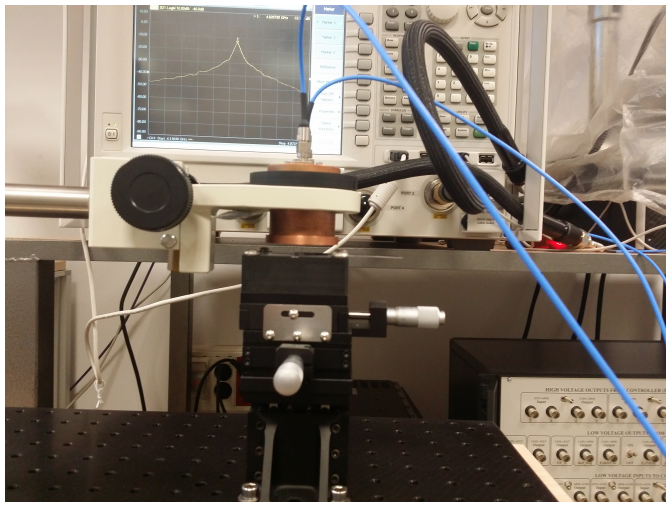

Figure 4.15: Fabricated coaxial cylindrical cavity resonator mounted to the NSMM platform.

It can be clearly noticed that there is a good agreement between the simulation and experimental results shown in the Figure 4.16. The frequency band from $f_r = [4.50 - 4.70]GHz$ has been chosen as the frequency of working during all our experiments because it is the most sensitive band that could figure out the variation of the resonance frequency when the tip is set far off or close to the material under test.

According to the experiment and the simulation results, the working frequency was selected at $f_r = 4.56GHz$ in the case of the cavity that is connected to the tip that is $l = 1.7mm$ of length extended out of the cavity. When the tip is extended $l = 2.2mm$ out from the cavity , it is connected to the inner conductor of the cavity, the working frequency then increased, and shifted with $7MHz$ to $f_r = 4.639GHz$.

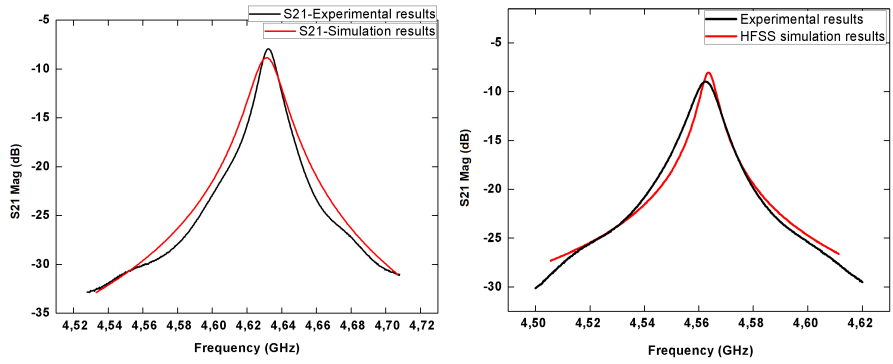

Figure 4.16: In the right side, the cavity connected to the probe tip with $l = 1.7mm$ of length. In the left side the cavity is connected to the tip with $l = 2.2mm$ of length.

4.4 Calibration of the NSMM system and characterization of some samples

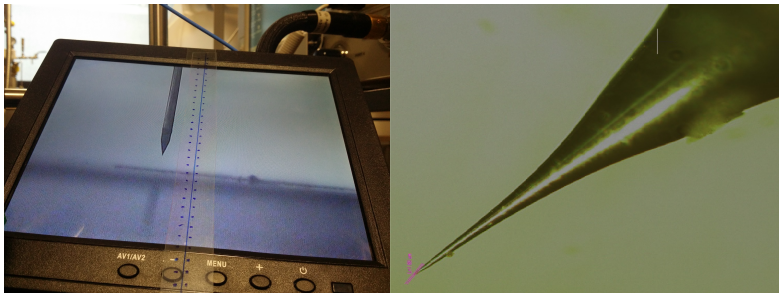

Figure 4.17: Tip used on the calibration of the NSMM system and the characterization of samples. In the left side, the cavity is connected to the probe tip with $l = 1.7mm$ of length and $d = 1.8\mu m$ in diameter. On the right side the tip connected to the cavity above the sample under test, using a LCD camera to capture a picture of the distance between tip-sample.

A calibration of the NSMM platform was done by characterizing a SiO_2 sample in order to check the functioning of the system. The tip used for calibration was $l = 1.7mm$ of length and $1.8\mu m$ of its sharpened diameter as it is clearly shown in Figure 4.17.

4.4.1 Set-up of NSMM and tip-sample distance control

During the measurements, as we mentioned before, the NSMM platform consists of a PNA-X vector network analyzer that works according to a given range $[0.10 - 26.5GHz]$. To do so, when the cavity resonator is connected to the vector network analyzer, a developed Matlab code is in charge to receive the scattering parameters of the cavity through the *GPIB* connection (port). The cavity resonator is synchronized with the vector network analyzer. Among those scattering parameters, we could store the transmission coefficient S_{21} to enable us to represent the behavior of the cavity resonator when it interacts with the material under test.

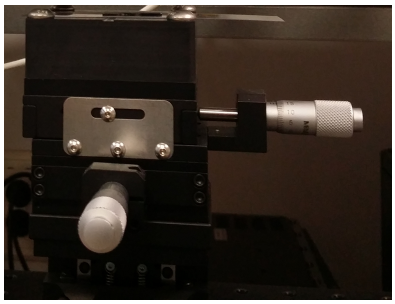

(a)

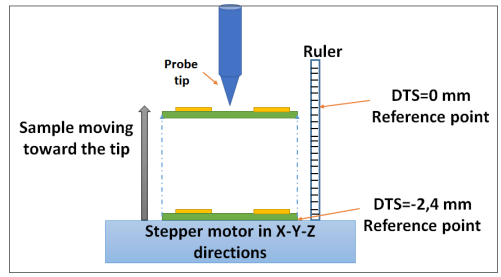

(b)

Figure 4.18: a) $X - Y - Z$ manual stage with micrometer motion-Thorlabs. b) Set-up of the sample approaching to the probe tip.

Once the experimental of the NSMM platform is set up, the tip is coupled to the inner conductor of the cavity, that allows us to test different kind of samples that are put on the X-stage support of the X-Y-Z micrometer stage. This latter allows for manual micrometer level motion as shown in Figure 4.18-a. The manual stage used in our experiments allows the motions in three directions: X-Y-Z. The sample was put on the X-Y stages and was approached toward the tip using different steps. The mentioned manual stage was working with a minimum step of $10\mu m$.

In order to present the interaction between the tip-sample under test, the tip which is connected to the coaxial cavity resonator has been fixed, otherwise, the sample was moving towards it. As it is seen in Figure 4.18-b, a ruler was set on the camera beside the tip to arrange its position and the motion reference of the sample. The tip was set up as a reference position of $DTS = 0$, whilst the sample was put down from the probe tip with separation distance $DTS = 2.4mm$. The spatial resolution is of the order of the diameter of the tip used which is $1.8\mu m$.

4.4.2 Characterization of graphene oxide and reduced graphene oxide using a cylindrical coaxial cavity resonator

Graphene, in the last decade, has become a promising material for electronics applications, especially in radio-frequency analogue circuits and transparent conductors in a wide range. Near-Field Microwave Microscopy is known generally as a non-destructive technique dedicated to the characterization of materials. Therefore, this material can be tested by this technique at nano scale range [89], [90]. A pristine graphene layer was put on the top of the substrate from Silicon and this later was analyzed using the AFM technique based on NSMM. This study was realized by Kundhikanjana et al [90], [91]. Furthermore, they succeeded in demonstrating the detection possibility of local inhomogeneities in the graphene derived chemically. Another approach was performed by Talanov et al [90], [92] that consists of a transmission line integrated to NSMM. It enables the quantitative imaging of a local impedance of graphene that contains mono layer and few layers. A multilayer material that is composed of a dielectric film and a few layers of graphene had been recently tested by Monti et al [90], [93]. The procedure was concentrated to achieve a non-contact measurement of the sheet resistance of this material that contains multilayer.
In this section, a sample fabricated in our lab (CITIC-UGR), consist a very thin layer of RGO on the top of a substrate layer of PET (polyethylene terephthalate). Several tests have been successfully done using coaxial cavity resonator connected to a shorter and longer probe tip. The idea was to characterize the sample being analyzed and simultaneously to determine the thickness of the RGO layer put on top of the GO as shown in Figure 4.19.

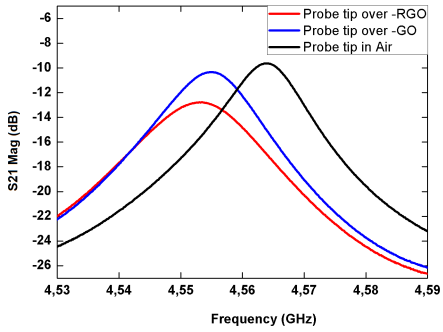

(a)

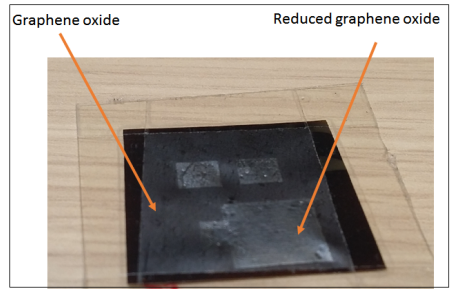

(b)

Figure 4.19: a) Tip in the Air, over graphene oxide, and reduced graphene oxide ($GO - RGO$) using a shorter tip, b) ($GO - RGO$) sample.

Figure 4.19-a shows a comparison of the transmission coefficient S_{21} of the cavity when the tip is in the air, and in the two other cases, when it is over a region of $GO-RGO$ respectively. The distance between the tip-sample was set according to the step of the manual stage which is $DTS = 10\mu m$.

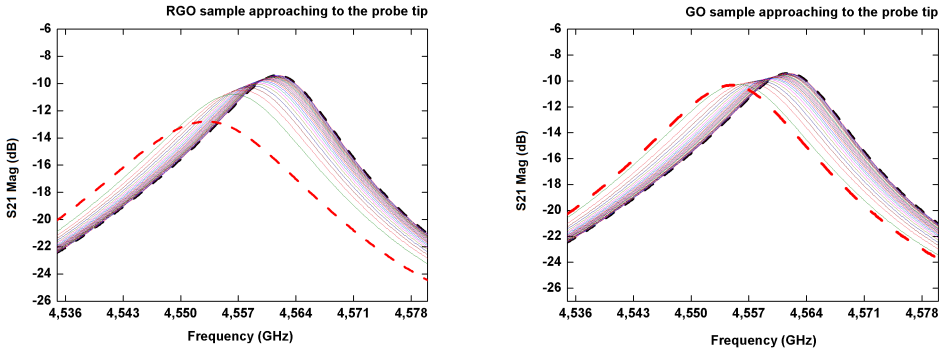

(a) (b)

Figure 4.20: a), b) A shorter tip with $l = 1.7\mu m$, with a diameter $d = 1.8\mu m$, when the sample composed of a graphene oxide, and reduced graphene oxide ($GO - RGO$) in approaching mode to the tip.

The measurements that were done as they are shown in Figure 4.20-a,b present test level of the tip over two different materials which are GO and RGO respectively and the tip in the air. The samples under test well carefully placed in the X-Y stage of the stepper motor with respect to keep the tip fixed.
In Figure 4.20-a,b, we can notice that there is a decrease in resonance frequency as well as in the transmission coefficient when the sample is well separated from the tip till the contact between them is produced. This result is obtained when the chosen area of GO and RGO sample approach step by step to the tip. The black and red dash curves represent when the tip is far from the sample and when is in contact mode respectively. The tip was separated to the samples under test with a $DTS = 2.4mm$. To control the tip-sample distance, a micrometer stage which is characterized by microns steps have been used in our experiments. As it seen in Figure 4.21, a transparent ruler has been used to make reference to the distance between the tip and the sample under test as it was mentioned previously.

Figure 4.22-a, therefore, exhibits clearly the drift level of the resonance frequency when the sample that contains (graphene oxide GO) is approaching to the tip in comparison with the other part of the sample being tested. The degradation in frequency as a function of the tip-sample separation distance is given from $DTS = -2.4mm$ by

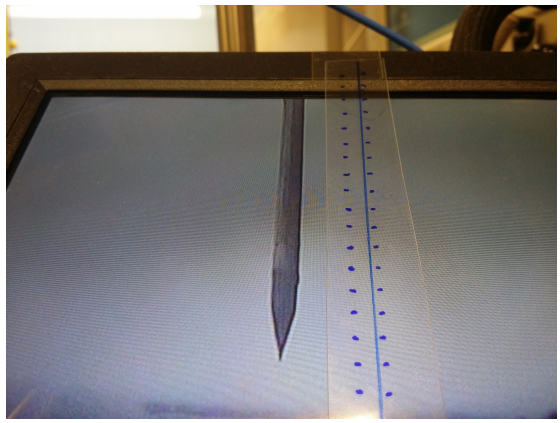

Figure 4.21: Tip-sample reference separation distance. The distance between tip-sample was set at $DTS = 2.4mm$ with a step of $100\mu m$.

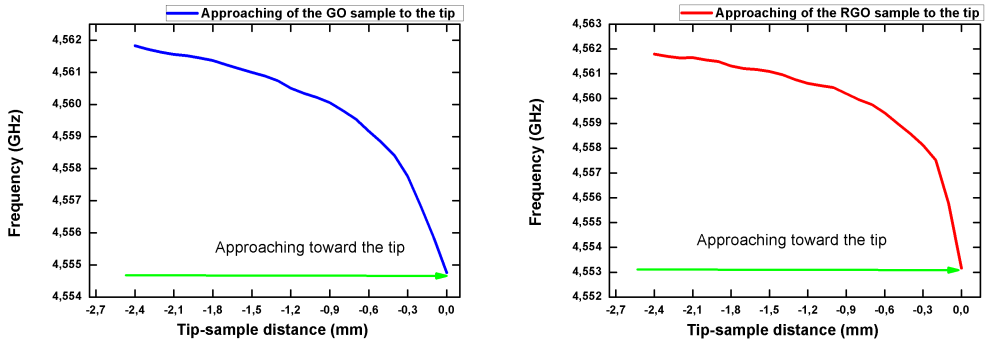

(a) (b)

Figure 4.22: a) Graphene oxide sample (GO) in approaching mode to the tip with a step of $100\mu m$. b) Reduced graphene oxide sample (RGO) in approaching mode to the tip with a step of $100\mu m$.

steps of $100\mu m$. On the other hand, when the (Reduced graphene oxide RGO) region of the sample under test is approaching also with the same step and the same separation distance of the tip-sample, there is also a remarkable decrease in resonance frequency which is illustrated in Figure 4.22-b.

The difference in the resonance frequency when the different regions of the sample are approaching toward the tip with a step of $100\mu m$ is illustrated in Figure 4.23-a and with a separation distance from the tip set at $DTS = -2.4mm$. At this distance, there is a small change in resonance frequency according to both different regions of the sample

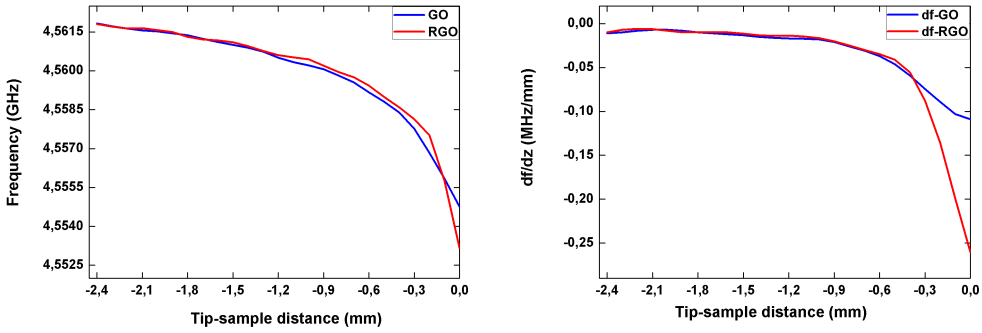

(a) (b)

Figure 4.23: a) Comparison of the resonance frequency in function of the tip-sample distance , the (GO, RGO) sample in approaching mode to the tip. b) Comparison of the derivative of the resonance frequency in function of the distance between the tip and the (GO, RGO) sample.

under test. When the sample is going to be near the tip especially when DTS in the range from $-2.4mm$ to $-900\mu m$, we can really distinguish that the drift in the resonance frequency of the different regions of the sample is increased.

In this case, we used a very large step of $100\mu m$ approaching to the tip, it is hard to figure out the thickness level of the RGO put on the GO substrate as illustrated in Figure 4.23-b. However, when the sample is approaching towards the tip with the noticed step and especially in the near field region, a loss of information according to the properties of the sample can occur. For that, another test with a small step of $10\mu m$ has been selected in which the smallest step that provides the translation stage is used in our experiments (Figure 4.24).

To reveal the difference between the different layers of material in the sample under test, the graph in Figure 4.25 represents the resonance frequency and its derivative in function with the stand-off distance that separates the tip from the sample. As we prepared the samples to be tested using this technique of non-destructive characterization, small squares of RGO have been on a thin layer of GO in which this layer was set as substrate.

The distance between the sample and the tip with small steps provides a high spatial resolution. Therefore, the precision of the measurement of the samples that are analyzed quantitatively is related to the control accuracy of that distance.

The quality factors shown in Figure 4.26 Q were obtained simultaneously and similarly with the resonance frequency f_r. These parameters decrease when the sample starts

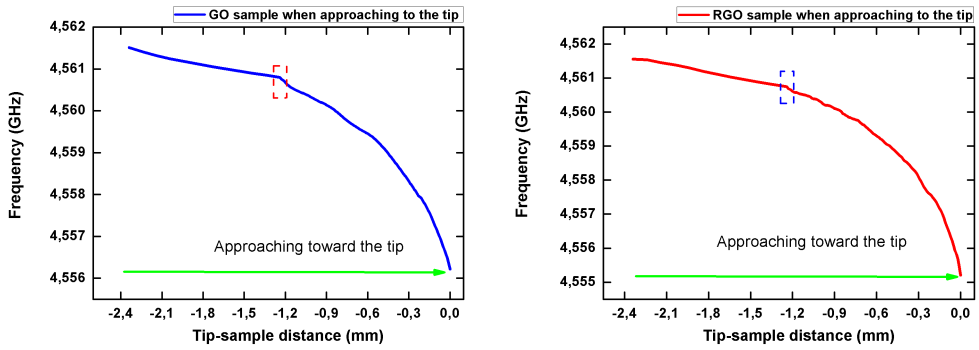

(a) (b)

Figure 4.24: a) Graphene oxide sample (GO) in approaching mode to the tip with a step of $100\mu m$ in the far field and $10\mu m$ in the near field regions. b) Reduced graphene oxide sample (RGO) in approaching mode to the tip with a step of $100\mu m$ in the far field and $10\mu m$ in the near field regions.

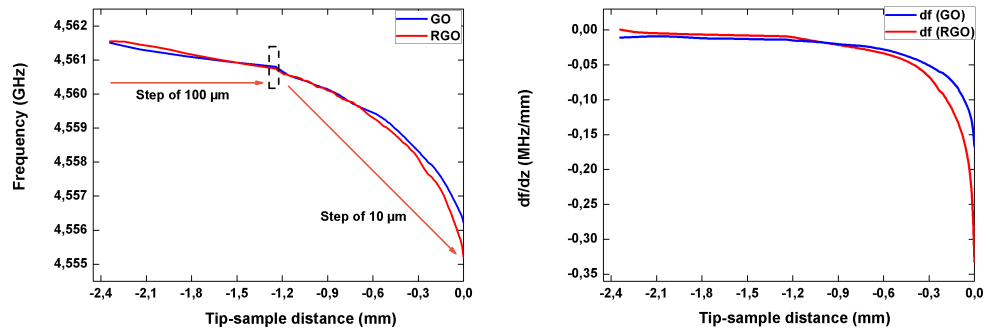

(a) (b)

Figure 4.25: a) Comparison of the resonance frequency in function of the tip-sample distance , the (GO, RGO) sample in approaching mode to the tip with a small step of $10\mu m$ in the near field regions. b) Comparison of the derivative of the resonance frequency in function of the tip-sample distance of the (GO , RGO) sample.

to approach towards the tip.

We can distinguish the quality factor $Q_{near-GO} = 336.09$ when the GO region of the sample is closer to the tip of few microns. Therefore the quality factor of the RGO region of the sample is $Q_{near-GO} = 307.95$ also when it is closer to the tip of few microns (around 1 micron). This is means when the sample is closer to the tip, the quality factor of the GO area of the sample is higher than the RGO area that gives a difference in the

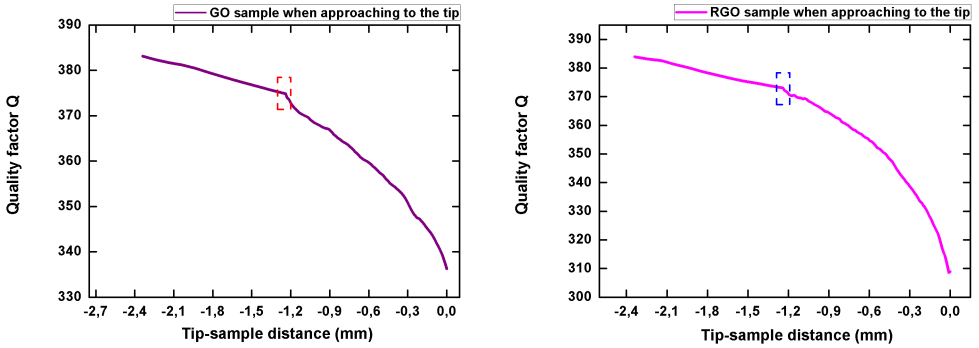

(a) (b)

Figure 4.26: Comparison of the quality factor in function of the tip-sample distance. a) Quality factor measured of the (GO) sample in approaching mode to the tip with a small step of $10\mu m$ in the near field regions. b) Quality factor measured of the (RGO) sample in approaching mode to the tip with a small step of $10\mu m$ in the near field regions.

quality factor of $\Delta Q = 28.14$. This difference signifies the thickness level of the RGO layer with a few microns put on top of the GO substrate.

4.4.3 Characterization of graphene oxide and reduced graphene oxide using a conical coaxial cavity resonator

The idea to design such a conical coaxial cavity resonator was at first improved by Luis.A and al [94], in which they had developed their scanning microwave microscopy platform by designing a tapered open-ended $\lambda/4$ coaxial cavity which had a conical form at its end. The idea to design such a resonator as shown in Figure 4.27 is to have more energy concentrated at the end of the cavity. The conical coaxial cavity resonator has a resonance frequency of $f_r = 2.16GHz$ that corresponds to the sensitive working frequency during the measurements. The resonance frequency corresponds to the response of the resonator when it is connected to the tip of $l = 2.2\mu m$ of length.

The conical coaxial cavity resonator consists of cylindrical cavity base with length of $l_{base} = 12mm$, diameter $d_{base} = 40mm$,and a cone length l_{cone} ended by a tapered shape with a diameter of $d_{coneend} = 3mm$. In total , the conical coaxial cavity resonator forms a $\lambda/4$ resonator with $l_{conicalcavity} = 37mm$ of length ended by a cone.

This resonator has been designed and fabricated at CITIC-UGR lab. During the fabrication of this conical resonator, we faced two problems; the first one was the fabrication of the cone geometry of the inner conductor, and the second obstacle was the connection between the tungsten tip with the head cone of the inner conductor. So, those constraints

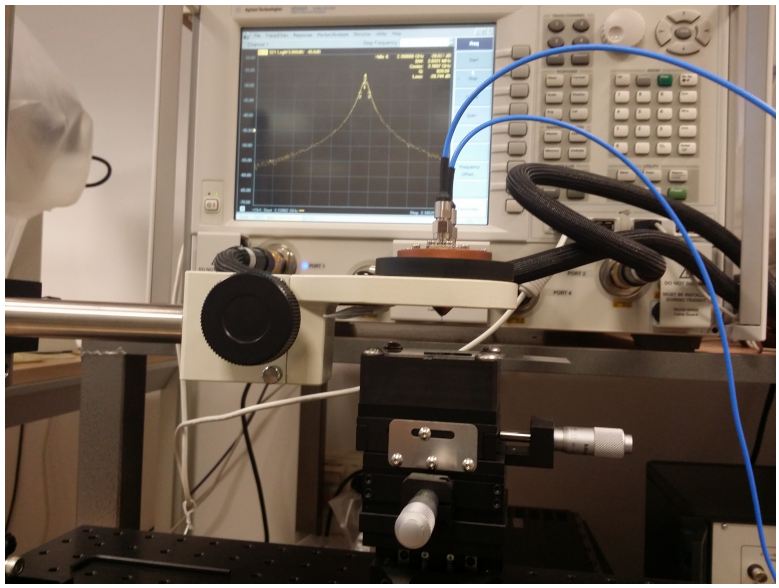

Figure 4.27: The fabricated conical coaxial cavity resonator mounted to the NSMM platform.

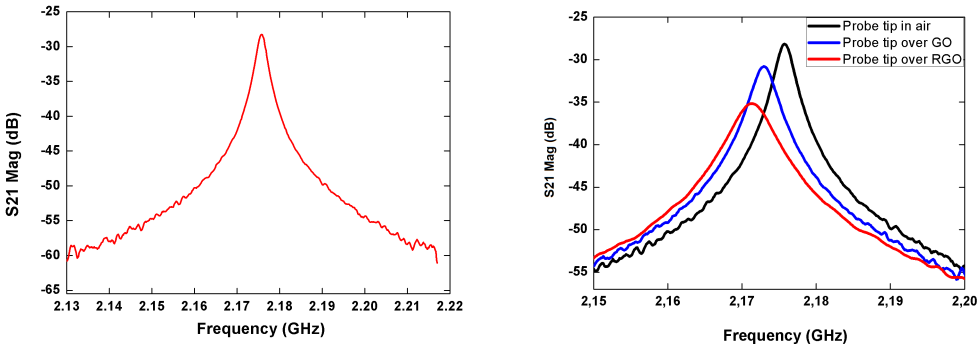

(a) (b)

Figure 4.28: a) The magnitude of the transmission coefficient S_{21} of the conical coaxial cavity resonator connected to a tip of $l = 2.2\mu m$ during the measurements. b) Tip in the Air, over graphene oxide, and reduced graphene oxide ($GO - RGO$) using a longer tip.

pushed our study to focus on the use of the coaxial cylindrical cavity that was easier to mount and make the tip connection with the inner conductor more efficient. Although this kind of conical cavity provides a very high-quality factor in which its design based

on, its response is a little noisy in comparison with the response of the cylindrical one.

The results obtained in Figure 4.28-b illustrate the interaction that happened between the same sample tested previously with the cylindrical cavity resonator. This measure consists of approaching the layer areas of the GO and RGO sample towards the tip connected to the conical coaxial cavity resonator.

This experiment allows us to validate these results with those that were taken by the cylindrical resonator. The measurements of the transmission coefficient S_{21} of this resonator were taken in the air, that means without the presence of the sample, the other ones were taken were the sample was approaching closer to the tip of few microns.

It is clear that there is a good match between the results of the characterization of the graphene oxide and the reduced graphene oxide $GO - RGO$ sample obtained with both coaxial cavity resonators. Moreover, the cylindrical resonator can provide more accuracy.

4.5 Conclusions

In conclusion, based on results from simulations and experiments, we have in a first part, developed multi resonators for the characterization of thin layers of semiconductors.

Scanning near-field microwave microscopy platform such the developed in our study permits to get more information about the material under test and its nature (dielectric, conductors, semiconductors). The platform allows also to record the reflection and the transmission coefficients during the measurements. Both of them can be used to analyze the samples under test.

In this study, indeed, the coaxial cavity resonators designed and simulated ones were well integrated into the NSMM platform. Furthermore, the cylindrical coaxial cavity has been more useful to our platform regarding its efficiency, ease of assembly, and its design. The change in the cavity length can affect the resonance frequency while the change in diameter affect the quality factor and also the resonance frequency. The tested samples were fabricated in our lab CITIC-UGR, and our main objective was to extract their properties to validate the NSMM proposed platform.

Chapter 5

NSMM integrated with a commercial atomic force microscopy (NSMM-AFM)

5.1 Introduction

Since the early eighteenth century, scientists have been able to observe small sizes of samples using optical lenses. Following the introduction of optical apparatus and fixed beam, electron microscopes have emerged, including microscopes that can utilize transmission and reflection in the near field-microscopy (i.e., tunnelling and atomic force). Today, these techniques can observe objects on the nano-atomic scale.

The characterization of materials can be achieved by examining the interaction of electromagnetic fields with matter [17], [95]. The scanning near-field microwave microscopy (NSMM) technique is one of such tools [96], which has been proposed as a way to achieve the non-destructive characterisation of localised material electrical properties at microwave frequencies [97], [98], [99].

A number of different techniques have been used in the characterization of materials, which has been the subject of notable research. Among these techniques, NSMM (which was demonstrated for the first time in 1962 by Soohoo [35]) has been well-described in the previous chapters. Since then, several researchers have been working on increasing the sensitivity and the resolution of this technique.

In the near-field regime, the quantitative measurement of these properties (resolution and sensitivity) can be carried out using length scales that are much smaller than the freely propagating wavelength of the radiation [77], [100], [101].

When a sharp probe tip protruding from a resonator cavity of high-quality factors is brought in close proximity to the sample surface, near-field microwaves can be utilised to obtain measurements of the reflection coefficient S_{11} as well as the transmission coefficient, quality factor and resonant frequency shifts of the resonant cavity that is coupled to the tip [100].

The local electrical properties such as conductivity, sheet resistance, and the dielectric constant can then be extracted through measured data [35], [97]. Of a particular interest is the study of the electrical conductivity of thin-film samples, including semiconductor nano structures [1], [67], [102], [103], [104].

In this chapter, we employed a performance network analyzer (PNA) that continuously feeds the conductive tip of an atomic force microscope (AFM), to which we have coupled a half-wavelength micro strip line resonator. The tip is then brought to the surface of the sample under study using the AFM control mechanism [105], which is operated in the usual way. Depending on the impedance of the tip-sample interface, part of the microwave signal is reflected and measured by the PNA as the reflection coefficient, S_{11}.

The scattering S_{11} parameter depends on the dielectric properties of this region; therefore, the high spatial resolution of the AFM allows us to non-destructively characterize semiconductor structures. Our method offers high sensitivity and nanometric resolution and is able to evaluate factors such as the quality of the interfaces, thickness variations, and doping and carrier concentrations [104], [106].

5.2 Configuration of an integrated AFM-NSMM

Several commercial solutions already exist [106]. However, we have developed a home-made adaptation that allows a commercial AFM to easily be integrated with an NSMM platform. To do so, we have coupled different types of an $\lambda/2$ micro-strip resonators to a commercial AFM (NT-MDT Integra) by employing a specially designed tip holder. The conductive tip (an n-doped silicon tip coated with gold) is connected at the edge of the micro strip, in contact with the conductive strip line of the micro-strip as shown in Figure 5.1.

To check the validity of the set-up, the device tested here was used in conjunction with different kinds of samples, including a silicon sample covered with a $300nm$ thick layer of SiO_2. To test our technique, we deposited different patterns of gold and aluminium in different sizes and shapes on top of the oxide through thermal evaporation; what is done is to deposit graphene oxide and then reduce it using the laser process [107].

We then used this structure of AFM-NSMM combination to calibrate the system (Figure 5.2, left-hand side). The thickness of the gold metallization is $60 - 70nm$.

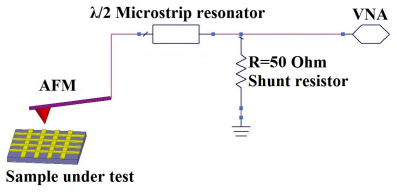

(a)

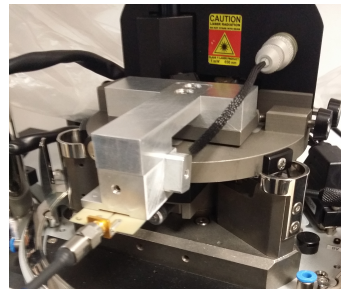

(b)

Figure 5.1: a) Experimental set-up using the combined NSMM-AFM technique; b) the holder head of the integrated AFM-to-NSMM solution.

Figure 5.1-a shows the set-up used in this work, while Figure 5.1-b shows some photos of the micro strip and the final setup.

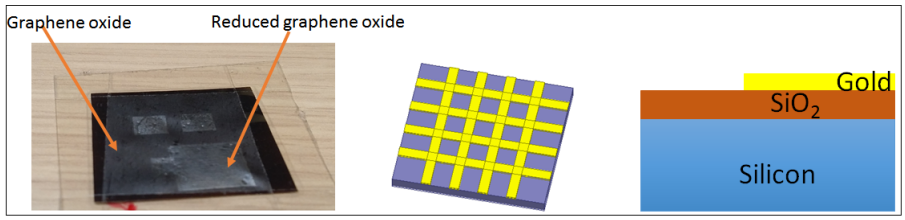

Figure 5.2: Samples analyzed using AFM-NSMM inegrated technique.

5.3 Integration of the NSMM and AFM

The combination of a NSMM platform combined with a commercial AFM increases the efficiency of the characterization of materials by simultaneously performing the material measurements and analyzing the topography of the surfaces on a micro/nano scale [13], [105].

Among the techniques that have been used to couple a commercial AFM with an NSMM platform is the use of a half-wavelength coaxial resonator. Keysight Technologies provided a commercial platform that integrates SNMM with AFM using a coaxial resonator, as is illustrated in Figure 5.3 [106].

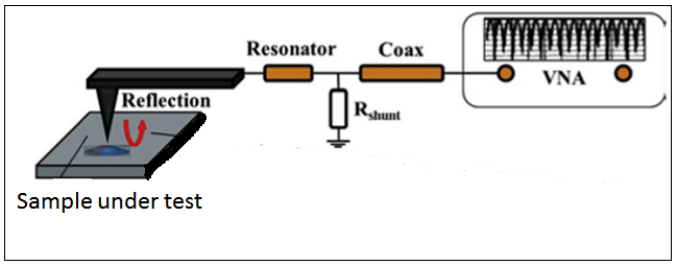

Figure 5.3: Basic shematic of integrated NSMM-AFM using a coaxial resonator with a 50Ω shunt resistor.

5.3.1 Microstrip line as resonator

The idea to use a micro strip line resonator in an NSMM application was used firstly by Tabib Azar et al. in 1993 [77]. They designed a quarter-wavelength micro strip line resonator connected at its end to a sharp probe tip. The idea was to measure the conductivity of the material used to form metallic lines on a glass and printed circuit boards. A micro strip resonator using a tuning Stub shown in Figure 5.4, had already been used by Wang et al. of the MINEC Group at the University of Lille [18], [52].

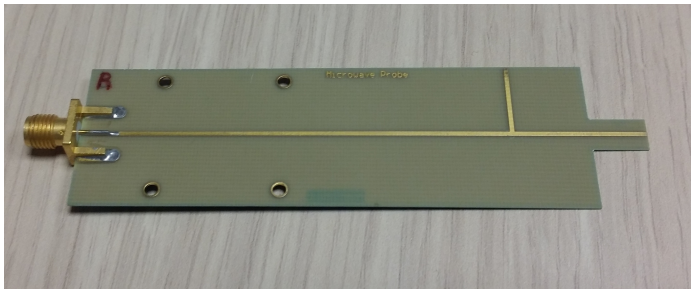

Figure 5.4: A micro strip resonator using a tuning Stub.

Wang et al. [18] thought to develop a micro strip line resonator that could be applied in order to achieve the non-destructive characterization of material using the microwave range. This micro strip line was tapered at its end, forming a probe; this shape helps to concentrate the energy that will be transferred into the material under test, making the interaction between this probe and the material that is being characterized more efficient.

The main goal when designing such a micro strip line resonator is to tune the minimum amount of reflected power from the microwave probe when the cantilever is on the surface of the sample. In this way, a small change in impedance will have a significant effect on

the reflected signal.

The micro strip line resonator uses the right-angled stub design referenced in Figure 5.4, there are two unterminated lengths of the strip line, they are $\lambda/4$ and $\lambda/2$ wavelengths. The longer stub is in electrical contact with the bottom of the cantilever chip. The additional length of the chip and the cantilever will affect the resonance of the structure. Our first aim, using this device, is to explore this micro strip line and determine the specific characteristics that will allow us to connect it with a commercial AFM platform [108].

Figure 5.5 shows the designed micro strip line resonator within HFSS environment. The experimental results of the reflection coefficient $S11$ spectrum are shown in Figure 5.6.

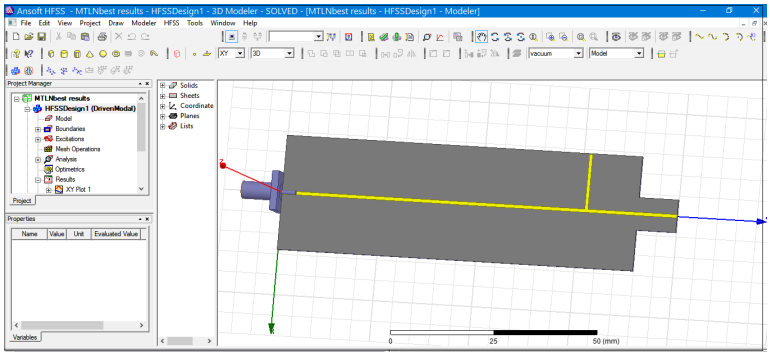

Figure 5.5: A micro strip line resonator designed and simulated within the HFSS environment.

In order to do so, firstly:

- We calculate the resonance frequency theoretically;

$$f_r = \frac{c}{4l\sqrt{\varepsilon_{eff}}} = 1.78GHz$$

where ; l_{stub} corresponds to tuned Stub length of the micro strip line.
ε_{eff} corresponds to the effective dielectric constant of the micro strip's line dielectric substrate (FR-4 fibreglass) $\varepsilon_{eff} = 3.385$.

Figure 5.7-a shows the magnitude of the $|S_{11}|$ scattering parameter as a function of the frequency. The selected fixed frequency for the experimental procedure was $f0 = 4.56GHz$. This presents a selective notch of working frequency that is more sensitive to the application of the NSMM-AFM technique, as well as providing a better interpretation of the interaction between tip-sample when the sample under test is put closer to the

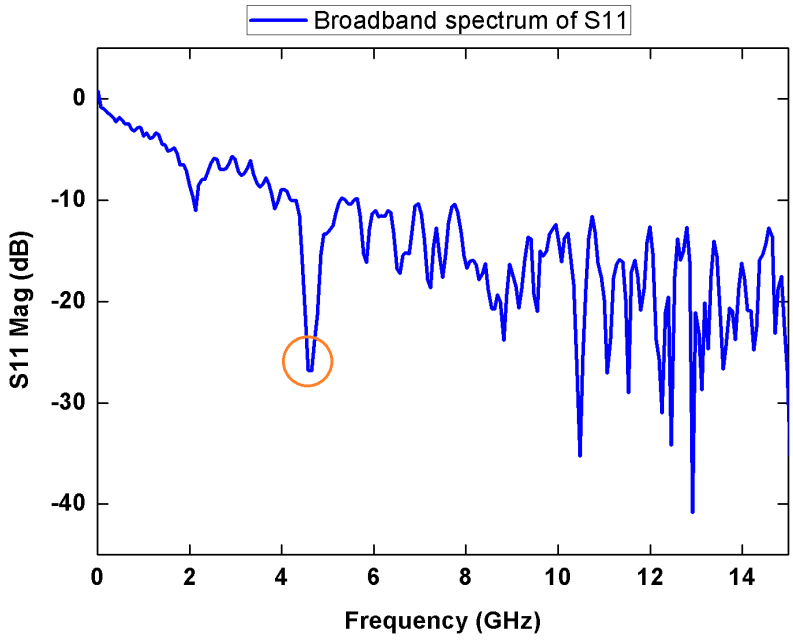

Figure 5.6: Spectrum of reflection coefficient S_{11} at $[10MHz - 10GHz]$ range, experimental results.

cantilever tip. The right -hand side of Figure 5.7-b shows the micro strip line resonator when it is connected to the modelled cantilever tip, which has been designed in an HFSS environment. It is also noted that there is a small shift in the resonance frequency when the cantilever tip is connected to the micro strip line resonator [108].

5.3.1.1 Characterization of SiO_2 sample using half wavelength micro strip line resonator

The results obtained in Figure 5.8-a using a half wavelength micro strip line resonator demonstrate a good function of this device regarding its test done when it is closer to a sample. The sample was placed at a distance of $DTS = 10nm$ from the cantilever tip, this proved to be the optimal distance when interpreting the interaction between Tip-sample being analyzed.

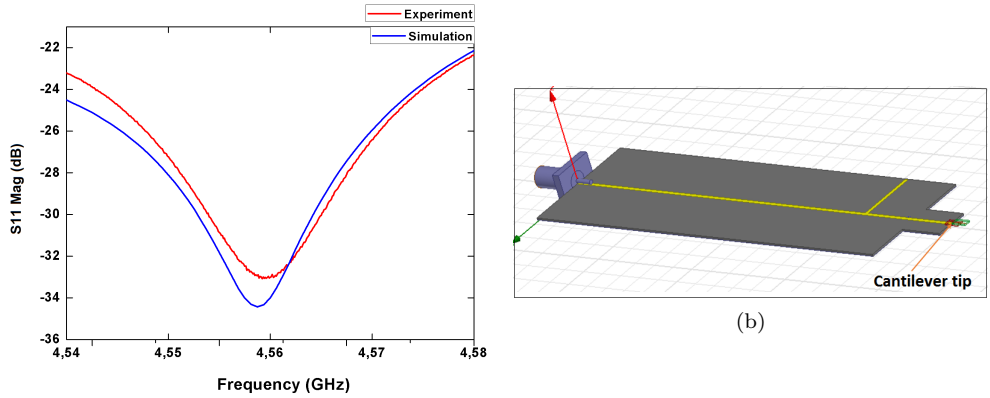

(a) (b)

Figure 5.7: a) Selected notch for the working frequency experimental and simulation results. b) Micro strip line resonator connected to the cantilever tip within the HFSS environment.

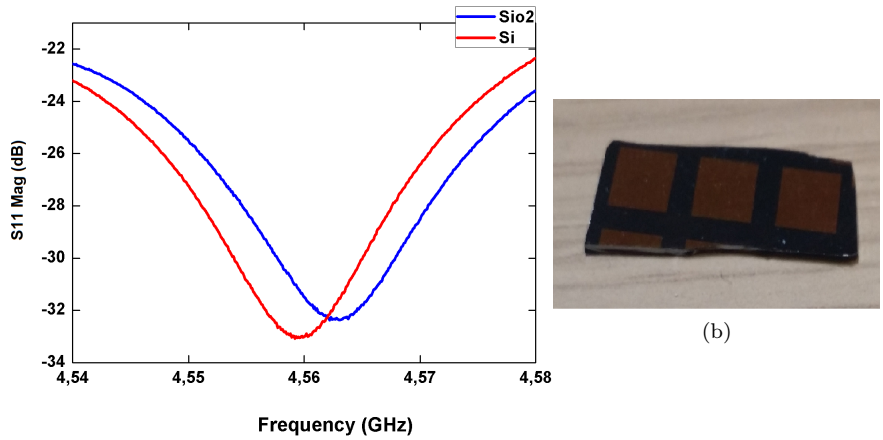

(a) (b)

Figure 5.8: a) The cantilever tip test performed over SiO_2 and Si regions of the sample with a separation distance of around $DTS = 10nm$ between Tip-sample. b) The sample being tested.

5.3.2 A half wavelength microstrip line using a 50Ω shunt resistor

The idea when designing this type of resonator is to make the connection easier between the resonator and the cantilever tip. In order to obtain the minimum reflected power at

the frequency of interest, we used a micro strip line, adding a termination resistor back by the SMA connector.

This produces a fundamental frequency of about $f_0 = 802MHz$ which forms a $\lambda/2$ wavelength resonator Figure 5.9. The termination resistance needs to be trimmed by adding a resistor in parallel or by removing it and changing the values. The resonance

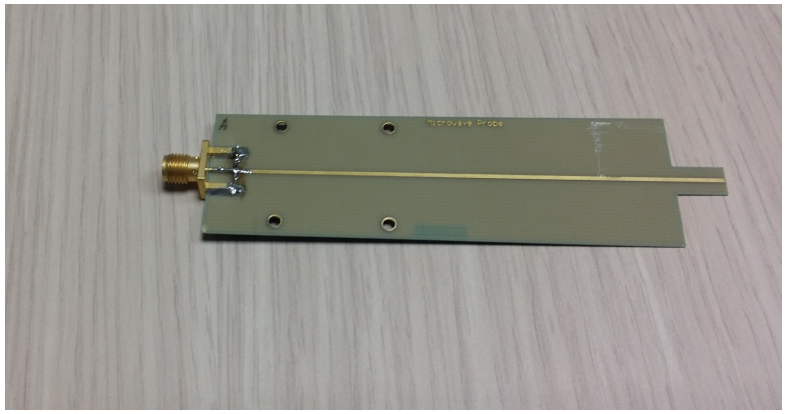

Figure 5.9: A $\lambda/2$ half wavelength micro strip resonator using a 50Ω shunt resistor.

frequency of the micro strip line using a shunt resistor was calculated as follows:

- Calculate the resonance frequency of the micro strip line using a shunt resistor:

$$f_r = \frac{c}{2l\sqrt{\varepsilon_{eff}}} = 802MHz$$

where ; $l_{line} = 100mm$ which corresponds to the length of the micro strip line. ε_{eff} corresponds to the effective dielectric constant of the microstrip line dielectric substrate (FR-4 fibreglass) $\varepsilon_{eff} = 3.511$.

The micro strip line resonator using a shunt resistor was also designed in an ADS environment. Furthermore, a block containing a resistor and capacitor has been integrated with the system in the NSMM-AFM simulation, which presents the modelling of the sample under test (Figure 5.10).

Once the sample under test has been placed in the AFM sample holder, the tip is brought to the sample and the reflection coefficient and the quality factor of the micro strip at the resonance frequency are recorded as a function of the sample-tip distance over different areas of the sample (over SiO_2 and over metal sample).

The frequency sweep in this time is performed from $10Mhz$ to $8GHz$. Figure 5.11 shows the magnitude of the S_{11} parameter as a function of the frequency.

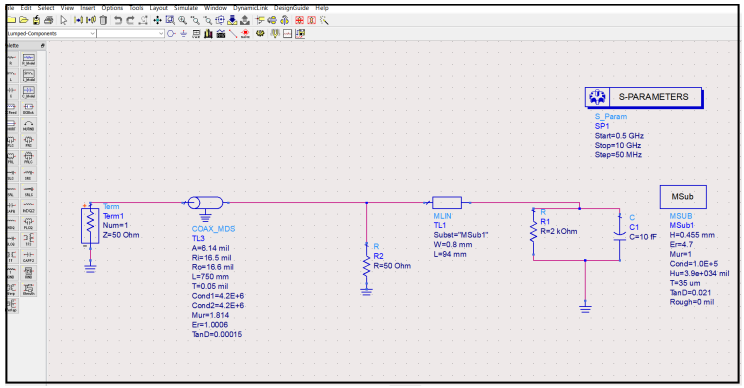

Figure 5.10: A $\lambda/2$ half wavelength micro strip line resonator using a 50Ω shunt resistor designed and simulated within the ADS environment.

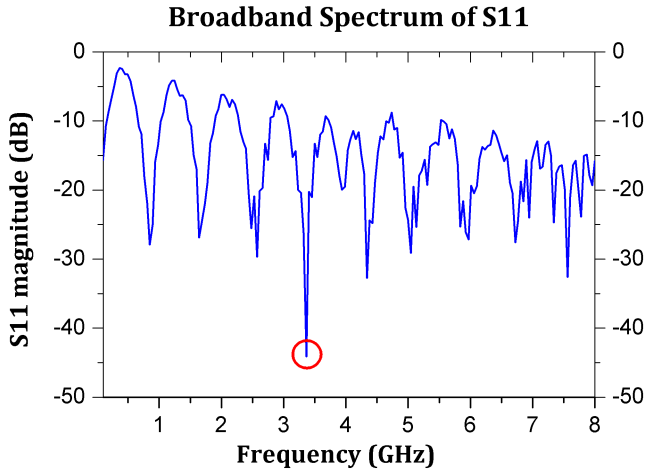

Figure 5.11: Spectrum of reflection coefficient S_{11} at $[10MHz - 8GHz]$ range, simulation and experimental results.

The selected notch determining the working frequency during the experimental procedures was $f_r = 3.365GHz$ (Figure 5.12).

5.4 Characterization of test materials

When the device under test (sample) is placed in the AFM sample holder the tip is approached to the sample and the resonance frequency is recorded as a function of the

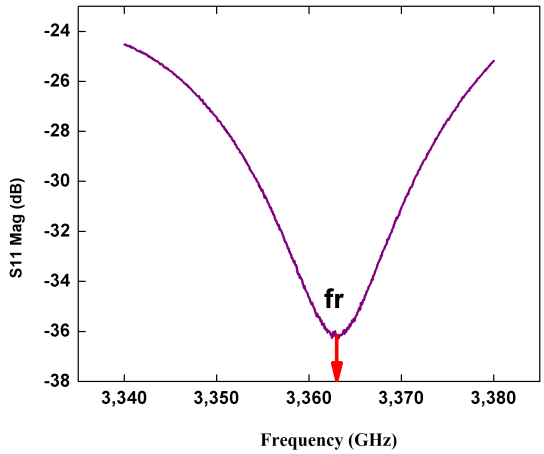

Figure 5.12: A selective notch for working frequency.

sample-tip distance over different areas of the sample as shown in Figure 5.13.

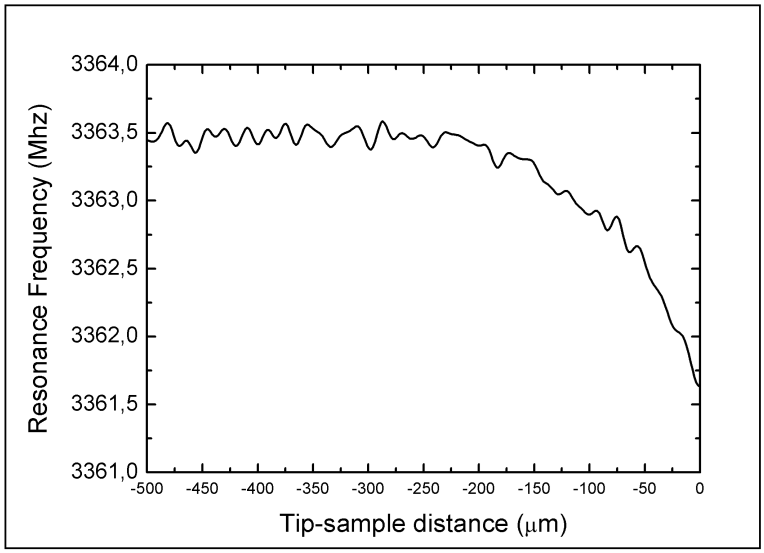

Figure 5.13: Evolution of the resonance frequency as the tip is approaching the sample.

As it has been mentioned previously, our device under test consists in a silicon sample, covered with $300nm$ of SiO_2. Different patterns of gold and aluminium that contain

different sizes and shapes are deposited on top of the oxide. This structure is used to calibrate the system (Figure 5.14).

Figure 5.14 also shows an AFM image of a gold ribbon on top of the SiO_2. The thickness of the gold metallization is $60 - 70nm$.

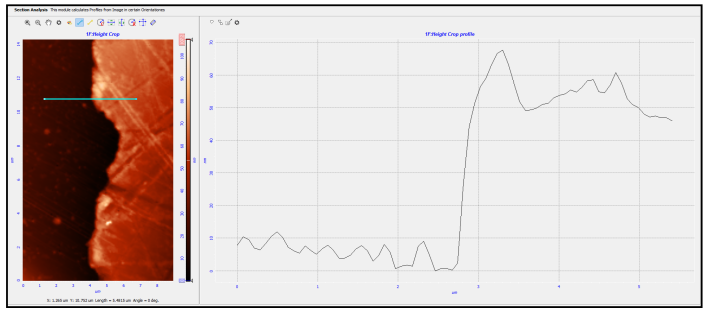

Figure 5.14: AFM image of the DUT, and profile of the Gold metallization (the step is $70nm$).

While Figure 5.15-a, 5.15-b show the 3D topography, and the 2D topography respectively of the sample under test.

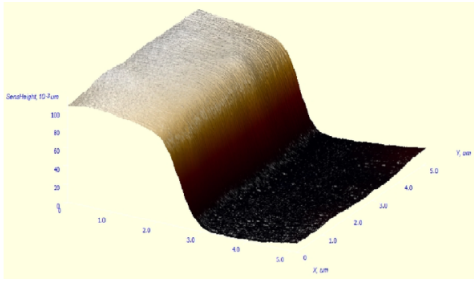

(a)

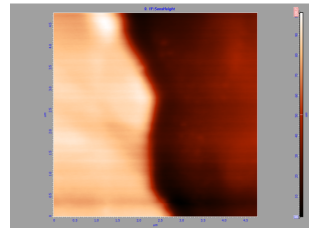

(b)

Figure 5.15: a) 3D topography image of the scanned sample. b) 2D topography image of the sample.

As the tip is approaching the sample, the resonance frequency of the micro strip remains constant until $150\mu m$ above the sample. A closer distance from the tip to the sample surface produces a decrease of the resonance frequency until the contact is produced. The magnitude of the S_{11} parameter also decreases as the tip is approaching the surface of the sample, and the value that this parameter gets near and right at the surface strongly depends on the local dielectric characteristics of the semiconductor sample right under the tip.

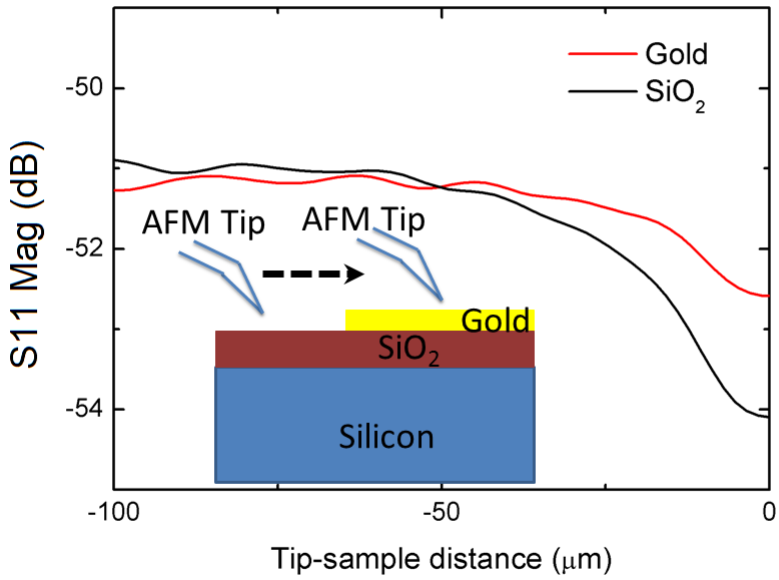

Figure 5.16: Magnitude of S_{11} as the AFM tip is approaching the surface of the DUT: (red line) the approaching is produced over a point on the gold metallization; (black line) the approaching is produced on the SiO_2 substrate.

Depending on the point where the approach is produced, the value of the reflection coefficient, S_{11}, (shown in Figure 5.16), the resonance frequency and the quality factor (not shown) of the micro strip are modified. The scanning of the tip on the surface will produce a map of the variations of $|S_{11}|$ on the surface of the DUT, with the spatial resolution that allows the spatial resolution of the AFM.

The modifications of these parameters are related to the local properties of the DUT. Although the maximum difference in the $|S_{11}|$ value is produced right at the surface, there is also a noticeable difference hundreds of nanometres above the surface. Therefore, the spatial variation of the properties of the DUT can be detected with this technique without touching the surface, and therefore without producing any defect in the sample. In addition, this technique can also be used to detect changes in the properties of the DUT under the surface, just as doping, carrier concentration, defects, etc.

5.5 Conclusion

In this chapter, we have endeavored to develop an integrated NSMM-AFM method of characterization of materials compatible with industrial applications. The choice of configuration of this type of measurement has to be closer to the sample to be characterized. We, therefore, proposed a technique for measuring the reflection coefficient, in monostatic and contactless mode.

The measurement data was acquired in the form of shifts in the resonant frequency and changes in the magnitude of the reflection coefficient S_{11} when the tip of the AFM is scanned on the device under test. The variations of the S_{11} parameter are related to the topographical and dielectric properties of the material under the tip.

Finally, to illustrate how this method works, we compare the results obtained at different distances between the cantilever probe and the sample under test as well as the values already published. We find that these results are very close. This comparison highlights the capacity of the proposed method.

Chapter 6

Conclusions and Future Work

6.1 Conclusions

The last chapter of this thesis is dedicated to the synthesis of the scientific results that have been discussed in the previous chapters and explains the possibility to develop future research lines.

Through a brief state of the art, we presented the main of scanning microwave microscopy techniques. We have put forward two blocks of these techniques that are on the one hand the instrumentation associated with this type of measurement which almost systematically requires the use of a network analyzer, and on the other hand the limitations of these methods in term of spatial resolution, of the order of the wavelength of use.

In order to overcome the problem of spatial resolution imposed by conventional microwave characterization methods, works on the development of NSMM methods using microwaves have been described. Indeed, one of the benefits offered by the NSMM platform is that the zero level can be tuned as a function of the material under test. Another advantage brought by the system is the possibility to operate at any frequency in $[1 - 26.5GHz]$. These local techniques have spatial resolutions that depend neither on the wavelength of use but on the size of the measuring probe. The NSMM demonstrates its ability in the extraction of the local electromagnetic properties of materials. In particular, we show that these encouraging works have generally focused on measurement probes tip.

The second axis of this work is the study and development of a new microstrip line, economical, sensitive, and easy to integrate into a commercial AFM technique also devoted for characterization of materials especially semiconductors. These techniques are based on a reflection or transmission coefficient measurement technique, in a monostatic

and contactless configuration. This type of measurement uses low-cost samples (SiO_2, Graphene Oxide, and Reduced Graphene Oxide) associated with modeling that makes it possible to estimate the effective permittivity of the material under test from the measured reflection or transmitted coefficient. From a more personal point of view, this study was also an opportunity for me to have experimental phases where I could apply part of my research to a concrete problem. As a conclusion, the AFM-based near-field microwave microscopy is able to locally characterize the materials/semiconductor structures in a broad frequency range with high measurement sensitivity.

6.2 Future Work

Much of the work done in this doctoral thesis have laid the groundwork on the development of scanning microwave microscopy techniques devotes to semiconductor characterization. As perspectives, there are several interesting research lines that can be thought as a continuation of the work presented which are listed below: one of our other objectives is to eventually offer a specialized instrumentation for the local electromagnetic characterization of nano-objects. Indeed, the exceptional properties of nano-objects make it possible to envisage applications in a multitude of domains. Local characterization of electromagnetic properties such as conductivity or complex permittivity is necessary for both understanding and analyzing or predicting the behavior of the nano-object. Conventional measurement techniques (free space, guided structures) that have spatial resolutions of the order of the wavelength of use are poorly adapted to local characterization. Consequently, the approach based on the use of evanescent waves appears as a promising solution to address this type of characterization. Another field of investigation relates to the realization of a near-field microwave microscope in transmission (or even simultaneous reflection / transmission).

For the second point, it will transpose the current equipment in the nanoscale to meet the current need for electromagnetic characterization tools in the microwave frequency band at a scale of a few nanometers. The fields of applications concerned are multiple. For example, in the field of semiconductors and particularly the micro / nano-electric, the miniaturization of components and the use of innovative dielectric materials is accompanied by the need to study these components and materials locally for their optimization.

In the field of Biology, scanning near field microwave microscopy is one of the few techniques that allows a direct characterization of complex permittivity at sub-micron scales. It therefore offers undeniable perspectives for the study of polarization and dielectric relaxation at the nanometer scale.

To meet these objectives, the design and manufacture of probes with nano apex

sizes is envisaged. The main difficulty consists in designing and producing propagation structures to bring and concentrate the electromagnetic energy at the end of the probe by limiting as much as possible the phenomena of standing waves. This reduction in size is accompanied by the need to operate in controlled atmospheres in terms of temperature and humidity. A particular effort during the design phase of the main parts of the NSMM platform will focus on the limitation of electronic and acoustic noise. Indeed, operating in millimeter frequency range makes it possible to further increase the measurement sensitivity and to miniaturize the electronic circuits. Thus, this axis makes it possible to offer interesting perspectives with regard to terahertz microscopy methods that remain difficult to implement and expensive.

Finally, the preliminary studies devoted to AFM based NSMM integrated technique presented in the last part of this manuscript showed the interest of this approach to image the surface and sub-surface of the device under test. In particular, the extension of this method to the study of materials or multilayers seems relevant. It is noted that Keysight Technologies TM (formerly AgilentTechnologiesTM) has initiated studies in this direction.

From the standpoint applications, the first step will be to develop the modeling part of the local electromagnetic interactions between the probe tip and the material under test. So, using these models the physical quantities of interest are extracted from the measurement. The works presented in this thesis have been particularly focused on the technical aspects of measurement, associated instrumentations with the aim of improving electrical and spatial sensitivities. In particular, the electromagnetic simulation used in this thesis is presented as a tool adapted to extract the parameters of interest. It will be in the following of these works to compare and test different simulators in order to compare them to the experiments. The characterization methods will be compared to conventional characterization techniques for measuring the permittivity and/or permeability of planar dielectric materials but also in the context of the measurement of the electrical conductivity of conductive materials. Analytical methods such as first order perturbation or quasi-static approaches will also be exploited. These parameters are more time-saving than numerical methods and can be implemented directly on the software part of the instrument.

6.3 Publications

Publications by date of delivery at the Graduate School of the University of Granada:

Journal publications derived from the Thesis

1) Bagdad, Bendehiba Abadlia, Carmen Lozano, and Francisco Gamiz. "Near-field scanning microwave microscope platform based on a coaxial cavity resonator for the characterization of semiconductor structures." Solid-State Electronics, **2019**.

Conference publications

1) Development of Near-Field Scanning Microwave Microscopy Technique for Characterization of Semiconductor Structures Bagdad BA, Gamiz F, A.Ahmadouche. *II Jornadas de investigadores en formación fomentando la interdisciplinariedad*, **Granada 2016 (Spain)**

2) Characterization of semiconductor structures using scanning microwave microscopy technique Bagdad BA, Gamiz F. *InUltimate Integration on Silicon (EUROSOI-ULIS), 2017 Joint International EUROSOI Workshop and International Conference*, **Athens 2017 (Greece)**.

3) Near field scanning microwave microscope based on a coaxial cavity resonator for the characterization of semiconductor structures. Bagdad BA, Gamiz F. *InUltimate Integration on Silicon (EUROSOI-ULIS), 2018 Joint International EUROSOI Workshop and International Conference.*, **Granada 2018 (Spain)**.

4) Applications of a near-field scanning microwave microscope technique for semiconductors characterization Bagdad BA, Gamiz F. *Women in Sciences Symposium*, **Erlangen 2018 (Germany)**.

Bibliography

[1] S. Gu, T. Lin, and T. Lasri, "Broadband dielectric characterization of aqueous saline solutions by an interferometer-based microwave microscope," *Applied Physics Letters*, vol. 108, no. 24, p. 242903, 2016.

[2] S. Barbet, "Étude par microscopie à champ proche de matériaux iii-n pour émetteurs électroniques planaires," Ph.D. dissertation, Lille 1, 2008.

[3] B. T. Rosner and D. W. van der Weide, "High-frequency near-field microscopy," *Review of Scientific Instruments*, vol. 73, no. 7, pp. 2505–2525, 2002.

[4] S. M. Anlage, V. V. Talanov, and A. R. Schwartz, "Principles of near-field microwave microscopy," in *Scanning probe microscopy.* Springer, 2007, pp. 215–253.

[5] K. Lee, H. Melikyan, A. Babajanyan, and B. Friedman, "Near-field microwave microscopy for nanoscience and nanotechnology," in *Scanning Probe Microscopy in Nanoscience and Nanotechnology 2.* Springer, 2011, pp. 135–171.

[6] M. Mehdizadeh, *Microwave /RF applicators and probes: for material heating, sensing, and plasma generation.* William Andrew, 2015.

[7] P. N. Minh, O. Takahito, and E. Masayoshi, *Fabrication of silicon microprobes for optical near-field applications.* CRC Press, 2002.

[8] R. A. Kleismit, M. K. Kazimierczuk, and G. Kozlowski, "Sensitivity and resolution of evanescent microwave microscope," *IEEE transactions on microwave theory and techniques*, vol. 54, no. 2, pp. 639–647, 2006.

[9] M. Tabib-Azar, D.-P. Su, A. Pohar, S. LeClair, and G. Ponchak, "0.4 μm spatial resolution with 1 ghz (λ= 30 cm) evanescent microwave probe," *Review of Scientific Instruments*, vol. 70, no. 3, pp. 1725–1729, 1999.

[10] G. Binnig and H. Rohrer, "Scanning tunneling microscopy—from birth to adolescence," *reviews of modern physics*, vol. 59, no. 3, p. 615, 1987.

[11] D. J. Barker, "Evaluation of microwave microscopy for dielectric characterisation," Ph.D. dissertation, University of Birmingham, 2010.

[12] Z. Wu, A. Souza, B. Peng, W. Sun, S. Xu, and C. Ong, "Measurement of high frequency conductivity of oxide-doped anti-ferromagnetic thin film with a near-field scanning microwave microscope," *AIP Advances*, vol. 4, no. 4, p. 047114, 2014.

[13] A. Karbassi, "Different probing techniques for scanning near-field microwave microscopy," Ph.D. dissertation, University of Wisconsin-Madison, 2007.

[14] A. R. de Souza, "Study of electrical conductivity of thin films with near-field scanning microwave microscopy," Ph.D. dissertation, National University of Singapore, 2014.

[15] B. Crowell, *Conceptual physics*. Light and Matter Books, 2016.

[16] C. Tsipogiannis, "Microwave materials characterization using waveguides and coaxial probe," *Student Paper*, 2012.

[17] D. M. Pozar, *Microwave engineering*. John Wiley & Sons, 2009.

[18] M. Wang, "Contribution à la conception et la réalisation de microscopes champ proche en bandes de fréquences microondes et millimétriques: application à l'évaluation non destructive," Ph.D. dissertation, Lille 1, 2010.

[19] H. Alaaeddine, "Contribution à la caractérisation de matériaux diélectriques par résonateurs submillimétriques en technologies planaire et ltcc," Ph.D. dissertation, University of Limoges, 2011.

[20] A. J. Bahr, *Microwave nondestructive testing methods*. CRC Press, 1982, vol. 1.

[21] A. W. Kraszewski, "Microwave aquametry-needs and perspectives," *IEEE Transactions on Microwave theory and Techniques*, vol. 39, no. 5, pp. 828–835, 1991.

[22] H. S.-l. Ku, F. Siu, E. Siores, and J. Ball, "Applications of microwaves in non-destructive testing," *Non-Destructive Testing-Australia*, vol. 38, no. 5, pp. 129–132, 2001.

[23] R. Zoughi, *Microwave non-destructive testing and evaluation principles*. Springer Science & Business Media, 2012, vol. 4.

[24] D. K. Ghodgaonkar, V. V. Varadan, and V. K. Varadan, "A free-space method for measurement of dielectric constants and loss tangents at microwave frequencies," *IEEE Transactions on Instrumentation and measurement*, vol. 38, no. 3, pp. 789–793, 1989.

[25] F. Wee, P. J. Soh, A. Suhaizal, H. Nornikman, and A. Ezanuddin, "Free space measurement technique on dielectric properties of agricultural residues at microwave frequencies," in *Microwave and Optoelectronics Conference (IMOC), 2009 SBMO/IEEE MTT-S International*. IEEE, 2009, pp. 183–187.

[26] M. H. Umari, D. K. Ghodgaonkar, V. V. Varadan, and V. K. Varadan, "A free-space bistatic calibration technique for the measurement of parallel and perpendicular reflection coefficients of planar samples," *IEEE Transactions on Instrumentation and Measurement*, vol. 40, no. 1, pp. 19–24, 1991.

[27] M. Zhao, J. D. Shea, S. C. Hagness, and D. W. van der Weide, "Calibrated free-space microwave measurements with an ultrawideband reflectometer-antenna system," *IEEE microwave and wireless components letters*, vol. 16, no. 12, pp. 675–677, 2006.

[28] G. Kent, "An evanescent-mode tester for ceramic dielectric substrates," *IEEE transactions on microwave theory and techniques*, vol. 36, no. 10, pp. 1451–1454, 1988.

[29] J. Rammal, "Capteurs microondes en bande ism pour la caractérisation de matériaux en champ proche et pour le suivi de l'évolution de la corrosion," Ph.D. dissertation, Université de Limoges, 2014.

[30] P. Guillon and Y. Garault, "Complex permittivity measurement of mic substrate," *Archiv Elektronik und Uebertragungstechnik*, vol. 35, pp. 102–104, 1981.

[31] M. D. Janezic and J. Baker-Jarvis, "Full-wave analysis of a split-cylinder resonator for nondestructive permittivity measurements," *IEEE Transactions on Microwave Theory and Techniques*, vol. 47, no. 10, pp. 2014–2020, 1999.

[32] M. D. Janezic, E. Kuester, and J. R. Baker-Jarvis, "Nondestructive permittivity and loss tangent measurements using a split-cylinder resonator," in *2002 URSI General Assembly*, 2002.

[33] M. D. Janezic, "Nondestructive relative permittivity and loss tangent measurements using a split-cylinder resonator," Ph.D. dissertation, University of Colorado at Boulder, 2003.

[34] E. Synge, "Xxxviii. a suggested method for extending microscopic resolution into the ultra-microscopic region," *The London, Edinburgh, and Dublin Philosophical Magazine and Journal of Science*, vol. 6, no. 35, pp. 356–362, 1928.

[35] R. F. Soohoo, "A microwave magnetic microscope," *Journal of Applied Physics*, vol. 33, no. 3, pp. 1276–1277, 1962.

[36] Y. Lu, T. Wei, F. Duewer, Y. Lu, N.-B. Ming, P. Schultz, and X.-D. Xiang, "Nondestructive imaging of dielectric-constant profiles and ferroelectric domains with a scanning-tip microwave near-field microscope," *Science*, vol. 276, no. 5321, pp. 2004–2006, 1997.

[37] Z. Wang, M. A. Kelly, Z.-X. Shen, L. Shao, W.-K. Chu, and H. Edwards, "Quantitative measurement of sheet resistance by evanescent microwave probe," *Applied Physics Letters*, vol. 86, no. 15, p. 153118, 2005.

[38] S. Huang, "Thin film dielectric properties characterization by scanning near-field microwave microscopy," Ph.D. dissertation, The George Washington University, 2009.

[39] S. Huang, H. Christen, and M. Reeves, "Parameter-free extraction of thin-film dielectric constants from scanning near field microwave microscope measurements," *arXiv preprint arXiv:0909.3579*, 2009.

[40] S.-C. Lee, C. Vlahacos, B. Feenstra, A. Schwartz, D. Steinhauer, F. Wellstood, and S. M. Anlage, "Magnetic permeability imaging of metals with a scanning near-field microwave microscope," *Applied Physics Letters*, vol. 77, no. 26, pp. 4404–4406, 2000.

[41] S. R. Snyder and H. S. White, "Scanning tunneling microscopy, atomic force microscopy, and related techniques," *Analytical Chemistry*, vol. 64, no. 12, pp. 116–134, 1992.

[42] G. Binnig, C. F. Quate, and C. Gerber, "Atomic force microscope," *Physical review letters*, vol. 56, no. 9, p. 930, 1986.

[43] H. Cercellier, "Etude par photoémission et microscopie à effet tunnel des relations entre propriétés structurales et électroniques des interfaces ce/sc (0001) et ag/au (111)," Ph.D. dissertation, Université Henri Poincaré-Nancy I, 2004.

[44] B. Calmettes, "Étude par microscopie à effet tunnel à basse température de l'adsorption moléculaire sur ag (111): de la molécule unique aux assemblages complexes," Ph.D. dissertation, Université de Toulouse, Université Toulouse III-Paul Sabatier, 2010.

[45] S. A. James, N. Hilal, and C. J. Wright, "Atomic force microscopy studies of bioprocess engineering surfaces–imaging, interactions and mechanical properties mediating bacterial adhesion," *Biotechnology journal*, vol. 12, no. 7, p. 1600698, 2017.

[46] I. Tessmer, P. Kaur, J. Lin, and H. Wang, "Investigating bioconjugation by atomic force microscopy," *Journal of nanobiotechnology*, vol. 11, no. 1, p. 25, 2013.

[47] G. Coulon, *Imagerie de Surface de Polymeres: Microscope a Force Atomique.* Ed. Techniques Ingénieur, 2000.

[48] F. SALVAN and F. THIBAUDAU, *Microscopie à sonde locale.* Ed. Techniques Ingénieur, 1999.

[49] J. Dellinger, "Imagerie hyperspectrale en champ proche optique: développement et applications à la nanophotonique," Ph.D. dissertation, Université de Bourgogne, 2013.

[50] M. Martin, "Caractérisation par microscopie en champ proche optique de composants de l'optique intégrée," Ph.D. dissertation, INSA de Lyon, 2003.

[51] O. M. Ramahi, "Near-and far-field calculations in fdtd simulations using kirchhoff surface integral representation," *IEEE Transactions on Antennas and Propagation*, vol. 45, no. 5, pp. 753–759, 1997.

[52] M. Tabib-Azar, P. Pathak, G. Ponchak, and S. LeClair, "Nondestructive superresolution imaging of defects and nonuniformities in metals, semiconductors, dielectrics, composites, and plants using evanescent microwaves," *Review of Scientific Instruments*, vol. 70, no. 6, pp. 2783–2792, 1999.

[53] T. Wei, X.-D. Xiang, W. Wallace-Freedman, and P. Schultz, "Scanning tip microwave near-field microscope," *Applied Physics Letters*, vol. 68, no. 24, pp. 3506–3508, 1996.

[54] C. Vlahacos, R. Black, S. Anlage, A. Amar, and F. Wellstood, "Near-field scanning microwave microscope with 100 μm resolution," *Applied physics letters*, vol. 69, no. 21, pp. 3272–3274, 1996.

[55] F. Keilmann, D. Van der Weide, T. Eickelkamp, R. Merz, and D. Stöckle, "Extreme sub-wavelength resolution with a scanning radio-frequency transmission microscope," *Optics Communications*, vol. 129, no. 1-2, pp. 15–18, 1996.

[56] N. Okazaki, H. Odagawa, Y. Cho, T. Nagamura, D. Komiyama, T. Koida, H. Minami, P. Ahmet, T. Fukumura, Y. Matsumoto *et al.*, "Development of scanning microwave microscope with a lumped-constant resonator probe for high-throughput characterization of combinatorial dielectric materials," *Applied surface science*, vol. 189, no. 3-4, pp. 222–226, 2002.

[57] Q. Zhang, *Near-field scanning microwave microscopy and its applications in characterization of dielectric materials.* University of Notre Dame, 2006.

[58] C. Gao and X.-D. Xiang, "Quantitative microwave near-field microscopy of dielectric properties," *Review of scientific instruments*, vol. 69, no. 11, pp. 3846–3851, 1998.

[59] F. Duewer, C. Gao, I. Takeuchi, and X.-D. Xiang, "Tip–sample distance feedback control in a scanning evanescent microwave microscope," *Applied physics letters*, vol. 74, no. 18, pp. 2696–2698, 1999.

[60] A. Tselev, S. M. Anlage, H. M. Christen, R. L. Moreland, V. V. Talanov, and A. R. Schwartz, "Near-field microwave microscope with improved sensitivity and spatial resolution," *Review of scientific instruments*, vol. 74, no. 6, pp. 3167–3170, 2003.

[61] A. Imtiaz and S. M. Anlage, "A novel stm-assisted microwave microscope with capacitance and loss imaging capability," *Ultramicroscopy*, vol. 94, no. 3-4, pp. 209–216, 2003.

[62] M. S. Kim, S. Kim, J. Kim, K. Lee, B. Friedman, J.-T. Kim, and J. Lee, "Tip–sample distance control for near-field scanning microwave microscopes," *Review of scientific instruments*, vol. 74, no. 8, pp. 3675–3678, 2003.

[63] S. M. Anlage, D. Steinhauer, B. Feenstra, C. Vlahacos, and F. Wellstood, "Near-field microwave microscopy of materials properties," in *Microwave Superconductivity.* Springer, 2001, pp. 239–269.

[64] H. El Matbouly, "Review on microwave metamaterial structures for near-field imaging," in *Microwave Systems and Applications.* InTech, 2017.

[65] G. López-Maldonado, N. Qureshi, O. Kolokoltsev, H. Vargas-Hernández, and C. Ordóñez-Romero, "Graphite thin film characterization using a simplified resonant near field scanning microwave microscope," *Revista mexicana de física*, vol. 60, no. 1, pp. 88–94, 2014.

[66] J.-L. Biarrotte, "Etude de cavités supraconductrices pour les accélérateurs de protons de forte puissance," Ph.D. dissertation, Paris 11, 2000.

[67] J. Smoliner, H. Huber, M. Hochleitner, M. Moertelmaier, and F. Kienberger, "Scanning microwave microscopy/spectroscopy on metal-oxide-semiconductor systems," *Journal of Applied Physics*, vol. 108, no. 6, p. 064315, 2010.

[68] H. Bakli, "Développement d'une plate-forme de microscopie champ proche hyperfréquence par interférométrie," Ph.D. dissertation, University of Lille1, 2015.

[69] M. K. M. Salleh, G. Prigent, O. Pigaglio, and R. Crampagne, "Quarter-wavelength side-coupled ring resonator for bandpass filters," *IEEE Transactions on Microwave Theory and Techniques*, vol. 56, no. 1, pp. 156–162, 2008.

[70] O. Tegel and H. S. Gill, "Cavity-stabilized microwave oscillator," Dec. 24 1985, uS Patent 4,560,952.

[71] L.-F. Chen, C. Ong, C. Neo, V. Varadan, and V. K. Varadan, *Microwave electronics: measurement and materials characterization*. John Wiley & Sons, 2004.

[72] C. W. Nelson, D. A. Howe, and A. S. Gupta, "Ultra-low-noise cavity-stabilized microwave reference oscillator using an air-dielectric resonator," NATIONAL INST OF STANDARDS AND TECHNOLOGY BOULDER CO, Tech. Rep., 2004.

[73] G. Broussaud and L. Malnar, "Influence des circuits hyperfrequences sur les performances d'un maser a cavites couplees," *Solid-State Electronics*, vol. 4, pp. 200–224, 1962.

[74] M. Kozlov and R. Turner, "A comparison of ansoft hfss and cst microwave studio simulation software for multi-channel coil design and sar estimation at 7t mri," *Piers online*, vol. 6, no. 4, pp. 395–399, 2010.

[75] S.-E. Laib, "Caractérisation de la ligne coplanaire à microruban volumique et ses discontinuités par l'approche full-wave basée sur la technique MPIE dans le domaine spatial," Ph.D. dissertation, University of Setif, 2018.

[76] O. M. Abderrahmane, "Hyperfrequency characterization of a material from frequency analysis of circuits with transmission lines," Ph.D. dissertation, University of Mostaganem, Algeria, 2014.

[77] M. Tabib-Azar, N. S. Shoemaker, and S. Harris, "Non-destructive characterization of materials by evanescent microwaves," *Measurement science and technology*, vol. 4, no. 5, p. 583, 1993.

[78] A. Imtiaz, T. M. Wallis, and P. Kabos, "Near-field scanning microwave microscopy: An emerging research tool for nanoscale metrology," *IEEE Microwave Magazine*, vol. 15, no. 1, pp. 52–64, 2014.

[79] C. Gao, B. Hu, I. Takeuchi, K.-S. Chang, X.-D. Xiang, and G. Wang, "Quantitative scanning evanescent microwave microscopy and its applications in characterization of functional materials libraries," *Measurement science and technology*, vol. 16, no. 1, p. 248, 2004.

[80] M. M. Jobbins, A. F. Raigoza, and S. A. Kandel, "Note: Circuit design for direct current and alternating current electrochemical etching of scanning probe microscopy tips," *Review of Scientific Instruments*, vol. 83, no. 3, p. 036105, 2012.

[81] A.-S. Lucier, "Preparation and characterization of tungsten tips suitable for molecular electronics studies," Ph.D. dissertation, McGill University, 2004.

[82] M. Kulawik, M. Nowicki, G. Thielsch, L. Cramer, H.-P. Rust, H.-J. Freund, T. P. Pearl, and P. S. Weiss, "A double lamellae dropoff etching procedure for tungsten tips attached to tuning fork atomic force microscopy/scanning tunneling microscopy sensors," *Review of scientific instruments*, vol. 74, no. 2, pp. 1027–1030, 2003.

[83] J. Kerouedan, "Design and realization of microwave probes for the detection of fatigue micro-cracks on the surface of metals," Ph.D. dissertation, Brest, 2009.

[84] B. A. Bagdad, C. Lozano, and F. Gamiz, "Near-field scanning microwave microscope platform based on a coaxial cavity resonator for the characterization of semiconductor structures," *Solid-State Electronics*, 2019.

[85] J. Perez Urquizo, "Microcircuits for application in ghz microscopy and thz," Ph.D. dissertation, National University Autonomous of Mexico, 2014.

[86] W. Sun, Y. Yang, Z. Wu, T. Feng, Q. Zhuang, L.-M. Peng, S. Xu, and C. K. Ong, "Penetrative imaging of sub-surface microstructures with a near-field microwave microscope," *Journal of Applied Physics*, vol. 116, no. 4, p. 044904, 2014.

[87] T. W. Shawn, "Live cell imaging with the near-field scanning microwave microscopy," Ph.D. dissertation, National University of Singapore, 2014.

[88] B. A. Bagdad and F. Gamiz, "Near field scanning microwave microscope based on a coaxial cavity resonator for the characterization of semiconductor structures," in *Ultimate Integration on Silicon (EUROSOI-ULIS), 2018 Joint International EUROSOI Workshop and International Conference on.* IEEE, 2018, pp. 1–4.

[89] A. Tselev, V. K. Sangwan, D. Jariwala, T. J. Marks, L. J. Lauhon, M. C. Hersam, and S. V. Kalinin, "Near-field microwave microscopy of high-κ oxides grown on graphene with an organic seeding layer," *Applied Physics Letters*, vol. 103, no. 24, p. 243105, 2013.

[90] S. Gu, "Contribution to broadband local characterization of materials by near-field microwave microscopy," Ph.D. dissertation, Lille 1, 2016.

[91] W. Kundhikanjana, K. Lai, H. Wang, H. Dai, M. A. Kelly, and Z.-x. Shen, "Hierarchy of electronic properties of chemically derived and pristine graphene probed by microwave imaging," *Nano letters*, vol. 9, no. 11, pp. 3762–3765, 2009.

[92] V. V. Talanov, C. D. Barga, L. Wickey, I. Kalichava, E. Gonzales, E. A. Shaner, A. V. Gin, and N. G. Kalugin, "Few-layer graphene characterization by near-field scanning microwave microscopy," *ACS nano*, vol. 4, no. 7, pp. 3831–3838, 2010.

[93] T. Monti, A. Di Donato, and M. Farina, "High resolution imaging of few-layer graphene by near-field scanning microwave microscopy," in *Silicon Monolithic Integrated Circuits in RF Systems (SiRF), 2012 IEEE 12th Topical Meeting on*. IEEE, 2012, pp. 109–112.

[94] L. A. Valiente, A. D. Haigh, A. A. Gibson, G. Parkinson, G. Jacobs, P. J. Withers, and R. Cooper-Holmes, "Coplanar waveguide scanning microwave profiler," in *2007 European Microwave Conference*, 2007, pp. 194–197.

[95] E. Ash and G. Nicholls, "Super-resolution aperture scanning microscope," *Nature*, vol. 237, no. 5357, p. 510, 1972.

[96] D. Steinhauer, C. Vlahacos, S. Dutta, B. Feenstra, F. Wellstood, and S. M. Anlage, "Quantitative imaging of sheet resistance with a scanning near-field microwave microscope," *Applied physics letters*, vol. 72, no. 7, pp. 861–863, 1998.

[97] H. Melikyan, T. Sargsyan, A. Babajanyan, S. Kim, J. Kim, K. Lee, and B. Friedman, "Hard disk magnetic domain nano-spatial resolution imaging by using a near-field scanning microwave microscope with an afm probe tip," *Journal of Magnetism and Magnetic Materials*, vol. 321, no. 16, pp. 2483–2487, 2009.

[98] Y. Wang, M. Reeves, W. Chang, J. Horwitz, and W. Kim, "Near-field imaging of the microwave dielectric properties of single-crystal pbtio 3 and thin-film sr 1- x b x tio 3," *MRS Online Proceedings Library Archive*, vol. 603, 1999.

[99] Y. Wang, M. Reeves, and F. Rachford, "Simultaneous imaging of dielectric properties and topography in a pbtio 3 crystal by near-field scanning microwave microscopy," *Applied Physics Letters*, vol. 76, no. 22, pp. 3295–3297, 2000.

[100] I. S. WC, K. W. Whites, and R. A. Lodder, "Theoretical and experimental characterization of a near-field scanning microwave microscope (nsmm)," *IEEE Transactions on Microwave Theory and Techniques*, vol. 51, no. 1, pp. 91–99, 2003.

[101] H. Bakli, K. Haddadi, and T. Lasri, "Interferometric technique for scanning near-field microwave microscopy applications," *IEEE Transactions on Instrumentation and Measurement*, vol. 63, no. 5, pp. 1281–1286, 2014.

[102] I. Humer, H. Huber, F. Kienberger, J. Danzberger, and J. Smoliner, "Phase and amplitude sensitive scanning microwave microscopy/spectroscopy on metal–oxide–semiconductor systems," *Journal of Applied Physics*, vol. 111, no. 7, p. 074313, 2012.

[103] J. Marzouk, S. Arscott, A. El Fellahi, K. Haddadi, T. Lasri, C. Boyaval, and G. Dambrine, "Mems probes for on-wafer rf microwave characterization of future microelectronics: design, fabrication and characterization," *Journal of Micromechanics and Microengineering*, vol. 25, no. 7, p. 075024, 2015.

[104] S.-S. Tuca, G. Badino, G. Gramse, E. Brinciotti, M. Kasper, Y. J. Oh, R. Zhu, C. Rankl, P. Hinterdorfer, and F. Kienberger, "Calibrated complex impedance of cho cells and e. coli bacteria at ghz frequencies using scanning microwave microscopy," *Nanotechnology*, vol. 27, no. 13, p. 135702, 2016.

[105] K. Lai, M. Ji, N. Leindecker, M. Kelly, and Z. Shen, "Atomic-force-microscope-compatible near-field scanning microwave microscope with separated excitation and sensing probes," *Review of scientific instruments*, vol. 78, no. 6, p. 063702, 2007.

[106] E. Brinciotti, G. Gramse, S. Hommel, T. Schweinboeck, A. Altes, M. A. Fenner, J. Smoliner, M. Kasper, G. Badino, S.-S. Tuca *et al.*, "Probing resistivity and doping concentration of semiconductors at the nanoscale using scanning microwave microscopy," *Nanoscale*, vol. 7, no. 35, pp. 14 715–14 722, 2015.

[107] C. Marquez, N. Rodriguez, R. Ruiz, and F. Gamiz, "Electrical characterization and conductivity optimization of laser reduced graphene oxide on insulator using point-contact methods," *RSC Advances*, vol. 6, no. 52, pp. 46 231–46 237, 2016.

[108] B. A. Bagdad and F. Gamiz, "Characterization of semiconductor structures using scanning microwave microscopy technique," in *Ultimate Integration on Silicon (EUROSOI-ULIS), 2017 Joint International EUROSOI Workshop and International Conference on*. IEEE, 2017, pp. 200–203.